ABSTRACT

Title of dissertation: MULTIPHOTON ABSORPTION POLYMERIZATION: ISSUES AND SOLUTIONS

Christopher N. LaFratta, Doctor of Philosophy, 2006

Dissertation directed by: Professor John T. Fourkas
Department of Chemistry and Biochemistry

Multiphoton absorption polymerization (MAP) is gaining importance as a means for fabricating 3-D micro-devices. By focusing an ultrafast laser inside a prepolymer resin, radical polymerization can be initiated by two-photon absorption of a photoinitiator. The result is a highly cross-linked solid polymer point, or voxel, which is extended to create complex shapes by scanning the laser beam in a 3-D pattern. The geometric freedom combined with sub-micron resolution provided by MAP is unparalleled by any other microfabrication techniques. However, MAP suffers from three issues; the novelty of the technique itself, the fact that it is inherently a serial process, and the restriction of device materials to cross-linking polymers. To better understand the technique, the MAP fabrication setup is described in detail. Specific techniques of fabrication, such as how to design and wash microstructures, are also described. To address the second issue, micro-transfer molding (μTM) has been applied

to make high fidelity molds of complex master microstructures, followed by a fast and easy replication step to make duplicate structures. This technique has even been extended to replicate structures with closed-loops, such as arches or coils, which should be topologically impossible to mold and replicate. The third issue has been addressed in two ways, by laser-direct-writing of metal patterns on 3-D substrates and by changing the surface chemistry of the polymer to contain primary amines. Laser-deposited metal can be made conductive by further electroless growth yielding 3-D conducting patterns. The amine surface modification can be used for any number of chemistries, including catalytic metal seeding, which could then be grown into a metal coating. This new flexibility in surface chemistry, along with the enhanced speed of μTM, ensures that MAP will be a practical technology to create micro-devices. Numerous electrical, mechanical, optical, and biological applications of MAP are described as well as potential future applications. To date this work has resulted in 9 peer reviewed publications, and 2 more which have recently been submitted.

MULTIPHOTON ABSORPTION POLYMERIZATION: ISSUES AND SOLUTIONS

by

Christopher N. LaFratta

Dissertation submitted to the Faculty of the Graduate School of the
University of Maryland, College Park in partial fulfillment
of the requirements for the degree of
Doctor of Philosophy
2006

Advisory Committee:

Professor John T. Fourkas, Chair
Professor Douglas English
Professor Sang Bok Lee
Professor Elisabeth Smela
Professor Michael R. Zachariah

DEDICATION

This work is dedicated in loving memory

to one of my first teachers, my great aunt,

Margaret “Winnie” Langone.

ACKNOWLEDGEMENTS

I would like to thank, from the bottom of my heart, my wife, Amanda, for her love and support through the adventure that is graduate school. She has made the good time twice as good and the bad times only half as bad. I am sure I cannot have done this without her. I am forever indebted to her for her tolerance during our 15 months apart while I completed the work in this thesis. I know how extremely hard it was for her. It was certainly the most trying time of our relationship, and I am confident that together we can weather any storm the 'real world' will present. Thank you. I love you.

I would also like to thank my parents and brothers for their life-long support. My parents instilled in me strong values of hard work, integrity, and they gave me the confidence to always strive for excellence. My brothers have been wonderful role models both for how to work hard and how to play hard. I will forever look up to them.

I consider myself fortunate to have been able to work under the guidance of Prof. John Fourkas. His breadth of knowledge and creativity in problem solving are inspirational. Nearly all the clever ideas in this thesis were his, and I simply had the pleasure of turning them into a reality. While I would have preferred to stay at Boston College for personal reasons, I am glad I followed him to Maryland, and I am sure that the University of Maryland is very lucky to have him.

I would also like to acknowledge all the members of the Fourkas group that I had the pleasure to work with, particularly; Dr. Richard Farrer, Dr. Tommaso Baldacchinni, Juliet Znovena, and Linjie Li.

Dr. Richard Farrer was a pillar of strength and hard work in the laboratory. Absolutely any question I could think of, he had an answer to. I aspire to be half the teacher and researcher that he is.

Dr. Tommaso Baldacchini has been a great scientific mentor and friend to me. His passion for science, particularly chemistry, is unmatched, and is second only to his love of practical jokes. All of the work I describe in this thesis is extended from work he began when I joined the group. His curiosity to work with PDMS led directly to the contents of chapter 3. If not for him, this thesis would not exist.

Juliet Znovena and Linjie Li joined the group after me, and while they may think I taught them a lot, in fact it was I who learned more from the experience. They have been great colleagues and friends, and I am sure good work will continue to pour out of the Fourkas lab because of them.

TABLE OF CONTENTS

TABLE OF CONTENTS (CONT.)

TABLE OF CONTENTS (CONT.)

LIST OF TABLES

LIST OF FIGURES

LIST OF FIGURES (CONT.)

ABBREVIATIONS

AC	Autocorrelation
AFM	Atomic force microscopy
BME	2-methoxy-1,2-diphenylethanone
BSB-S_2	*bis*[(diarylamino)styryl] benzene with two dimethylsulfonium groups
DC	Direct current
DIDMA	N, N,-dimethyl-2,6-diisopropylaniline
GM	Goeppert-Mayer
GVD	Group velocity dispersion
HMDS	hexamethyldisilizane
ITX	2(4)-isopropylthioxanthone
LCVD	Laser chemical vapor deposition
LECD	Localized electrochemical deposition
LIGA	Lithographie, galvanoformung and abformung
MAM	Multiphoton absorption metallization
MA-μTM	Membrane-assisted microtransfer molding
MAP	Multiphoton absorption polymerization
μCP	Micro contact printing
MEMS	Microelectromechanical systems
MIMIC	Micromolding in capillaries
MPA	Multiphoton absorption
μTAS	Micro total analysis systems

ABBREVIATIONS (CONT.)

μTM	Microtransfer molding
NA	Numerical aperture
PAG	Photoacid generator
PDMS	Polydimethylsiloxane
PSF	Point-spread function
PVP	Polyvinylpyrrolidone
RLC	Resistor inductor capacitor circuit
SEM	Scanning electron microscope
STED	Stimulated emission depletion
TPA	Two-photon absorption
TPS	Triphenylsulfonium salt
XPS	X-ray photoelectron spectroscopy
YAG	Yttrium aluminum garnet

Chapter 1: Microscopic Patterning

1.1 Introduction

Technological developments in microscopic pattern generation have led to the current information revolution. State-of-the-art computer processors have been made with >1 billion transistors per chip and with individual features on the scale of tens of nanometers.[*] A comparable revolution is brewing for microtechnology of a different sort. What if all the benefits of microelectronic's speed, cost, and portability could be extended to mechanical, chemical, or biological systems? This is the basic premise for such ideas as 'labs-on-a-chip', microelectromechanical systems (MEMS), and micro-total analysis systems (μTAS). These concepts have been in the air for about two decades and are poised to make a leap in applicability in the near future.

Advances in microscopic pattern generation will be required for these technologies to come to full fruition. Thus far photolithography, the technique developed for making micro-circuitry, has been applied to create MEMS. Photolithography uses a mask to expose patterns in two dimensions. After development, these patterns can be etched, doped, or coated to create structures such as insulating layers, p- or n- doped regions, or conducting wires. The combination of these processes results in transistor logic switches, memory gates, amplifiers, filters and many other functional electronic components. The primary benefits of photolithography are its resolution, currently 30

[*] The dual-core Intel® Itanium® processor, code-named "Montecito," already uses 1.7 billion transistors. See www.intel.com for more information.

nm,[1] and its ability to create hundreds of chips, each with millions of features, in parallel. This batch fabrication enables highly complex devices to be produced at a low cost.

While photolithography has been tremendously successful, it suffers from several issues that prevent it from being used to full advantage in MEMS. One drawback is, "it poorly suited for introducing specific chemical functionalities; it is directly applicable to only a limited set of materials used as photoresists."[2] Such control is essential for chemical and biological applications. Another issue is the cost and facility requirements for photolithography, which are typically beyond the reach of most researchers. Finally, photolithography is an inherently two-dimensional technique. Patterns are duplicated from a 2-D mask, and while they can be stacked or released to create to layers in three dimensions, true 3-D fabrication simply cannot be done with photolithography.

The ability to fabricate in three dimensions is much more important for MEMS than it is for more conventional microelectronics. Circuits would stand to gain from increased component density if extended into three dimensions, but the performance of these circuits would remain essentially the same. Conversely, many MEMS or μTAS devices will require 3-D capability to function in the same manner as their larger-scale counterparts. Take, for instance, typical components of full scale electro-mechanical systems or analytical equipment, such as electromagnetic motors, combustion engines, diffraction optics, mixing vessels, pumps, valves, or separation columns. Some of these components can and have been made in two dimensions,[3,4] but their functionality may be compromised due to the limited dimensionality. However, if they could be made in three dimensions, but smaller than usual, they could function in a manner analogous to the corresponding macro-scale devices. Creating 3-D devices is possible with

photolithography although it generally requires sequential fabrication of many layers and accurate registration between them. This thesis will discuss and alternative fabrication technique that can fabricate complex 3-D microstructures in a single fabrication step.

1.2 3-D Pattern Generation

A number of techniques have been developed to generate microscale patterns in three dimensions. These methods fall into two categories, based on the ability to create either arbitrary or restricted 3-D features. A restricted patterning technique may not be able to create undercut or free-moving features. Another example of a restricted 3-D patterning technique is one that can only make periodic patterns. Restricted patterning techniques include X-ray lithography, soft lithography, self-assembly, layer-by-layer assembly, and holographic photopolymerization. Direct-write technologies, such as stylus- or laser- based techniques, enable arbitrary pattern formation.

1.2.1 Restricted 3-D Techniques

One of the first attempts to extend fabrication into the third dimension was a process known as LIGA, which was invented in the early 1980s. LIGA is a German acronym for X-ray lithography (X-ray **li**thographie), electroplating (**g**alvanoformung), and molding (**a**bformung). As its name implies, LIGA uses X-rays to create patterns.[5] The synchrotron-generated X-rays have small divergence angles due to their extremely short wavelength, which allows for micrometer-resolution patterning in photoresists with depths exceeding 1 cm. The result is high-aspect-ratio patterns, such as channels and gears, which can be used as molds to electrodeposit metals such as nickel. The metal

pattern can be used as is, or the shape can be inverted again by using the metal pattern as a mold for polymeric parts. Structures made by LIGA have good surface smoothness and sharp vertical features, but are of limited 3-D complexity because of the line-of-sight nature of the X-ray exposure. Undercut structures can be produced by stacking layers or by exposing the resist and an angle. Complex structures have been demonstrated, but their application has not been widespread, despite the maturity of the technique, likely because of the availability of synchrotron radiation sources and X-ray masks.

Another technique capable of producing restricted 3-D features is soft lithography, a class of techniques that includes micro-contact printing (μCP) and micromolding.[2] Soft lithography uses photolithography or electron-beam lithography to generate patterns that are then molded by an elastomer, typically polydimethylsiloxane (PDMS), to create a stamp. For micromolding, this stamp can be used to duplicate 3-D structures with tens of nanometer resolution[6] and with restrictions on geometry. Methods will be discussed in chapter 3 that overcome most of these topological limitations. For μCP, the PDMS stamp is used to transfer the pattern to any number of substrates using a variety of 'inks'. One typical example is the μCP of an alkanethiol ink placed in contact with a gold surface. The alkanethiol forms a self-assembled monolayer on the gold, making that region hydrophobic. Aqueous etching solutions can then be applied to pattern the gold with ~100 nm resolution. This technique offers greater control of surface chemistry than does conventional photolithography, and is cheaper and easier. μCP can also be applied to non-planar surfaces; however, if the first step is photolithography, μCP cannot be used to create truly 3-D structures. Soft lithography is the most popular 'unconventional' lithography because of its low cost, great convenience, and broad

chemical capability; however, it has severely limited 3-D freedom because the starting point is usually photolithography.

Self-assembly has the capability of creating arbitrarily complex 3-D patterns, as demonstrated by biological systems; however, this degree of 3-D complexity on the micron- or submicron-scale is currently beyond the reach of science.[7-10] What is possible is the fabrication of periodic structures from materials such as colloids or block copolymers. Colloidal solutions can be dried carefully to yield close-packed crystals.[11] Block copolymers, consisting of polymeric units such as …AAABBBAAABBB… can microphase separate, due to differences in hydophobicity between the A and B subunits, to yield 3-D patterns. Block copolymers thus offer attractive ways to make useful devices such as photonic crystals.[12] However, without arbitrary control, these techniques cannot be used to create more complex systems.

Layer-by-layer assembly has been demonstrated to create 3-D patterns from 2-D substructures made using photolithography or soft lithography. This technique is also useful for creating photonic crystals and other periodic structures, but geometric constraints prevent the creation of arbitrary 3-D shapes.[13] Another problem is that each layer has to be registered correctly to the existing shape, which is not trivial.

Holographic fabrication generates periodic patterns in three dimensions using the interference properties of coherent laser light. By intersecting multiple laser beams in a photoresist, a 3-D light intensity distribution is generated that consists of constructive and destructive interference regions. This pattern induces photochemistry that can be used to develop the pattern into a 3-D lattice structure.[14] Like the previously mentioned techniques, this is only applicable for periodic geometries.

1.2.2 Arbitrary 3-D Patterns

Direct-write technologies are the second class of 3-D techniques, and are the only ones to offer true 3-D freedom. Direct-write refers to methods involving moving a pattern-generating source, such as an ink-delivery nozzle or a laser focal point, in three dimensions with respect to a substrate in a way that is analogous to writing in two dimensions.

Ink-based writing can be performed by either drop-based or filament-based techniques that are referred to as ink-jet printing and robotic deposition, respectively. A nozzle can deliver inks made of colloids, polymers, or polyelectrolytes, whose rheological properties can be tailored for the particular deposition technique. Structures can span a range of sizes, from small structures with individual features having micron scale resolution to larger structures made of ~100-μm-wide lines.[15] While 3-D control is offered in principle, in practice the inks are not rigid enough to create structures with completely arbitrary geometries.[16-19] For example, lattice type scaffolds have been demonstrated, but without compact structural support individual lines will not remain freestanding.

The other adaptation of direct-writing, using a laser focal point, does allow for true 3-D control. This method has been used in a technique called microstereolithography (μSL);[20] larger-scale versions also go by the name of rapid prototyping or 3-D printing. The basic idea is simple: a laser is focused onto the surface of a liquid prepolymer resin, photochemically inducing cross-linking. After scanning the desired 2-D pattern, additional resin is added to create a new surface layer, and the process is repeated. The liquid resin is removed after fabrication, yielding a 3-D

microstructure. The feature size is determined by the thickness of the added layer and the size of the laser focal spot. Features that are submicron in all three dimensions have been demonstrated.[21] One issue with this technique is the speed with which layers can be added. Generally, the resin has a low viscosity, but it may still take nearly one minute to reflow an additional layer.[20]

An alternative technique, recently developed, eliminates the need to reflow the resin by focusing directly inside the sample and polymerizing only at the focal point.[22, 23] This local polymerization is made possible through multiphoton absorption, and the process has been named multiphoton absorption polymerization (MAP).[†] MAP has a

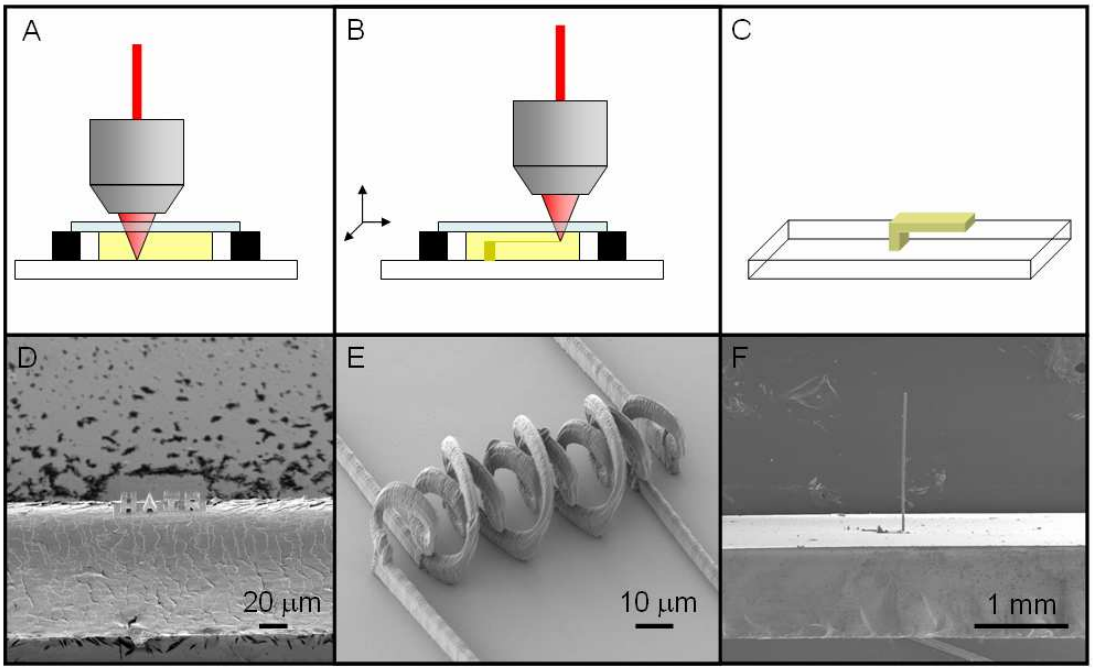

Figure 1.1 A) In step 1 of MAP, a laser is focused inside a prepolymer resin. B) In step 2, the focal point is scanned in a 3-D pattern creating the desired part. C) In step 3, the unpolymerized resin is washed away in solvent, leaving the freestanding part. D) An example of a MAP microstructure of the word 'HAIR' created on a human hair.[35] E) A coil within a coil (unpublished). F) Side view of a tower with dimensions 20 μm × 20 μm × 1.5 mm.[35]

[†] This process has also been called 3-dimensional lithography (3DLM), two-photon induced polymerization (TPIP), and two-photon polymerization (TPP or 2PP) in the literature.

higher resolution than μSL and employs a simpler experimental setup. The setup will be described in detail in the next chapter, but briefly MAP is performed in 3 steps: 1) focus an ultrafast laser into a drop of resin; 2) move the focus relative to the resin in X, Y, and Z to fabricate the desired pattern; and 3) rinse in a solvent to remove the unpolymerized resin. Some examples of MAP microstructures are shown in Figure 1.1.

1.3 Multiphoton Absorption

At the heart of MAP is the nonlinear optical process of multiphoton absorption (MPA). First predicted in 1931 by the Nobel laureate physicist Marie Goeppert-Mayer in her doctoral dissertation,[‡24] the process was not verified experimentally until the advent of the laser.[25] An intuitive explanation of MPA is that the transition from the ground electronic state to an excited electronic state that is usually achieved by the absorption of one high-energy photon is instead reached by simultaneous absorption of multiple low-energy photons. The most common implementation of this is degenerate two-photon absorption (TPA), where both photons have the same energy.

A more accurate physical picture is obtained using a quantum mechanical treatment of MPA that can be derived with perturbation theory.[26,27] Using the time-dependent Schrödinger equation and a Hamiltonian that contains the vector light field, E_γ, and the position vector, r, solutions can be obtained for single- or multiple- photon interactions. The first-order solution corresponds to the one photon case, the second-order to the two-photon case, etc. The transition probability for TPA between a final |f> and initial |i> state is given by:

[‡] While Prof. Goeppert-Mayer is well known for her early work on the multiple quanta events, her 1963 Nobel prize was earned for explaining the stability of 'magic number' nuclei.

$$P \approx \left| \sum_m \frac{\langle f | \vec{E}_\gamma \cdot \vec{r} | m \rangle \langle m | \vec{E}_\gamma \cdot \vec{r} | i \rangle}{\varepsilon_\gamma - \varepsilon_m} \right|^2 , \qquad \text{(eqn. 1.1)}$$

where ε_γ is the energy of the light field E_γ and ε_m is the difference in energy between the ground state and the virtual state *m*. A virtual state is unique to quantum mechanics and can be thought of as a transient state between stable states. The lifetime of a virtual state is extremely short, ~1 femtosecond, and defines how 'simultaneous' photons need to be in order to interact. Equation 1.1 reveals why TPA is spatially localized: its probability is proportional to the light intensity squared, I^2, or more generally I^n for *n* photons.

This localization was first utilized by Denk *et al*. in two-photon fluorescence microscopy.[28] In two-photon fluorescence microscopy an excitation wavelength is used that is approximately double the peak absorption wavelength of a given fluorophore. TPA occurs at the focal point, resulting in fluorescence that is then imaged. What is fundamental for two-photon fluorescence microscopy and for MAP is that excitation occurs only within the focal volume. This is shown in Figure 1.2, where the total one-photon and two-photon absorption per transverse section of a focused laser beam are plotted as a function of axial position. Because the transition rate of two-photon absorption is proportional to the light intensity squared, a maximum occurs at the focal point.[29]

Since the seminal work of Denk *et al*; hundreds of groups worldwide have used multiphoton absorption for fluorescence imaging, 3-D data storage, photodynamic therapy, and microfabrication. In almost all applications MPA uses pulsed laser light and strongly focusing lenses, e.g. high numerical aperture (NA) objectives, to create the necessary photon density for nonlinear absorption. Denk *et al*. showed that for such a

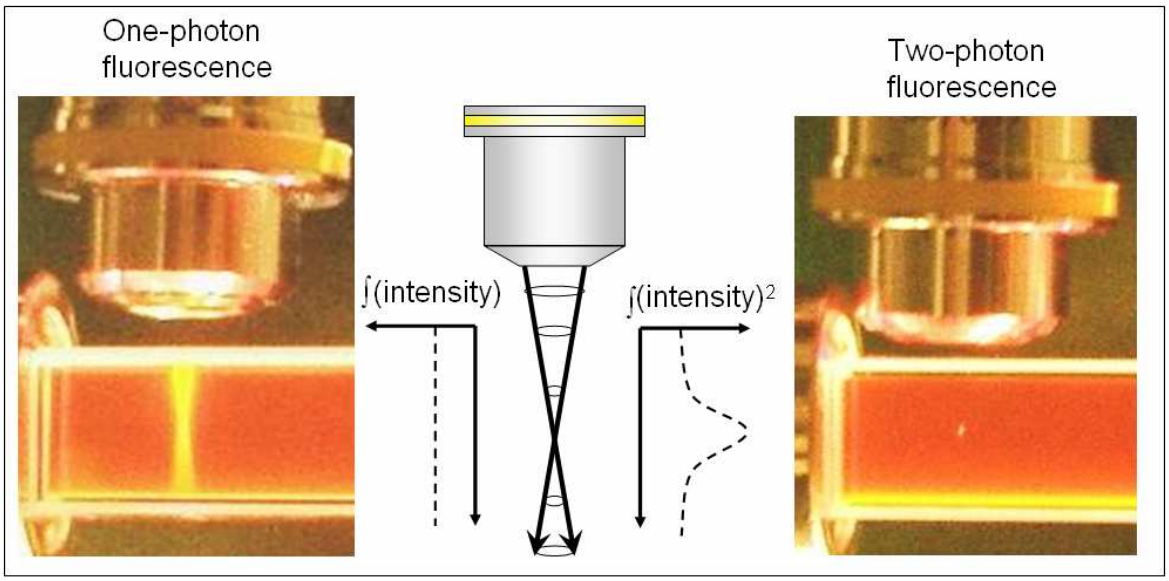

Figure 1.2 Fluorescence from a solution of Rhodamine B caused by single-photon excitation from a UV lamp (left) and by two-photon excitation from a mode-locked Ti:sapphire operating at a wavelength of 800 nm (right). The integrated intensity in each transverse section of the beam does not depend upon position for single-photon excitation, but is tightly peaked in the focal region for two-photon excitation.

system with pulse duration τ and pulse repetition rate f_p, the number of photons absorbed per molecule per pulse, n_a, is proportional to

$$n_a \approx \frac{p_0^2 \delta}{\tau \, f_p^2} \left(\frac{(NA)^2}{2\hbar c \lambda} \right)^2 , \qquad \text{(eqn 1.2)}$$

where p_0 is the time-averaged laser power, λ is the excitation wavelength, and δ is two-photon absorption cross-section. The units for δ are named Goeppert-Mayer (GM) and defined as 1 GM = 10^{-58} m^4 s photon. As an example, δ for the good two-photon-absorbing fluorophore fluorescein is 38 GM.[27]

1.4 MAP in the Literature

For MAP the spatial confinement of excitation is used to induce a chemical reaction only at the laser focal point. This polymerization reaction can take place by

either of two reaction mechanisms, radical or cationic, depending on the photoinitiator and monomer being used.

1.4.1 Radical Polymerization

Upon excitation, a radical photoinitiator can either cleave homolytically or transfer its energy to a coinitiator to begin the reaction. The two types of photoinitiator are classified as Type I and II, respectively.[30] There exist a number of commercially-available Type I initiators, most of which are aromatic carbonyl compounds. The photolysis of these molecules usually occurs by homolytic α-cleavage.

A number of groups have demonstrated the use of Type I initiators for MAP. The most commonly used Type I photoinitiator is found in a commercial resin called JSR500 (Japanese Rubber Company). JSR500 contains two of the Type I radical initiators shown in Figure 1.3, which are available under commercial names of Irgacure 369 and Iragcure 184.[31] The polymerization reaction is started from the benzoyl radicals created by photolysis of these molecules, and continues until two chain termini couple with one another or until radicals are quenched by inhibitors, such as molecular oxygen. The reacting species are urethane acrylate oligomers (MW 400 and 1200 g/mol) and monomers. The δ for these molecules is relatively low, ~20 GM, but MAP is still possible using a Ti:sapphire oscillator with average powers in the milliwatt range.

Another Type I photoinitiator, which has been used extensively by the Fourkas group, is Lucirin TPO-L.[32-35] This photoinitiator has a low δ, likely around 1 GM, but works quite well for MAP. Upon photoexcitation Lucirin TPO-L homolytically cleaves, leaving a carbonyl radical and a phosphinoyl radical. While both are reactive, the phosphinoyl radical is tetrahedral in shape and is therefore sterically more reactive. This is important because despite its low δ, Lucirin TPO-L is still a highly efficient photoinitiator. It should also be noted that Lucirin TPO-L is a liquid at room temperature, making it easy to mix with monomers, which are often viscous. We have demonstrated MAP of a wide range of acrylate and methacrylate resins with this initiator

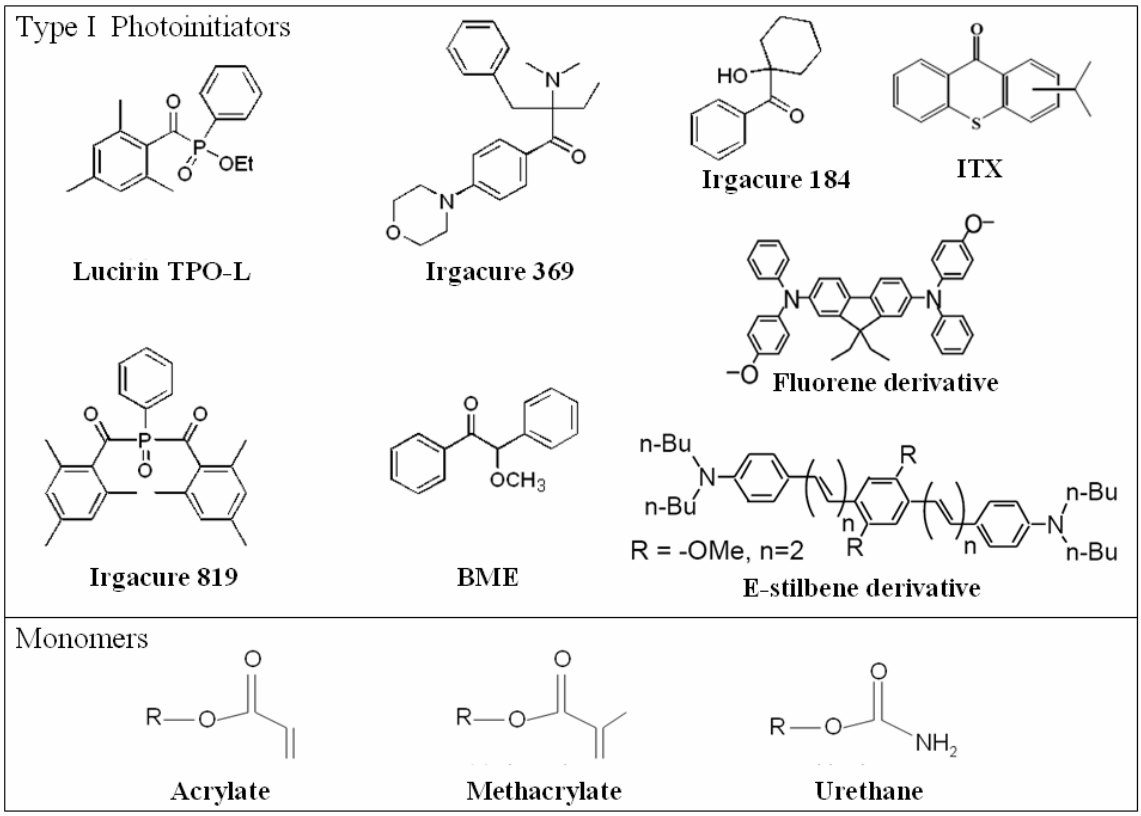

Figure 1.3 Type I photoinitiators used in MAP and typical monomer components

using low average power from a Ti:sapphire oscillator.

Other commercially available photoinitiators that have been used for MAP are shown in Figure 1.3 and include Irgacure 819 (bis(2,4,6-trimethylbenzoyl)phenylphosphine oxide), BME (2-methoxy-1,2-diphenylethanone), and ITX (2(4)-isopropylthioxanthone).[36]

Several groups have chosen to synthesize custom photoinitiators and optimize them for TPA. Such photoinitiators have enabled the use of lower fabrication powers and less sophisticated, less expensive laser systems. These engineered molecules can also be used for other applications that take advantage of TPA such as optical data storage, optical limiting, photodynamic therapy, and two-photon imaging. Work in this field centers on molecules that are composed of a conjugated central region flanked on either side by electron donating (D) or accepting groups (A). The various core moieties that have been used in MAP include E-stilbene, bis(stryl)benzene,[22,37,38] naphthalene,[39] biphenyl,[40] and fluorene.[41]

Marder, Perry and coworkers have done extensive work with the E-stilbene and bis(stryl)benzene systems by symmetrically altering the strength and positions of electron donating and accepting groups. Configurations such as D-π-D, D-π-A-π-D, and A-π-D-π-A have been tested (π represents a conjugated bridge) and molecules with δ as high as 1250 GM have been made. Studies show that symmetric charge transfer from the molecular center to the ends, or vice versa, is responsible for a high δ. Extending the conjugation length increases δ, as does increasing the electron donating/accepting strength. A side effect of these changes is a shift of the TPA wavelength peak, which red-shifts with increasing conjugation length. This shift could allow a molecule to be

optimized for different excitation wavelengths, but for the most common and simplest case of 800 nm excitation it may also mean inefficient pumping. After the molecule has been excited by TPA it is thought to undergo electron transfer to an acrylate monomer/oligomer, initiating the polymerization reaction. The molecule 4,4'bis(N,N-di-n-butylamino)-E-stilbene has been used for MAP at powers as low as a few hundred microwatts using a Ti:sapphire oscillator, thanks to its high δ value of 1,250 GM.

Andraud and coworkers have used a substituted fluorene system to initiate MAP, but have achieved this with a cheaper, smaller light source by using a Nd-YAG Nanolase microlaser operating at 532 nm.[40, 42] The aminobiphenyl substituted fluorene is of the D-π-D type and has a δ value of 80 GM at 532 nm. Acrylate monomers have been polymerized using 532 nm light with an average power of around 1 mW (0.5 ns pulses at repetition rate of 6.5 kHz). This was the first demonstration of MAP using a non-ultrafast laser.

The resins described above consist primarily of acrylates, which have a number of properties that are useful for MAP. Acrylates are used extensively in industry and so are commercially available with an assortment of functionalities, sizes, and compositions. They are generally safe and are easily processed by spin-coating or drop casting. The unreacted resins are soluble in common solvents such as ethanol. Using tri-, or tetra-functional acrylates results in polymeric solids that are highly cross-linked and are able to withstand the development step after fabrication. Perhaps the most important quality is the speed at which acrylates polymerize, because it enables the use of fast laser scanning speeds during MAP. All of these qualities explain the widespread use of acrylates and their derivatives, urethane acrylates and methacrylates, in radical polymerization.

Unlike type I photoinitiators, type II photoinitiators are used with a coinitiator, which is generally a bulky tertiary amine. This reaction takes place when the excited photoinitiator forms an exciplex and abstracts an α-hydrogen from the amine, followed by electron transfer.

Several groups have used type II photoinitiators for MAP, because they can have a high δ value and are commercially available. Campagnola, Pitts and coworkers have shown the use of a xanthene based chromophore, Rose Bengal, along with triethanolamine as a coinitiator, for the radical polymerization of acrylates, acrylamides, and several biopolymers.[43] Rose Bengal has a δ of about 10 GM at 800 nm and requires ~100 mW of Ti:sapphire light to make sustainable structures.

Belfield and coworkers have used a commercial fluorone dye, H-NU 470, along with an arylamine, N, N,-dimethyl-2,6-diisopropylaniline (DIDMA), for type II radical polymerization of acrylates and methacrylates.[36] Also Li *et al.* have reported the use of 7-diethylamino-3-(2'benzimidazolyl) coumarin with a coinitiator of diphenyliodonium hexafluorophosphate and showed <1 mW fabrication powers from a Ti:sapphire oscillator.[44]

In summary, the photoinitiators used for radical MAP vary from small molecules to large conjugated molecules in binary systems. A number of groups have reported the successful application of radical MAP using a variety of resins, homemade and commercial, and different excitation sources. Custom photoinitiators have been designed by several groups and have been shown to be effective both for low threshold powers and for the ability to use less expensive laser systems. While the benefits of custom initiators are clear, their availability is limited. Commercial resins or resins made of commercial

components have the benefit of accessibility but suffer from a slightly higher power threshold for fabrication. However, for all of the laser systems used, the threshold for these resins is always well below the available power and therefore their use is completely practical.

1.4.2 Cationic Polymerization

A cationic photoinitiator works by generating a strong Brønsted acid that is capable of polymerizing epoxides or vinyl ether monomers.[30] The generated photoacid is catalytic and can begin many polymerization reactions. Because these monomers react by a different mechanism, they are not subject to quenching by singlet oxygen, as are radical initiated polymers.

Epon SU-8 is the most widely used epoxy polymerized by MAP.[45-47] SU-8 has eight epoxy groups per monomer and contains a triphenylsulfonium salt (TPS) photoacid generator (PAG). SU-8 is used extensively in conventional photolithography for making MEMS because of its ability to make high-aspect-ratio structures. This ability is due in part to the thickness of the films that can be cast (up to 500 μm). The availability and well-documented use of SU-8 make it a convenient choice as a cationic resin; however, extra processing steps, such as a pre- and post-bake, are required. Teh *et al.* have performed extensive studies of MAP with SU-8.[45, 46] Using a low-NA objective, high-aspect-ratio structures (50:1) could be made with about 1.0 nJ/pulse energies. Wegener and coworkers have demonstrated the use of SU-8 for the fabrication of a functional photonic crystal at telecommunications wavelengths.[48] This photonic crystal required

large side walls for support against shrinkage. SU-8 is known to shrink about 7.5% upon crosslinking.[49]

Two commercial PAGs have been combined with monomers to make custom resins for MAP. These are diaryliodonium (CD1012) and triphenylsulfonium (TPS) salts and they can be used alone or with a photosensitizer. Belfield and coworkers used these salts, individually, to polymerize cycloaliphatic diepoxides.[36] While the δ is $\leq$10 GM, they are still able polymerize structures with modest average powers and speeds.

Two groups have also reported the use of homemade PAGs. Ober and coworkers used the coumarin/iodonium salt, because of its high two-photon sensitivity. Marder, Perry and coworkers adapted their high δ molecules with the bis(styryl)benzene core to become PAGs by changing the pendant groups to contain sulfonium moieties. This molecule, label BSB-S_2, has a δ of 690 GM and is more than ten times more sensitive than commercial cationic photoinitiators.[50-52] BSB-S_2 is shown in Figure 1.4.

The PAGs used for cationic polymerization can also be used in positive-tone photoresists. This promises to be an extremely useful way to fabricate 3-D microfluidic devices. Perry and coworkers have shown that the photoacid can induce an ester-cleavage reaction in a solid polymer.[50] The newly formed polar groups make the volume in which they are present soluble in an aqueous base developer. Channels 4 μm × 4 μm in cross-section have been made 10 μm below a surface with a mere 40 μW of average power from a Ti:sapphire oscillator.

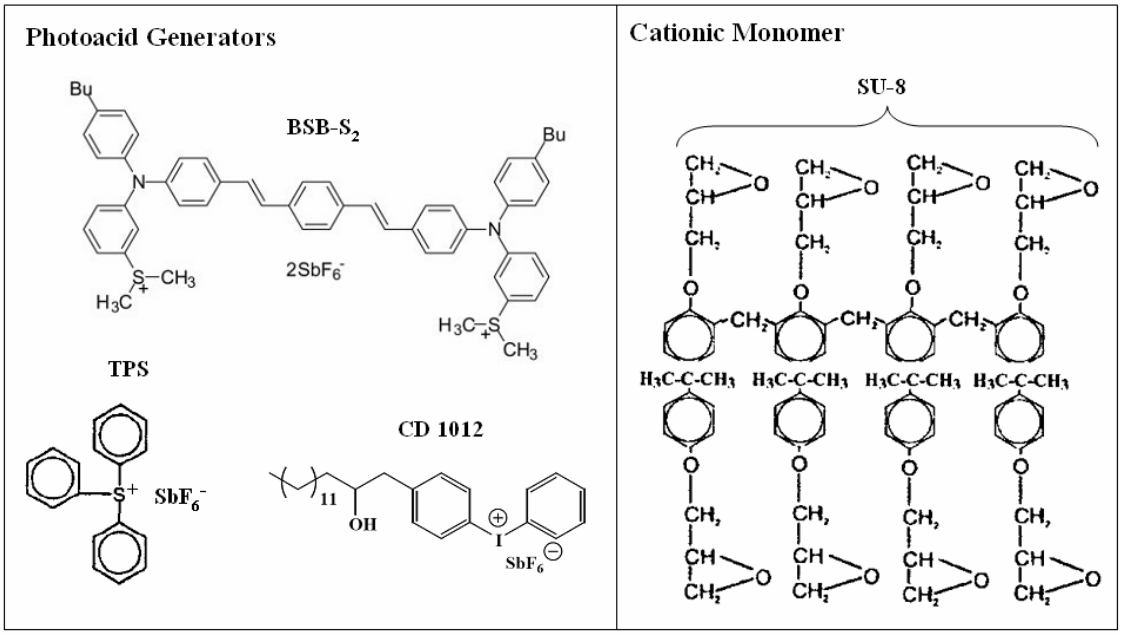

Figure 1.4 Chemical structure of three PAGs; *bis*[(diarylamino)styryl] benzene with two dimethylsulfonium groups (BSB-S_2), triphenylsulfonium hexafluoroantimonate (TPS), and [4-[2-(hydroxytetradecyl)oxy]phenyl] phenyliodonium hexafluoroantimonate (CD1012). The monomer structure of SU-8 is shown on the right. Note the eight epoxy rings per monomer.

1.5 Resolution of MAP

Due to a combination of optical and chemical nonlinearity, MAP can achieve resolution that is considerably better than that predicted by the diffraction limit. The smallest individual voxel thus far reported using 800-nm excitation was 100 nm in diameter.[53] Suspended lines with waists as small as 30 nm in one dimension have also been fabricated in SU-8, although this kind of resolution has not yet been achieved for more complex structures.[54] Voxels are generally ellipsoidal, and the two minor axes perpendicular to the optical axis are about 3-5 times smaller than the major axis.[55] This shape is determined in part by the point-spread function (PSF) of the light intensity near the focus.

The probability for TPA is proportional to I^2, which effectively narrows the PSF of the beam near the focal point so that it is smaller than the diffraction limit at the excitation wavelength. However, this narrowing alone is not sufficient to explain the decrease in voxel size that is observed experimentally.[56] In fact, voxels of comparable size have also been fabricated using single-photon absorption.[21] The real benefit of the optical nonlinearity of TPA lies in the negligible absorption away from the focal point. Photoinitiator concentrations can be employed that are approximately ten times higher than would be feasible for single-photon excitation without any fear of out-of-plane polymerization.

Chemical nonlinearity is also an important factor in the creation of voxels that are smaller than the diffraction limit. Due to quenching processes, there exists a threshold intensity below which the polymerization reaction cannot be sustained to create a solid structure. By careful control of the laser intensity, this threshold can be exceeded only in only a small fraction of the focal volume. For instance, a beam that is focused to a 400-nm diffraction-limited spot may exceed the intensity threshold only in a 100-nm region in the center of the spot.

1.6 Thesis Outline

MAP has been demonstrated by a number of groups and is a promising technology, but comparing MAP to other techniques that make 3-D microdevices reveals that MAP has several issues that prevent its widespread use. One issue is the novelty of the system itself. This issue will be described in detail in the next chapter, because scientists and engineers interested in microdevices are not necessarily familiar with the

intricacies of ultrafast lasers. Since no commercial all-in-one system is yet available to fabricate by MAP, the systems so far reported are all homemade. This has limited the use of MAP to specialists, but only for technical reasons. As lasers become smaller and cheaper and piezo-driven stages become more prevalent, MAP systems will become accessible to a wide variety of scientists. In chapter 2, details of how a system should be assembled and used will be described.

Another issue with MAP is that it is a slow serial process. Not only must parts be made one at a time, but each part is made one point at a time. Two groups have made progress in addressing this problem. Kawata and coworkers have demonstrated the ability to fabricate with multiple focal spots simultaneously. We have used soft lithographic techniques to mold and replicate microstructures made by MAP. The latter work will be the subject of chapter 3.

The chemistry available for MAP also poses a restriction. For example, the systems described already have been confined to the synthetic organic polymers, such as acrylates, methacrylates, epoxies, or urethanes. There has been little work on adding electrical functionality or biological compatibility to MAP systems. Chapter 4 will describe efforts to modify the surface chemistry of polymeric microstructures, enabling the incorporation of an assortment of functionality.

Applications of functional microstructures, specifically, the electrical applications of metal coated polymeric microstructures, will be summarized in chapter 5. Devices such as a microinductor and a circuit for the detection of gold plasmon absorption have been made by MAP. A brief description of devices made by other groups, such as

photonic crystals, will be discussed. Finally some of the many potential future applications of MAP from micro-NMR to nanophotonics will be discussed.

Chapter 2: Experimental Setup and Techniques

2.1 Introduction

MAP was first demonstrated over 15 years ago,[57] yet a survey of recent publications shows that groups still differ on how to assemble the fabrication system for optimal performance.[22,35,40,57-59] In this chapter the various components necessary for a MAP system will be analyzed. The configuration for a basic working system will be shown and additional features to make it more powerful will be explained. Five subsystems are required in order to fabricate by multiphoton absorption: a laser, a microscope, a sample, a device to move the beam with respect to the sample (or vice versa), and software to control the motion. For each subsystem there exist many choices that will be compared and contrasted. Also, an explanation of the software we use will be given and some of its time saving features highlighted.

Finally, specific methods of fabrication, rarely reported in the literature, will be explained. For instance, the logic for choosing a particular scanning pattern for a given 3-D shape will be spelled out. These techniques have been learned through experience and the reasoning behind them sheds light on the properties of polymeric microstructures.

2.2 The Laser

The laser most commonly used for MAP is a Ti:sapphire oscillator, although a few alternatives have also been reported. The Ti:sapphire oscillator offers sub-100 fs pulses with hundreds of milliwatts of average power from modestly priced ($100k

including pump laser) commercial systems. These systems can vary from turnkey operation to kit assembly, and span a broad window of output powers and pulse durations. One especially nice feature of the Ti:sapphire laser is the potential tuning range from 650 – 1100 nm.[60] More advanced systems, such as a regeneratively amplified Ti:sapphire have also been used for MAP; however, the level of intensity available from such lasers is not necessary unless the beam is divided for parallel fabrication.

Simpler lasers, such as an Erbium doped fiber laser, have also been used.[61] An Erbium laser outputs at a wavelength of 1550 nm with ~100 fs pulses and can be frequency doubled to 780 nm with tens of milliwatts of average power. These lasers are more compact and less expensive than Ti:sapphires.

A diode-pumped, frequency doubled, Q-switched Nd:YAG laser has also been used to fabricate by MAP.[40,62] This laser has a footprint of a mere 4 cm × 15 cm and costs less then $6,000. This laser operates at a wavelength of 532 nm and can generate 3.5 μJ pulses at 6.5 kHz for an average power of ~20 mW. At 600 ps, pulses are long compared to those from a Ti:sapphire laser, but are still intense enough for multiphoton absorption to occur. Clearly, this is the most cost-effective option, but it offers the least control over the available power, wavelengths, and pulse duration.

Getting the laser beam to the microscope can also vary from simple to complex. Two scenarios are sketched in Figure 2.1. The simple case consists of steering mirrors, a beam expanding telescope/spatial filter, a half-wave plate/polarizer, and a shutter. The spatial filter is critical to ensure that a clean $TEM_{0,0}$ mode enters the microscope and overfills the back aperture. Overfilling the back aperture provides a more uniform wavefront to take full advantage of the numerical aperture (NA) and focusing power of

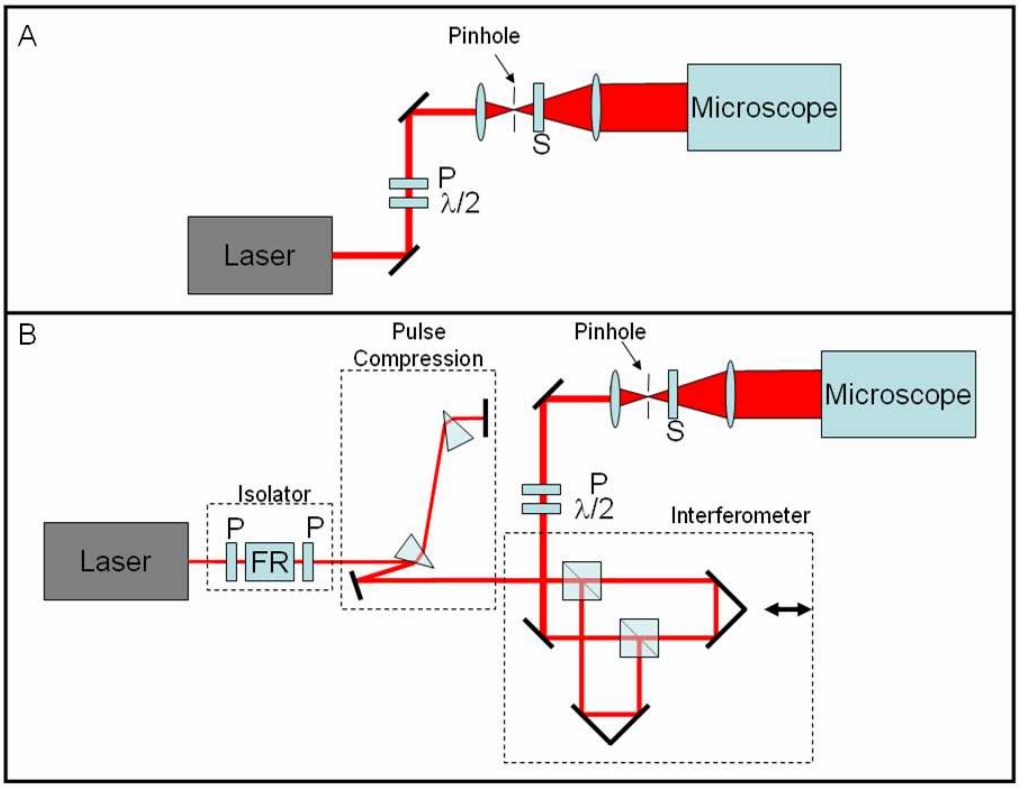

Figure 2.1 A) A simple MAP setup consisting of a laser, polarizer (P), a half-wave plate (λ/2), a spatial filter and a shutter (S). B) A more complex MAP setup for ultrafast lasers with an optical isolator based on a Faraday rotator (FR), a pulse compressing prism arrangement, and an interferometer for autocorrelation measurements.

the objective lens. The half-wave plate/polarizer is used to adjust the average power, and the shutter is used to control exposure of the sample.

The more complex setup (Figure 2.1B) includes three additional components that improve the performance of ultrafast systems. The first component is an optical isolator that consists of a polarizer – Faraday rotator – polarizer combination. This isolator prevents back-reflections from going into the laser cavity and disrupting the modelock.

The next component is an arrangement of prisms for pulse compression. Arranged in this way, negative group velocity dispersion (GVD) can be achieved, which is used to eliminate chirp and to ensure transform-limited pulses at the sample. Normal or positive GVD occurs when spectrally-broadband light passes through glass and the

shorter wavelengths travel more slowly than longer wavelengths, causing the pulse to spread out in time. This dispersion imparts chirp in the pulse, which means that different frequency components are present at different times. Pulses with duration less than 100 fs are highly susceptible to pulse broadening due to dispersion.

The third additional component in this setup is a novel in-line autocorrelator. An autocorrelator (AC) measures the temporal width of a laser pulse. By dividing a beam into two pieces and then recombining them with a known time delay, a signal can be obtained that is proportional to the time gap. Scanning the time delay enables the pulse duration to be measured. To obtain the signal proportional to the beam overlap (in time), a nonlinear process, such as second harmonic generation, is employed. The signal can be interferometric if the beams are collinear. If the beams instead meet at an angle, their interference pattern will produce fringes that average out to give a smooth curve known as an intensity autocorrelation. Most ACs use a second-harmonic crystal and detect the second-harmonic generated from the mixing of the two beams. However, this method makes pulse measurement after a high-NA lens difficult, because the working distance is too small for a doubling crystal and a detector to fit on a microscope stage. Recently, a new technique has eliminated the need for a doubling crystal and a detector by instead using a solid-state detector with a bandgap greater than the fundamental frequency of the light. These detectors are insensitive to the fundamental frequency but exhibit second-harmonic generation and/or two-photon absorption within the semiconducting crystal. An AC signal can therefore be obtained by simply focusing an ultrafast beam onto a photodiode detector and scanning the interferometer. One detector with this capability is made from GaAsP.[63] It has been shown to detect near-infrared light by both the second

harmonic generation and two-photon absorption.[64] This detector has been used after a 1.4 NA objective lens and has measured pulse widths as short as 6 fs.[65,66]

The generic AC described above consists of an interferometer that enables the pulse width to be measured after the microscope objective at the position of the sample. However, when actually fabricating by MAP one does not want an interferometer in the beam path because tiny sub-micron motion of the mirrors can cause dramatic fluctuations in the light intensity due to interference. Of course, one arm of the interferometer could be blocked, but then 75% of the power would be lost. A more elegant solution is to divide the beam by polarization; this is sketched in Figure 2.2A. Using polarizing beamsplitting cubes and a half-wave plate before the interferometer, the power in each leg can be adjusted arbitrarily without changing the path of either beam. Thus, the legs can be of equal intensity for the AC measurement and then the polarization can be adjusted to send all the light into only one leg of the interferometer for fabrication. Also, since the polarization of the combined beams is orthogonal, the beams should not interfere and should therefore give an intensity AC from which it is easy to measure the pulse width. In practice, the GaAsP diode is an anisotropic crystal and exhibits second-order interference between the cross-polarized beams. However, the interference can be eliminated by bringing the beams together at an angle, as is done for intensity autocorrelations. Figure 2.2B shows the reduction in interference as the beams are combined at a greater and greater angle. The number of fringes in the plot refers to the visible fringes present if a polarizer is used to make the two beams the same polarization, and the greater the number of fringes the greater the angle between the beams. The AC shown in Figure 2.2A enables ultrafast pulses to be measured at the sample position of a

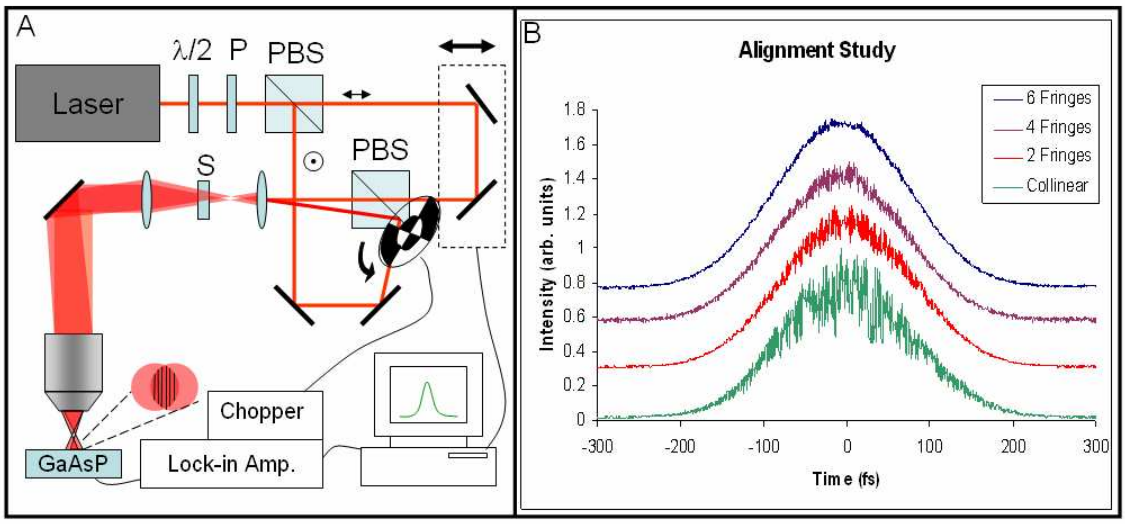

Figure 2.2 A) In-line autocorrelator. λ/2 is a half-wave plate, P is a polarizer, PBS is a polarizing beamsplitter, S is a shutter. The beams are brought together at a slight angle to create a fringe pattern on the detector. B) The autocorrelation signal as a function of alignment. When the beams are collinear an interference pattern can be seen that becomes weaker and weaker as the number of fringes increases. The top curve is obtained when the angle between the beams is approximately 1 mrad.

microscope and can be simply adjusted to 'turn off' the interferometer portion enabling it to be used 'in-line' that is, without altering the measured beam path in any way.

This in-line autocorrelator has the additional benefit of being easily converted to a cross-correlator. A cross-correlator measures a signal that is proportional to the time delay between pulses from two lasers. It works in exactly the same way as an AC except the combined beams originate from different sources. Figure 2.3 shows an arrangement that uses kinematic mounts with a fixed base plate but exchangeable top plates, allowing the in-line autocorrelator to autocorrelate either of two ultrafast lasers or to cross-correlate them. One requirement to cross-correlate two ultrafast lasers is that they operate at the same repetition rate (pulses/s) and with a fixed phase difference, which can be achieved through a commercial system such as a Synchro-Lock (Coherent). Such a system could be used for a number of different applications, such as dual-color pump-

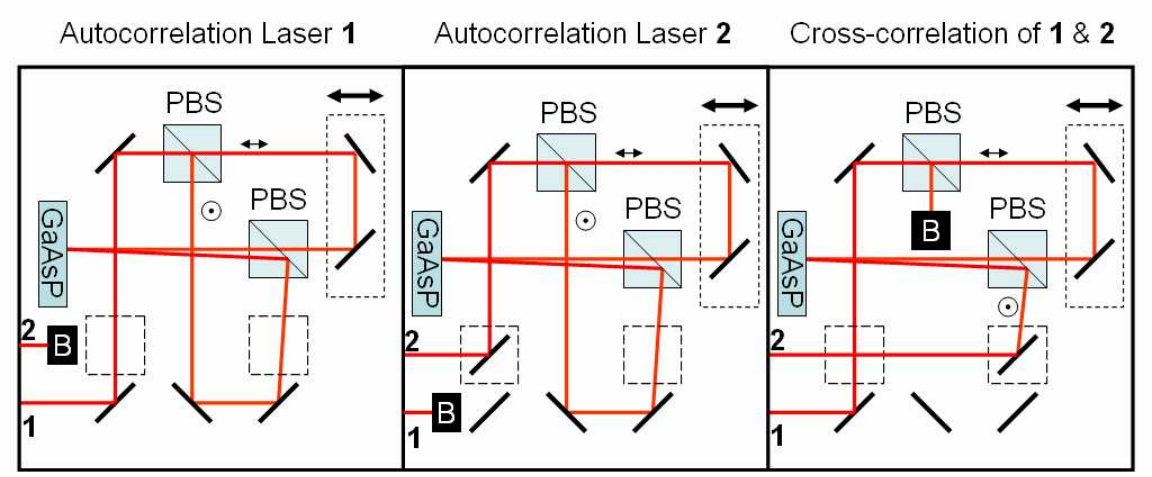

Figure 2.3 Using kinematic mounts (dashed-line squares), the in-line autocorrelator can be quickly modified to autocorrelate a second laser or to cross-correlate two lasers. 'B' is a beam block.

probe experiments, stimulated emission depletion (STED) microscopy, or STED MAP. This last application will be described in chapter 5.

2.3 The Microscope

A microscope is used in MAP both to focus the beam for fabrication and to generate an image to view the process in real time. At the heart of the microscope is the objective lens. The image it creates can be viewed either through oculars or on a television connected to a CCD camera. A short pass (i.e. blue) filter should be used to prevent reflected laser light from entering the oculars or the CCD camera.

The other important aspect of imaging is illumination of the sample. This is usually done by focusing light through a condensing lens and transmitting it through the sample. It should be noted that a long-pass (i.e. yellow) filter is necessary to prevent unintended photopolymerization of the sample. However, it is also possible to view an opaque sample by sending the illumination through the imaging objective. In this arrangement, substrates such as silicon can be used. This reflected illumination is

slightly more involved than transmission because a second microscope port containing tube lenses is needed to transmit collimated illumination light after the objective. In this way, the objective focuses the laser light and collimates the illumination. A schematic is shown in Figure 2.4.

The style of microscope, namely inverted or upright, should also be considered. The difference between the two is the direction of the objective lens, as shown in Figure 2.4. For an upright microscope the sample is mounted below the objective lens while for an inverted microscope the sample is above the lens. Both arrangements are optically equivalent, and for MAP there is little difference because the sample can be placed upside-down with no ill effects. In general, inverted microscopes provide two slight

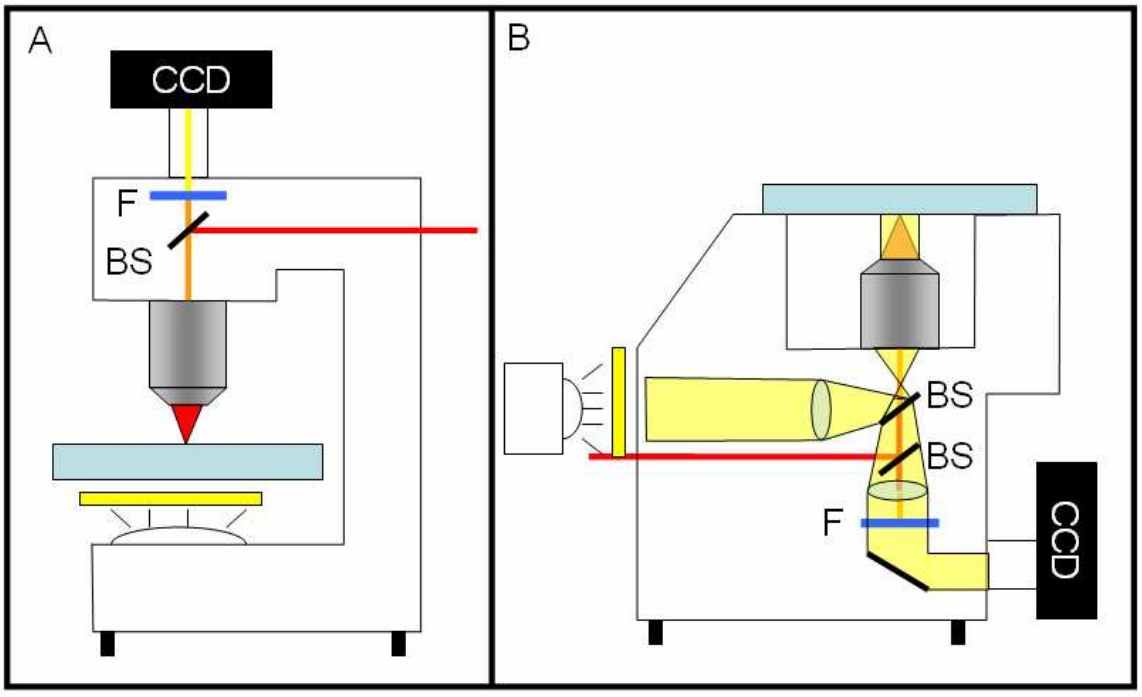

Figure 2.4 A) An upright microscope in transmission mode with one beamsplitter (BS) to reflect the laser and transmit the illumination. A short pass filter (F) blocks the laser and a yellow filter is used for the illumination to prevent photopolymerization. B) An inverted microscope in reflection mode with two beamsplitters for the illumination source and the laser.

advantages over upright microscopes for mechanical reasons. The first is that the position of the stage on an inverted microscope is fixed and the objective can be moved up and down along the optical axis. This means the focal plane is less likely to drift in the z direction compared to an upright microscope, where an entire stage is capable of moving in this direction and can gradually fall over extended periods of time. The other feature that is useful for inverted microscopes is that there is generally more room between the objective and the condenser in which to place the sample and stage. This is important because a 3-axis stage used in MAP may be too big to fit on an upright microscope.

Another option is building a microscope from rail mouted lenses. This is a viable option, but is not as easy as it sounds. Commercial microscopes can be purchased at a reasonable price and are usually worth it for a simple optical arrangement like MAP in which a basic inverted microscope will work well. Also, one of the most expensive parts of a microscope is the objective lens, which must be purchased whether the microscope is home-built or purchased commercially.

2.4 The Sample

The sample either consists of a liquid or solid prepolymer film. As mentioned in Chapter 1, acyrlates, methacrylates, and epoxies have been used in MAP, as have other materials such as siloxanes,[67] hydrogels,[68] chalcogenides,[69] and organic modified ceramics.[70] For most of our experiments a resin is prepared by mixing equal parts ethoxylated (6) trimethylolpropane triacrylate (Sartomer, SR-499) and *tris*(2-hydroxy ethyl)isocyanurate triacrylate (Sartomer, SR-368) with 3 wt. % 2,4,6-

trimethylbenzoylethoxyphenylphosphine oxide (BASF, Lucirin TPO-L).[35] The resin is sandwiched between a substrate and a coverslip with a spacer in between (Figure 2.5). The spacer is on the order of 100 μm thick, but can be made several millimeters thick depending on the sample. In general, the spacer thickness should be less than the working distance of the objective lens. The substrate is usually glass whose surface has been modified to promote adhesion of acrylate microstructures. The modification is done by O_2 plasma cleaning the glass followed by immersion for 24 hours in an ethanol solution with 3 % by volume 3-acryloxypropyltrimethoxysilane. This reaction puts acrylate groups on the surface of the glass that can then be polymerized into the microstructure, connecting it to the substrate. This modification can also be done on the oxide layer of a silicon wafer. The resin itself should be optically clear and transparent to the laser light used. This is usually not a problem at near-IR wavelengths. In general, a high viscosity resin is preferable to a low viscosity resin because the sample will be moved while in contact with an oil immersion objective lens. The pressure from the objective can cause the resin to flow that can distort incomplete structures. To achieve a higher viscosity, some groups have incorporated the polymer binder poly(styrene-co-acrylonitrile) in 1:3 ratio of binder : monomers.[71-73] After evaporation of a solvent used to mix the components, a clear solid film is left. The solid film enables fabrication of

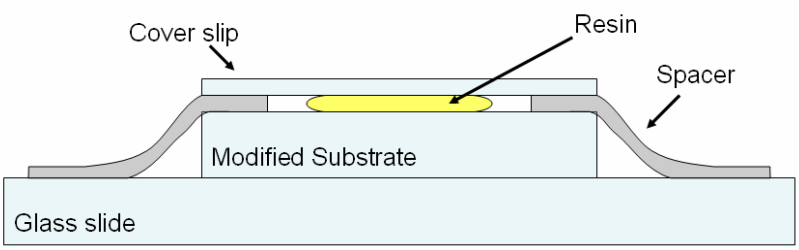

Figure 2.5 A typical sample configuration.

parts without fear of them floating away; however, preparing the film may take several days.

2.5 Creating the 3-D Pattern

Focusing an ultrafast laser into a prepolymer sample generates a cross-linked polymeric voxel. In order to create a 3-D shape the laser must be scanned in three dimensions with respect to a fixed sample; alternatively, the sample can be scanned with respect to a fixed laser beam. In principle the two are equal, but in practice scanning the sample offers greater flexibility and a simpler experimental setup.

Scanning mirrors are employed for scanning microscopies such as confocal or two-photon fluorescence microscopy, and in many cases are already present in a laboratory attempting MAP. They are designed for raster scanning or line scanning and are not well suited for creating arbitrary patterns in three dimensions. In fact, they can only scan in two dimensions; another stage, such as a piezoelectric mounted to the objective lens, must be used to move in the third dimension. Also, scanning mirrors only allow fabrication to the edge of the field of view, which may be only 300 μm × 300 μm or less, depending on the objective lens used.

The alternative, using a 3-axis stage to move the sample with respect to a fixed focal point, has several advantages over using scanning mirrors. A 3-axis stage is designed for synchronous motion and is not limited to the field of view of the objective. Mechanical stepper motor stages can have accuracies of 100 nm with ranges of over 10 cm. Piezo driven stages can have sub-nanometer resolution over a 1 millimeter range with velocities of up to 20 mm/s. Both systems are easily programmed in Cartesian

coordinates. MAP systems often employ two stages, a short-range, high-resolution stage riding atop a long-range, low-resolution stage. This enables small parts to be made accurately on the wafer scale.

2.6 Software

Neither scanning mirrors nor 3-axis stages have been designed by the manufacturer with 3-D patterning in mind. Most likely the scanning system is intended for automated inspection of semiconductors or biological samples or for generating images by raster or line scanning. Software must be written with the capabilities and limitations of MAP in mind. In the Fourkas lab we initially used scanning mirrors for pattern generation but quickly realized their limitations and changed to a stepper motor stage with 100 nm resolution in the x-y plane (Ludl) and 25 nm resolution along the z-axis (Zeiss). The software for this stage was created in LabView by Dr. Richard Farrer and provided the basis for the software I wrote to control our next-generation stage, a piezoelectric XYZ stage (Physik Instrumente) with a 200 μm × 200 μm × 200 μm range and sub-nanometer resolution. A screen shot for this software is shown in Figure 2.6.

The program has two basic modes of operation, a command-response mode and an automated mode. In the command-response mode velocities and position can be set/queried and the shutter can be opened/closed. This mode enables rudimentary fabrication of lines and points. For complex shapes the automated fabrication mode is used, whereby a text file containing command codes and coordinates is read and translated into the desired 3-D part. Other features of the program include a program log that records the time/date stamp of the text files that have been run as well as a help menu

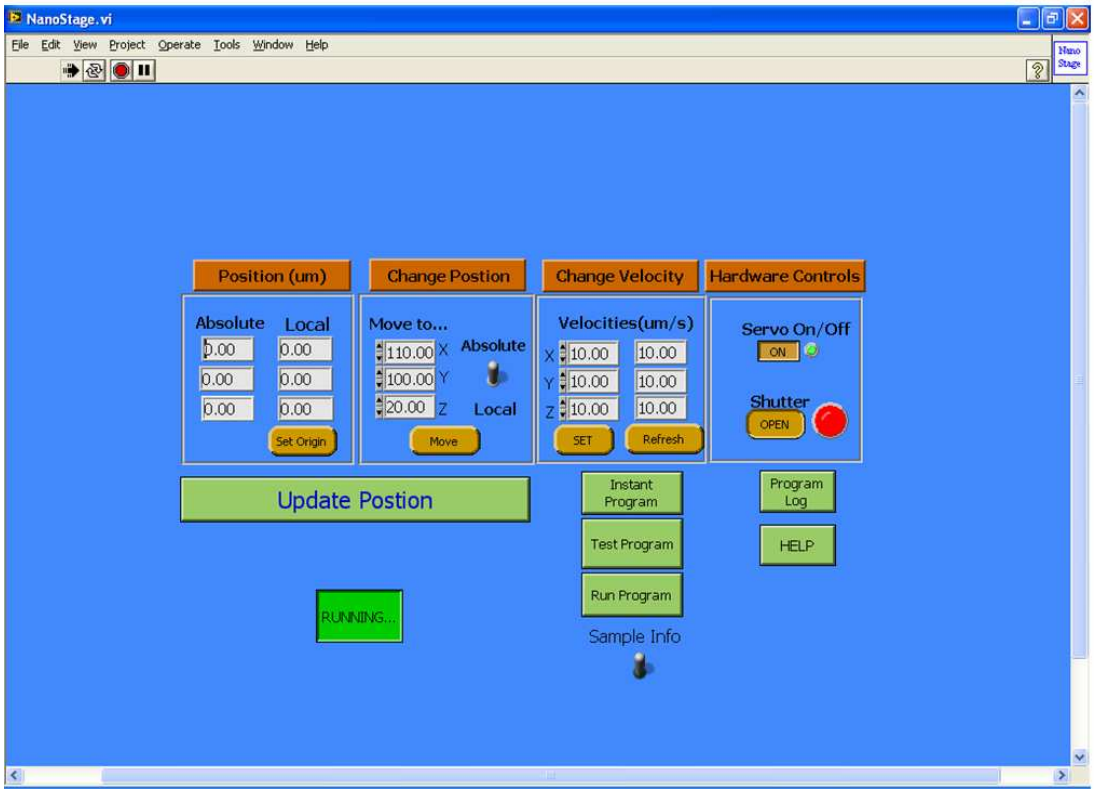

Figure 2.6 Front panel of the 'Nanostage.vi' program that controls a P-562.3CD (Physik Instrumente) stage.

that explains the available commands for automated programs. While an automated program is fabricating, a second window opens giving details of its progress, such as the current (x, y, z) coordinate, and the time remaining until completion.

Each line of an automated program begins with one of seven commands (-1 → 5) that dictate how that line of the program will be interpreted. Commands -1, 1, and 0 tell the stage to move to the subsequent (x, y, z) coordinates with the shutter closed, with the shutter open, with the state of the shutter unchanged, respectively. This (x, y, z) coordinate is with respect to the origin, which is defined as the position when the program was started. Command lines beginning with the number 2 set the velocity of x, y, and z axes in μm/s. Command 3 moves to (x, y, z) and then opens the shutter for a

fixed period of time in milliseconds. Command 4 is used to make waves or circles. The diameter, period, axes, and number of cycles are all adjustable parameters. The 4 command is useful for concise coding of waves or circles, but if an arbitrary curve is needed it is also possible simply to input a series of points to approximate a polygon. This procedure is very easy in a spreadsheet program if an equation can be written for the shape. Finally, command 5 resets a specified position as the origin. This enables already coded patterns to be cut and pasted into another program to piece together modular structures. Designing modular parts can make programming new structures significantly faster. Figure 2.7 shows a sample program, and its implementation.

2	20	20	20		
-1	0	10	0		
1	0	0	10		
0	0	-10	0		
3	5	0	0	500	
3	10	0	2	500	
3	15	0	4	500	
-1	20	0	0		
1	20	0	15		
5	20	0	25		
2	1	20	20		
4	20	10	2	3	3
0	30	0	-5	-1	
0	30	0	-25		
2	20	20	20		
5	30	0	-25		
-1	0	10	0		
1	0	0	10		
0	0	-10	0		
3	5	0	0	50	
3	10	0	1	50	
3	15	0	2	50	

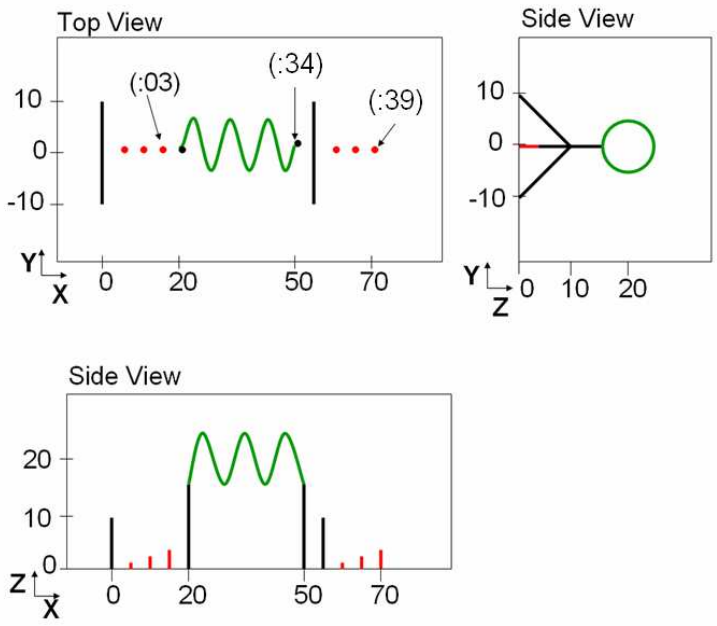

Figure 2.7 The text file on the left will generate the pattern shown above. The first column is the command (-1 → 5). The next three columns are (x,y,z) coordinates or velocities, except in the 4 command where they represent diameter (μm), period (s), and one of the axes for the circle. The axes in the 4 command are enumerated 1, 2, 3 for x, y, z and are programmed into columns 4 and 5. The sixth column in the 4 command specifies the number of cycles. The center of the coil is redefined as the origin with a 5 command before the coil is made. Note the last six commands are cut and pasted from the top and simply repeat the structure in a different location. The numbers in parenthesis in the top view are elapsed time in seconds at that point.

2.7 Putting it All Together

The combination of these subsystems produces a tool that can fabricate useful devices by MAP. An inexpensive, basic version can be assembled for less than $100,000. This system would be composed of a compact microlaser, a few optics for power control and steering, and a simple commercial microscope with a CCD camera. A computer controlled 3-axis piezo stage could be used for pattern generation. The footprint of the system could fit on a 2’ x 2’ optical breadboard, not including the accompanying PC. This system should enable fabrication of micro-devices within the range of the piezo stage (300 μm × 300 μm × 300 μm), but registration would be difficult beyond this range without another computer controlled stepper motor stage. An inexpensive manual stage could be used to translate the stage but not with significant accuracy for registering parts over a range greater than that of the piezo stage.

A more powerful system could be assembled using the advanced subsystems already described. For example, an ultrafast laser system with transform-limited pulses and an in-line autocorrelator could be used to ensure the most efficient polymerization by multiphoton absorption. An advanced optical microscope capable of reflection imaging would enable both transparent and opaque substrates to be used. The stage could be composed of a 3-axis piezo stage mounted to a computer-controlled, 2-axis stepper motor stage for fabrication on the centimeter scale with submicron accuracy.

Three additional improvements could also be made to increase the automation of the MAP process. The first is the addition of automatic power control. This could be achieved by either rotating a motorized half-wave plate or by transmitting the beam through a device such as an acousto-optic modulator or a spatial light modulator. This

would offer dynamic power control while fabricating a single part and could be useful for creating features such as thin walls or membranes, which are useful for micromolding of parts.

Programming the software to translate the substrate such that it is always parallel to the objective would be another useful improvement. If the substrate is not parallel with the stage, then features made on the surface at one point may be significantly above or below the surface far away from that point. By finding the surface at three distant points, the real plane of the substrate can be calculated and used to translate the programmed points into a new coordinate system. Using a simple 3×3 matrix, a space transform can be applied to correct for this type of problem in which a flat substrate is tilted with respect to the stage.

Finally, a third improvement that can be made is the use of a microfluidic sample chamber. This chamber would enable the exchange of resins without losing registration of existing parts. A schematic of such a chamber is shown in Figure 2.8. The chamber consists of three ports; inlet, outlet, and vacuum. The inlet and outlet provide the flow channels for the rinsing out the first resin and exchanging it with a second resin. The vacuum line is used for reversible adhesion of the chamber to the substrate. Resulting structures, composed of two types of polymers, are useful because of their different mechanical, optical, or chemical properties. For instance, dual-component fabrication can be useful for creating the core and cladding of an optical fiber, adjacent cantilevers with different spring constants, or structures in which only selective portions undergoes a reaction after fabrication.

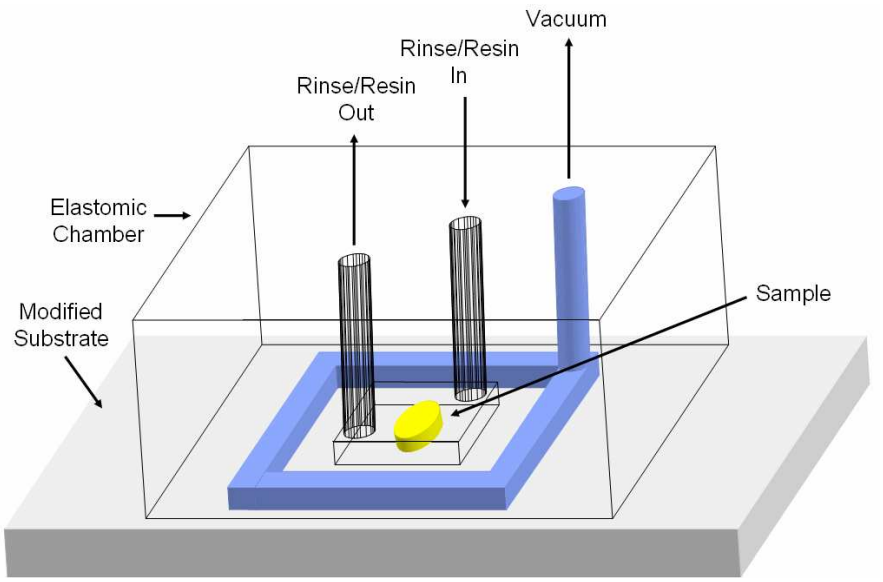

Figure 2.8 A microfluidic sample chamber. The vacuum channel reversibly holds the elastomeric chamber to the substrate. The sample compartment has two ports to bring resin or solvent in and out. The modified substrate is transparent and the laser would be focused through the bottom of the substrate into the resin (not shown).

2.8 Practical Procedures of MAP Fabrication

2.8.1 Structural Design

The most important part of structural design is the method by which the structure is fabricated. This has been reported in the literature as either a raster scan or a vector scan. During a raster scan the part is made in the same way an image is formed on a television. The beam scans a square area and points are either exposed or not exposed to create a 2-D pattern. This is usually done with scanning mirrors and a shutter. Another option for raster scanning that improves its efficiency is to vary the scanning speed to control polymerization.[46] If the beam is scanned quickly, the exposed polymer will not be cross-linked enough to survive washing; thus by scanning a single line slowly then quickly then slowly again, two line segments can be created with a gap in between them. This scheme increases the speed of raster scanning, but such scanning is still less efficient than tracing the desired shape. The vector scan method only traces the part of interest

and does not scan outside this part at all. Clearly, the vector scan is the most efficient, and so it is the fabrication method of choice, especially when using a 3-axis stage instead of scanning mirrors. The three scanning methods are shown in Figure 2.9.

Whether or not to make the shape solid is also an important issue. Significant time can be saved by only polymerizing the shell of a given shape, such as the walls of a cube instead of the entire 3-D volume. If the shell is closed, the liquid resin will be trapped within it during washing and can be polymerized later under a UV lamp. One problem with this is shrinkage upon cross-linking, which can cause the shape to collapse partially (Figure 2.10). This collapse will not occur if the part is made solid initially by MAP or if the part is left open so the liquid resin can be washed out. For this reason parts are rarely made as shells and polymerized after washing.

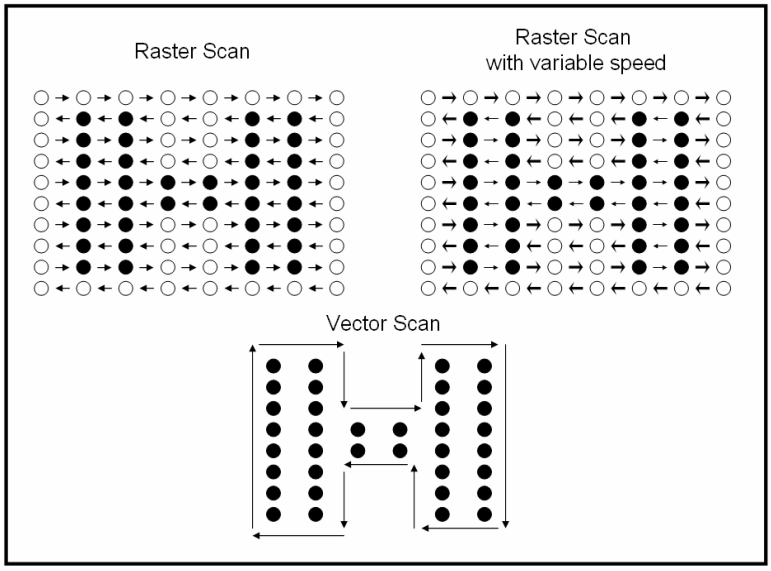

Figure 2.9 Raster scan with constant speed uses a shutter to expose points. Raster scanning with variable speed, denoted by large and small arrows, is faster because unpolymerized regions are scanned quickly. Vector scanning is the most efficient method and only traces the points to be polymerized.

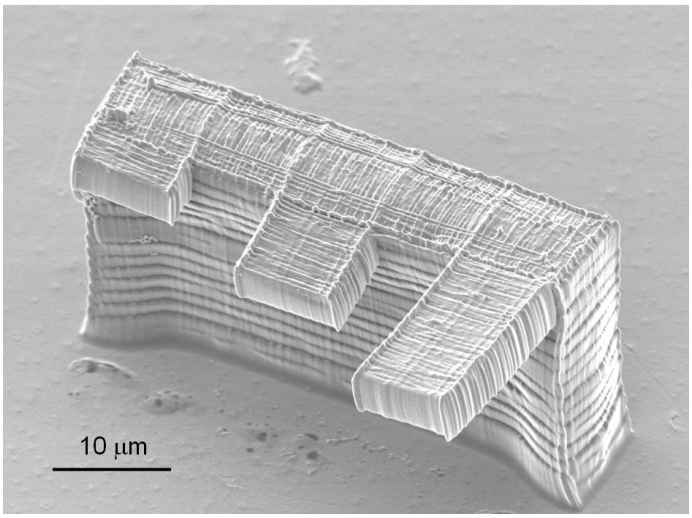

Figure 2.10 The support wall for these cantilevers was made as a shell and was partially collapsed by further polymerization after fabrication.

One final consideration in designing a program is the amount of overlap in adjacent points/lines. As mentioned in section 1.5, a typical voxel used for fabrication is ~ 400 nm in diameter and ~ 2 μm in height. Based on these dimensions, the distance between points in the x-y plane must be < 400 nm and < 2 μm in the z-x or z-y planes to form continuous objects. Making the spacing 2× or 3× smaller will increase the overall fabrication time but will also make the structure stronger. No systematic study has been reported showing the effect of the polymerization density on mechanical strength of the microstructures. Part of the difficulty lies in the accurate measurement of the mechanical properties of polymeric microstructures. For most structures in this thesis an overlap of at least 50% was used.

2.8.2 Fabrication Techniques

Knowledge of voxel size is critical for designing structures. The voxel dimensions can be measured using a technique known as an ascending scan. By fabricating voxels higher and higher above the substrate, the amount of truncation is reduced until the voxel is no longer touching the surface. Just before this happens, the voxels can be slightly attached and will fall over during washing, enabling the true height of the voxel to be measured (Figure 2.11A).

The ascending scan technique highlights an important issue for fabrication by MAP: accurately finding the substrate surface. If a part is made and it is not in solid contact with the substrate IT WILL wash off during rinsing. Luckily, finding the surface is easy. One simply needs to focus inside the resin and fabricate a line while moving the substrate towards the focal point. When the focal point becomes submerged in the substrate polymerization will stop. The surface can be found by moving the substrate

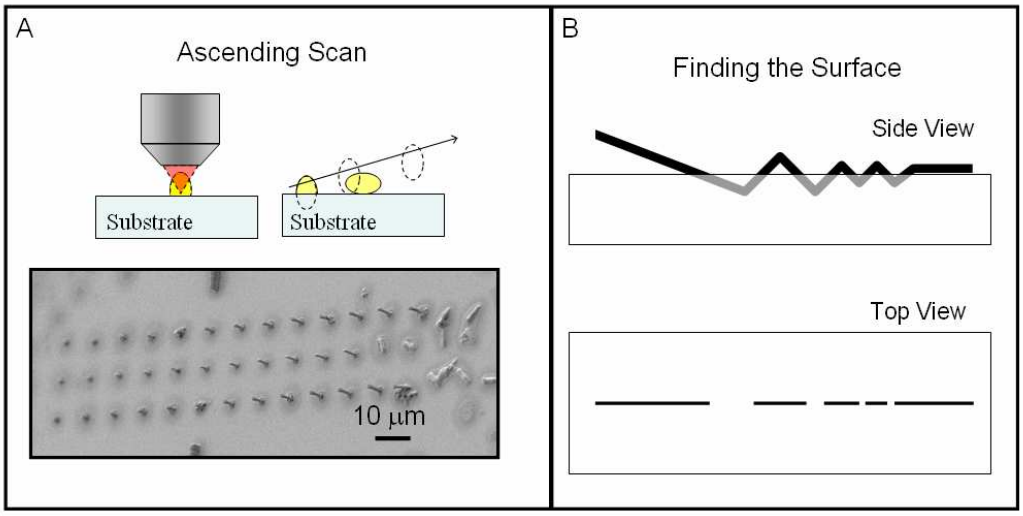

Figure 2.11 A) An ascending scan measures the true height of truncated voxels. B) To find the surface, the focal point is initially above the substrate then moves inside it stopping polymerization. The substrate is moved up and down to hone in on the correct surface location.

back a small amount, <1 μm, to a point where polymerization is visible. The process of finding the surface is shown in Figure 2.11B. The surface may be in a slightly different position than the one where the substrate surface is in focus, depending on how well the laser beam is collimated. One point worth noting is that the velocity used for this procedure should be greater than or equal to the velocity used for fabrication; otherwise the voxel used to find the surface could be too large, resulting in a seemingly lower surface when in fact the voxel is actually taller. An indication that the lines are in contact with the surface is that the lines the remain straight, while after several minutes lines made slightly above the surface get wavy and lines that are far above the surface bow into arches.[74]

Another important concept for MAP is the use of anchoring. Whenever possible, newly formed polymer should be connected to an existing polymer that is secured to the surface. This procedure will prevent the structure from moving if the resin should flow, which can occur when moving the sample along the optical axis with an oil-immersion objective. Tethering is also useful to prevent the bowing of parts, such as beams, that can occur during building. One way to avoid such problems is to fabricate many lines in the short direction instead of a few lines in the long direction when making something like a beam. The time to complete a structure this way will be slightly longer because the short lines will have more stopping points, and therefore on average have a lower average velocity, due to brief acceleration/deceleration cycles. This brings rise to another problem when fabricating at high speeds: the rate of acceleration/deceleration may be too slow, resulting in a dwell time at turning points that is long enough to cause over-polymerization. The easiest way to avoid this problem is to fabricate slowly; however, a

better solution is to make the end points slowly and stitch them to the rest of the line, which is made quickly. The fabrication of the quick line can be stopped prematurely by the closing the shutter while still in motion, allowing it to decelerate without overexposure.

Another issue that must be considered in fabrication is beam defocusing while traversing a microstructure. Defocusing occurs despite the fact that the polymerized material is optically transparent,[35] because this material has a slightly higher index of refraction, 1.5222, than the liquid resin, 1.4930. Defocusing poses a problem if something near the substrate is to be made after something tall has already been fabricated. For instance, the bridge in Figure 2.12 was made and then a thin wall under the bridge was fabricated. The thin wall polymerized correctly in the center but not near the edge, because a large fraction of the beam was defocused by the leg of the bridge. This problem can be circumvented by changing the sequence of fabrication or by using dynamic power control to increase the power in regions prone to defocusing.

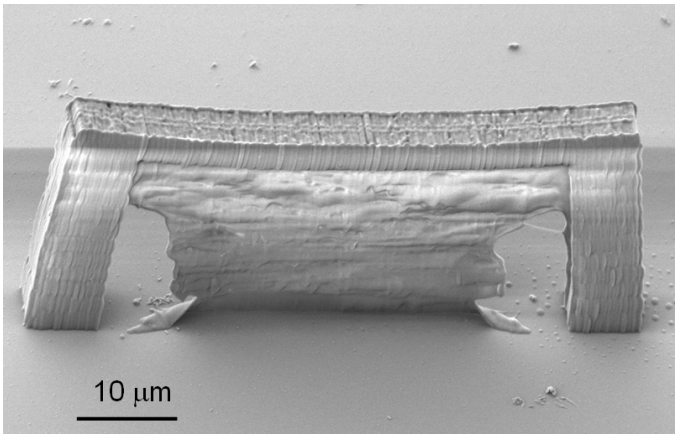

Figure 2.12 Polymerization can be impeded if the laser focuses through a thick polymer structure, as shown here near the support legs of a bridge. The holes near the legs were intended to be filled in.

2.8.3 Post-fabrication Processing

After washing unpolymerized resin from a microstructure, the capillary forces of the drying solvent can collapse delicate portions of the structure. For example, if a coil is washed in ethanol and then dried, the surface tension can be enough to cause adjacent turns to stick together (Figure 2.13). This problem can be avoided by using a solvent with a lower surface tension or by using supercritical drying. Supercritical drying requires additional equipment and is a slow process. Instead, we exchange ethanol with the solvent hexamethyldisilizane (HMDS) whenever fragile parts of a structure are susceptible to collapse during drying. HMDS is commonly used in photolithography as a surface modification agent and not for its low surface tension.

Another way in which surface tension can be overcome is by designing the structure differently and using another tool of laser microfabrication, ablation. Polymer laser ablation can be performed by focusing the same ultrafast beam used for fabrication into a cross-linked structure made by MAP. The polymer vaporizes at the focal point, resulting in the ability to make relatively smooth cuts in structures. This process can be

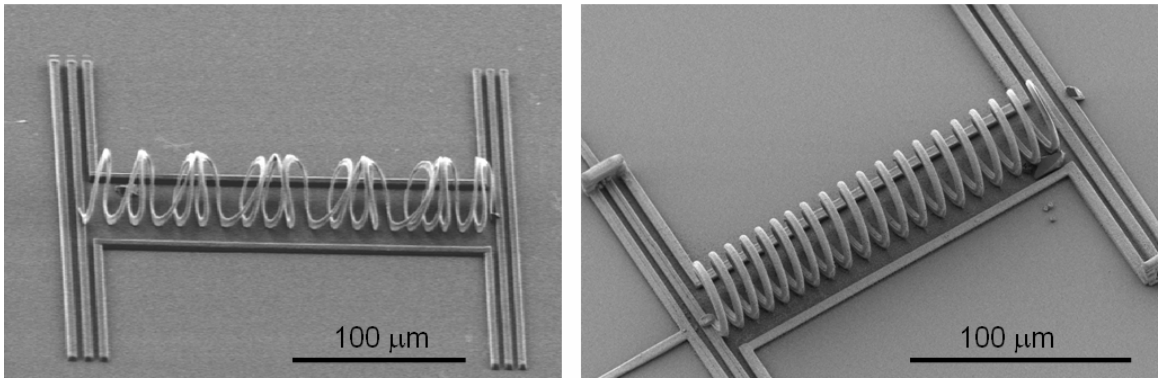

Figure 2.13 The coil on the left was dried in ethanol causing its turns to stick together. The coil on the right was dried in HMDS and did not stick together.

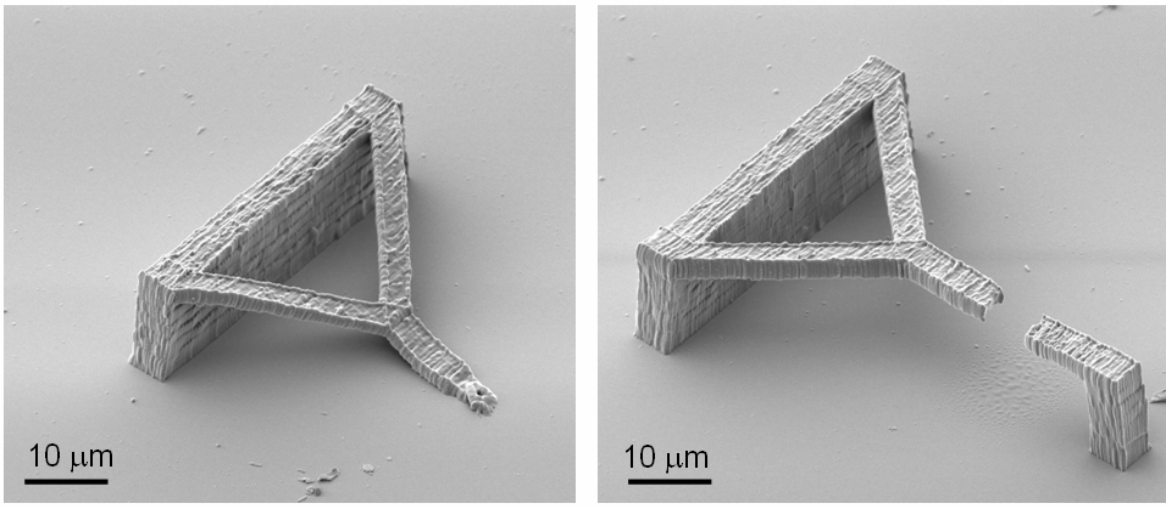

Figure 2.14 The cantilever on the left was made without a support. After washing in ethanol it was pulled down by surface tension. The cantilever on the right was made with a support post and was not affected by the surface tension during drying. The cantilever was cut free after drying by laser ablation. Note also the ridges at the edge of the cantilevers, which are unintentional. These are caused by acceleration/deceleration of the stage at the turning points.

used to free parts that were tethered during fabrication or to cut away another kind of support used to prevent collapse during washing. Figure 2.14 shows a pair of cantilevers. One was made without a support and fell after washing, while the other had a supporting tower that was disconnected by laser ablation. Ablation takes about ten times as much power as is required for fabrication, and while the cut edge is relatively smooth, if a large volume of material is ablated the surface can be littered with debris that is difficult to remove.

2.9 Summary

This chapter has described the five components necessary for fabrication by MAP: a laser, a microscope, a sample, a stage, and software. The available options for each have been described, as well as the rationale for selecting one option over another.

A wide range of systems can be assembled, depending on the desired level of capability. Simple systems, capable of fabricating arbitrary 3-D shapes, can be assembled for < $100,000 from a turnkey picosecond laser with a 3-axis stage. The software to control such stages is fairly simple. Also, samples can easily be prepared from commercially available components. Highly complex systems can also be envisioned to push the limits of automation and at the same time the efficiency and resolution of MAP. Using dynamic power control, planarizing software, and a microfluidic sample chamber would greatly extend the speed and quality of devices made by MAP.

Hopefully, the simplicity of the setup described here will reassure those without optics experience that they too can assemble a MAP system. The design and fabrication techniques discussed should enable beginners to avoid common mistakes such as not finding the surface correctly. Also, in highlighting the pitfalls, such as the collapse of shell structures (Figure 2.10), a better feel can be gained for the mechanical properties of microscopic polymer structures.

Chapter 3: Micro-Transfer Molding

3.1 Introduction

While MAP has remarkable 3-D capability and resolution, it is inherently a serial technique and is therefore of limited use in manufacturing. Structures made by MAP are not only made one at a time, but each structure is fabricated voxel by voxel. Thus a complex structure can take hours to make. Two solutions have been demonstrated to the make MAP a parallel process, enabling hundreds of structures to be made in the same time it takes to make one. The first technique uses a micro-lens array to create multiple laser foci that fabricate copies of the same structure next to one another. In the other method, one makes one master structure serially, molds it, and then makes replicas in parallel. The figure below summarizes these techniques.

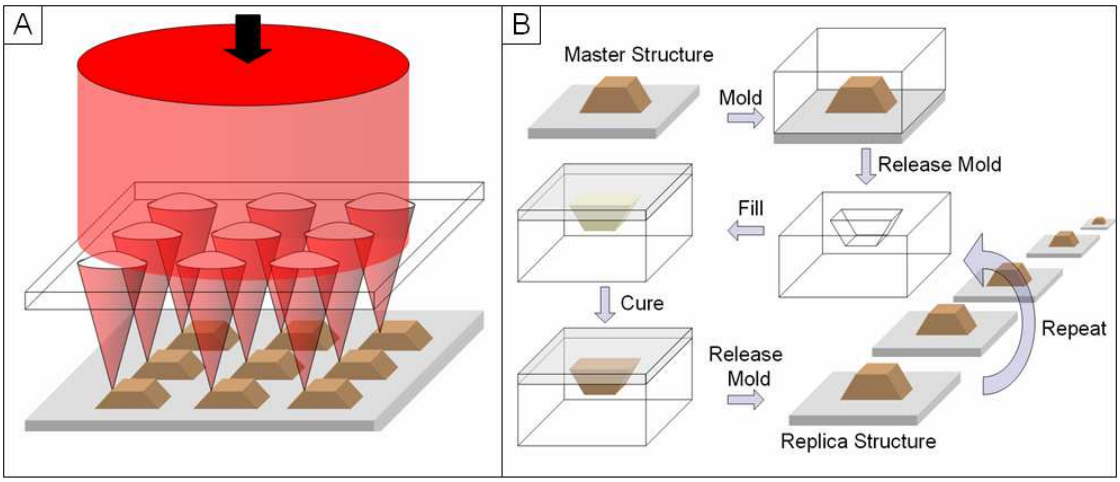

Figure 3.1 A) Micro-lens array for parallel fabrication. B) Micro-transfer molding (μTM). After molding a master structure, the mold is filled with resin, cured, and the replica is released. The mold can then be reused to make additional copies of the master.

The first technique has been demonstrated by Kawata and coworkers, and allows more than one hundred identical structures to be formed simultaneously with only one stage.[75] These structures must be in close proximity to one another (~10 μm), and care must be taken to ensure the laser beam is uniform across the micro-lens array to make each structure identical. Also, since the beam is divided into many sub-beams, the original beam must be very powerful, so an amplified laser is used. This technique is particularly useful for creating periodic structures such as photonic crystals, in which a unit cell could be made by each lens.[76]

The second technique uses MAP to create a structure in the usual manner. The structure is then molded, and the mold is used to make copies. The mold effectively takes the role of a mask in photolithography (which is also made in a serial manner) but then allows for subsequent parallel production. This technique has a number of advantages compared to the micro-lens array approach, as well some limitations. The remainder of this chapter will discuss this, which is known as micro-transfer molding (μTM), in detail.

3.2 Micro-Transfer Molding with PDMS

Transfer molding dates back to the early days of plastics engineering, but has more recently been applied to the micro-scale with the development of soft lithography. In the soft lithographic implementation the mold is made of an elastomer, typically poly(dimethyl)siloxane (PDMS).[2] The commercially available PDMS formulation most commonly used is Sylgard 184 from Dow Corning, which is composed of a 10:1 ratio of base to curing agent. The base is a cross-linkable, vinyl-functional T-type silicone resin

with a small amount of organo-platinum catalyst. The curing agent contains vinyl-terminated PDMS prepolymers and trimethylsiloxy-terminated poly(methylhydrosiloxane) prepolymers as cross-linkers. Upon mixing, the vinyl groups react with the hydrosilane hydrogens through a Pt-catalyzed hydrosilylation reaction to form a highly cross-linked elastomer.[77] The properties of Sylgard 184, which are summarized table 3.1, make it ideal for μTM.

Sylgard 184 Property	Benefit	Disadvantages
Low surface energy (19.8 mJ/m^2)[78]	Highly wetting surface	-
Low modulus (2 N/mm^2)[79]	Mold flexibility	Limits resolution
Chemically inert	Wide range of replica materials	Swells in organic solvents
Readily dissolves gas (air)	Facile filling of molds	Requires degassing after mixing
Optically transparent	Photopolymerization	-
Controllable surface chemistry	Controlled wetability or adhesion	-
Low shrinkage (~2%)	High fidelity replicas	-

Table 3.1 Benefits and disadvantages of Sylgard 184 as a molding material

The procedure for molding and replicating is simple, as shown in Figure 3.1B. A mold is made by weighing out a few grams of Sylgard 184 in a 10:1 mass ratio of base to curing agent. The resulting mixture is poured into a PDMS form containing a 1 cm × 1 cm × 2 mm well that has previously been modified with (tridecafluoro-1,1,2,2-tetrahydrooctyl) dimethylchlorosilane, and is vacuum degassed at 100 mTorr for ~1 min. The microstructure is then placed onto this degassed PDMS upside down and heated at 110 °C for 30 minutes. The PDMS mold is removed from the PDMS form and carefully peeled off of the substrate with tweezers. To create a replica, a drop of resin is placed

between the mold and a piece of acrylate modified-glass and is UV cured (at 365 nm) for 5 minutes. While any number of materials can be used to create replicas, here we use the same resin that was employed for MAP fabrication. After the replica is cured the mold is removed with tweezers. It should be noted that for all the replicas shown here there is a film (~100 μm) of acrylate between the replica and the glass substrate. No attempt has been made to remove this film, although it could either be made thinner by using a smaller drop of resin or presumably etched away by reactive ion etching with O_2, as is commonly done in nanoimprint lithography.

3.3 μTM Resolution

Micro-transfer molding has predominately been applied to 2-D patterns made by photo- or e-beam lithography with resolution down to the sub-100 nm scale.[80] The resolution is limited by the low Young's modulus of the Sylgard 184 which can distort small features if the mold deforms. Here, μTM is applied to the replication of 3-D microstructures made by MAP. As shown in Figure 3.2, these replicas are faithful down to at least the 100 nm scale. This level of resolution is comparable to that of the MAP process itself. The fact that the mold can deform will be used to our advantage to replicate complex shapes such as those with reentrant features and high aspect ratios.

One seemingly unavoidable resolution issue is shrinkage. Both the PDMS mold and the polymeric replica shrink upon cross-linking. Sylgard 184 is known to shrink from 1 to 5 % depending on the speed of curing (faster curing results in higher shrinkage).[81] The polymer replica shrinkage will also depend on cure speed and the

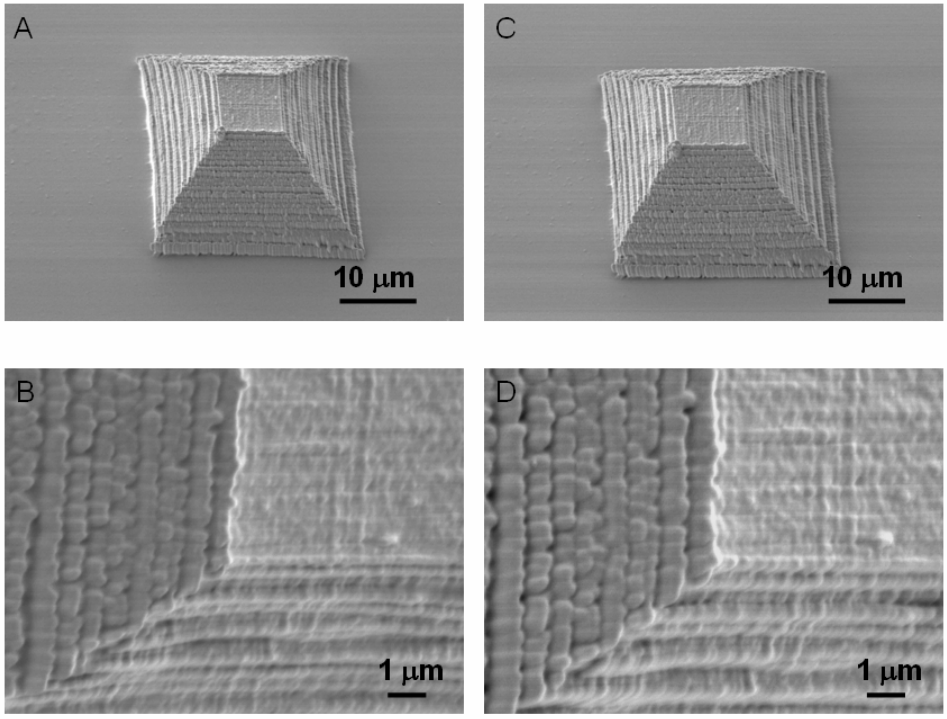

Figure 3.2 A) Scanning electron micrograph of a master truncated pyramid made by MAP. B) Higher magnification of A). C) Replica of structure in A), cured under a UV lamp. D) Higher magnification of C).

monomer composition. For the experiments described here, these effects combine to yield replicated microstructures that are about 5% smaller than the originals.

Other problems, stemming from the low Young's modulus of Sylgard 184, can make the replica different from the original. Figure 3.3 summarizes two common failure mechanisms that can result in poor reproduction quality.[78] A method involving a composite mold, made of 'hard'-PDMS supported of Sylgard 184, has been demonstrated to alleviate these problems, making possible an astonishing resolution of 2 nm.[82] However, in this work we sought to take advantage of the low Young's modulus to enable replication of topologically challenging, and even "impossible", microstructures that cannot be made by conventional lithography.

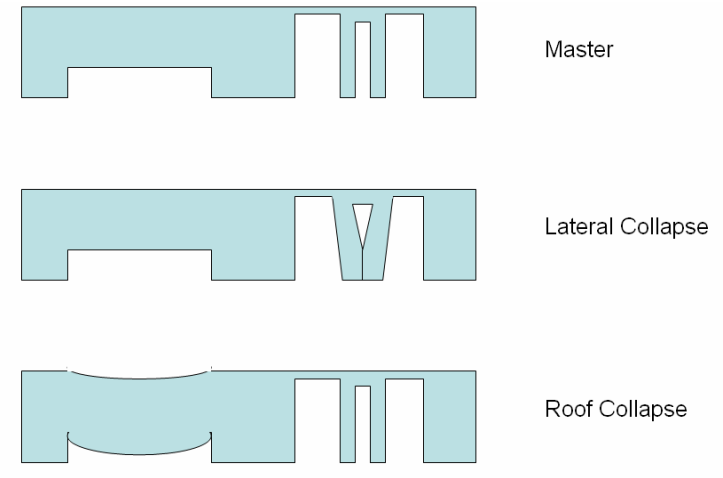

Figure 3.3 Typical deformation mechanisms of Sylgard 184 molds.

3.4 Limitations of Topology, Part I - Undercut/High Aspect Ratio Structures

3.4.1 Undercut Structures

Micro-transfer molding is a convenient way to replicate 3-D microstructures made by MAP, but there are limitations on the allowable geometries. For example, a structure that is smaller at the bottom than the top should get locked within a mold. This type of shape is called undercut or reentrant. If an undercut structure were surrounded by a rigid molding material, then upon removal of the mold, the structure would be trapped within the mold or destroyed. However, if the molding material is compliant, then it can flex around the replica and be released without damaging the copy. This has been mentioned in the literature was has not been systematically studied due to the difficulty of fabricating reentrant structures with conventional techniques.[83,84] Figure 3.4 shows a schematic of this idea.

Replication of reentrant structures was tested using a trapezoidal structure with varying open angles. Figure 3.5 shows three such shapes with undercut open angles of

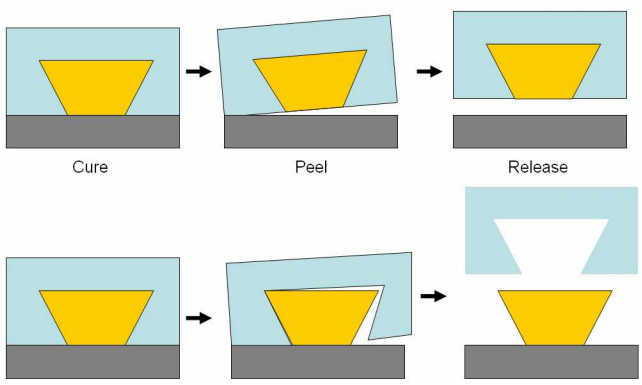

Figure 3.4 The top scheme shows a rigid mold that is unable to release an undercut structure, while the bottom scheme uses a flexible mold that can release the structure and then return to its original shape.

75°, 45° and 30°. Note that because the undercuts are opposed, there is no release direction that avoids flexing of the mold.[85]

Replication of structures with even more severe undercuts, such as cantilevers, was also tested. Cantilevers are of great practical importance in microfabrication because they are easily characterized mechanically and can be coupled to the macroscopic world optically or electrically. Cantilevers are ubiquitous in scanning probe microscopy and are

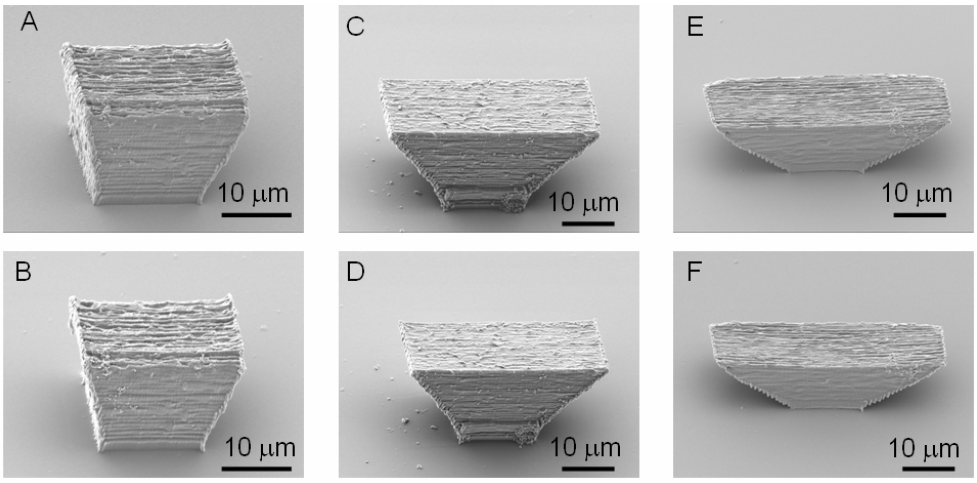

Figure 3.5 A, C, and E, undercut master structures with 75, 45, and 30° open angles respectively, and B, D, and F are their replicas.

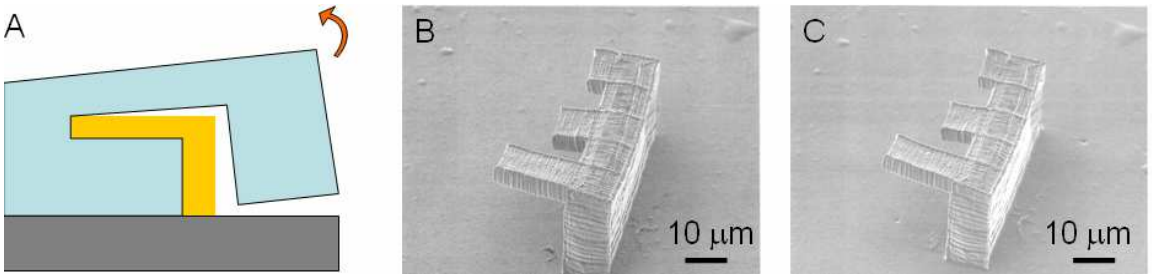

Figure 3.6 A) Peeling direction for cantilevers B) Master cantilever array with cantilevers 5, 10, and 20 μm long. C) replica of B).

finding use in numerous applications in silicon-based MEMS. Figure 3.6 shows three cantilevers, with lengths of 5, 10, and 20 μm, on a common support.[85] In this geometry there is a preferential direction in which to release the mold that puts the least amount of stress on the cantilevers. If the mold is not released in this direction the supporting wall will be released but the cantilevers will break off within the mold.

3.4.2 High-Aspect-Ratio Structures

Another type of structure that should be difficult to mold is towers. These high-aspect-ratio structures can be thought of as vertical cantilevers. While there is no

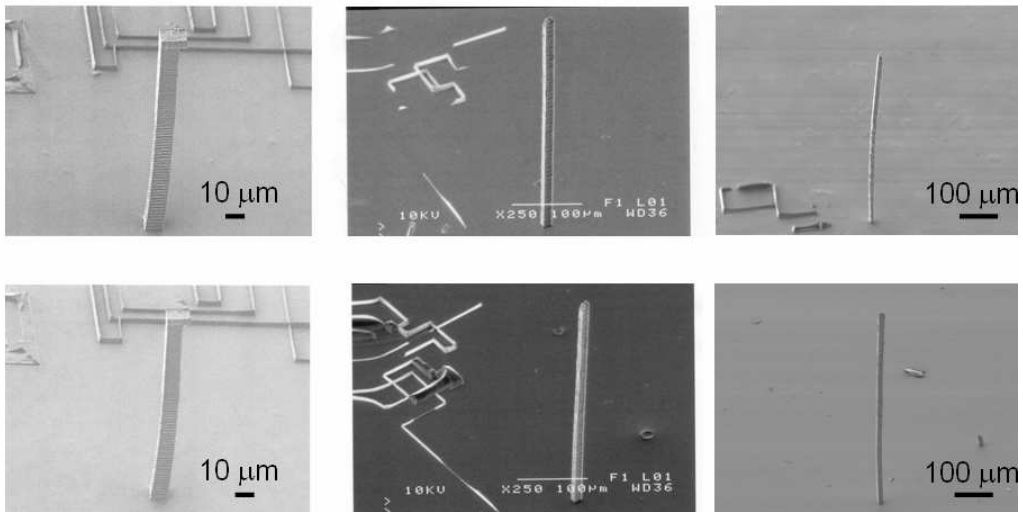

Figure 3.7 High-aspect-ratio towers. 100, 300 and 500 μm in height. All are 10 x 10 μm in cross-section.

topological constraint to prevent replication of towers, there is the practical difficulty of removing the mold without breaking the tower. Thus, for successful replication, the polymeric *replica* should also be somewhat flexible and the mold should be easily releasable from the replica. The Young's modulus of polymer microstructures made by MAP is about 0.5 GPa, as measured by AFM and nanoindentation,[86] which indicates that the polymer is fairly flexible. The lower surface energy of PDMS will help to minimize the shear stress along the length of the tower that otherwise would act to detach it from the substrate. Figure 3.8 below shows replicated towers with different aspect ratios.

It has been demonstrated, then, that some topological constraints, such as undercuts or very high aspect ratios can be replicated by an elastomeric mold. Figure 3.8 shows the replication of towers with undercut features as well.

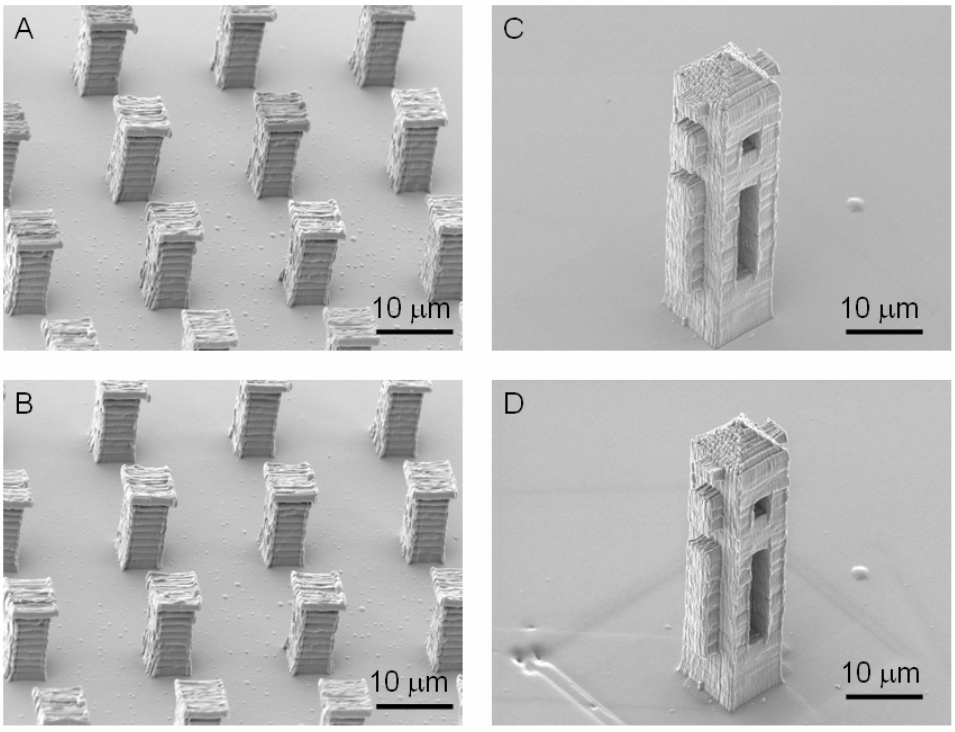

Figure 3.8 Towers with undercuts. A) Master structure of 16 tower array with caps that are larger than the towers. B) Replica of A. C) Master tower with cavities and protrusions. D) Replica of C. .

3.5 Limitations of Topology Part II - Closed Loops

3.5.1 Membrane-assisted micro-transfer molding (MA-μTM)

It has been shown in the previous section that the favorable properties of PDMS allow for many seemingly forbidden structures to be replicated. There exists, however, a class of structures that are topologically impossible to mold and replicate directly. Structures that contain closed loops, such as an arch, cannot be removed from the mold without destroying the structure and/or the mold. To circumvent this problem, we have created structures that are carefully designed not to have closed loops, but that after molding yield daughter structures that contain closed loops.

The secret to our technique is in the way in which the closed loop structure is made to not contain a closed loop: through the use of a thin membrane. The membrane is nothing more than a polymer wall, made in the same fashion as the rest of the microstructure, except that is particularly thin in one dimension and broader in the other two. For instance, if a membrane were made under an arch that was then molded, the molding material could not close under the arch. Upon removal of the mold, with no membrane to stop it, the mold can reversibly seal in the area where the membrane was. This is a favorable process due to the low surface energy of PDMS, which readily 'wets' other surfaces. The now-sealed mold looks like the mold of a closed loop, so upon filling with resin only the arch fills. The mold can then easily be released from the arch because the portion under the arch can unseal and flex around the arch. The figure below summarizes the closed-loop problem and the membrane assisted micro-transfer molding (MA-μTM) solution.[87]

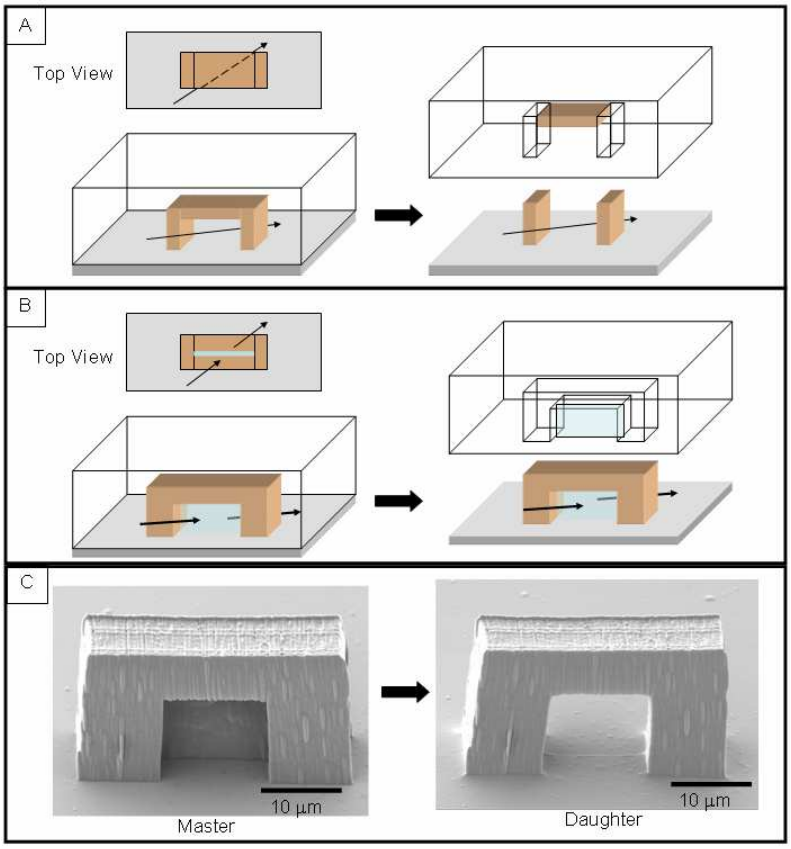

Figure 3.9 A) Closed-loop problem. The cured PDMS prevents the arch from being removed without destroying the structure. B) The closed loop with a membrane is easily removed from the mold and contains an area that is reversibly sealable (in light blue). C) Master arch with a membrane made by MAP, molded by MA-µTM, and then replicated to remove the membrane, creating a closed-loop daughter structure.

A more detailed mechanism of how MA-µTM works involves the interplay among the interfacial energies of air, PDMS, and resin, as well as the mechanical properties of the PDMS. The phenomenon of sealing a membrane is closely related to the failure mechanism of lateral collapse (Figure 3.3), which has been studied for micro-contact printing. The models used for lateral collapse involve parallel plates of PDMS, separated by a small gap, which stick together depending on their thickness, height, and separation. Unfortunately, in the membranes described here the two 'plates' that come

together to close the membrane cannot be described as plates because their thickness cannot be defined.

While a rigorous model has not yet been developed, a qualitative analysis can still be of use. The membrane areas of the mold are sealed by an initial compressive force that is slowly released in an attempt to maintain adhesion. Whether or not the membrane regions remain closed depends on the balance between the stress in the now deformed mold and the surface energies of the PDMS/PDMS and PDMS/air interfaces. Adding resin can also affect the seal, as the liquid may tend to wick into the membrane region. Wicking will occur if it is energetically favorable and if permitted by the kinetics of the flowing resin. It is possible, for instance, that a given resin formulation may energetically be able to wet a sealed membrane region but that this process may not be kinetically favorable if the resin viscosity is too high.

An experiment was performed to test whether a low viscosity resin that wets PDMS well would wet and separate a sealed membrane region. Three photocurable resins commonly used in soft lithography were tested, along with our homemade acrylic mixtures. The commercial resins used were Norland Optical Adhesive 73, Norland Optical Adhesive 61, Summers Optical J-91. Two homemade formulations consisted of a 1:1 ratio of monomers from Sartomer, SR 368:SR 499 and SR 368:SR 399, both of which contained 3% Lucirin TPO-L as a photoinitiator. All the resins were used with a freshly cured mold of a bridge structure, similar to that in Figure 3.9C, whose membrane region had been sealed. The results showed that none of the replicas contained membranes and that the various resins all yield identical looking bridges. The contact angle against a freshly cured PDMS surface was measured for all resins. The most strongly wetting, or

lowest contact angle, resin coincidentally also had the lowest viscosity. This worst-case scenario resin still does not wick into the membranes, indicating that the PDMS/PDMS adhesion that serves to close the membrane region of the mold is fairly robust.

The sealed membrane adhesion may be fairly strong, but this region can be pulled apart by macroscopic force and, if the mold is relaxed to the unstrained position gently, the membrane region will remain open. Daughter structures can therefore be directed either to contain a closed loop or to be faithful replicas of the master structure, including the membranes. The flexing is done by a simple device that consists of little more than a hose and a vacuum. By placing the mold over the opening and pulling vacuum on one side, the mold is flexed into a hemispherical shape. If the cavity of the mold is facing atmospheric pressure it will be pushed together and 'sealed', while if it faces the vacuum

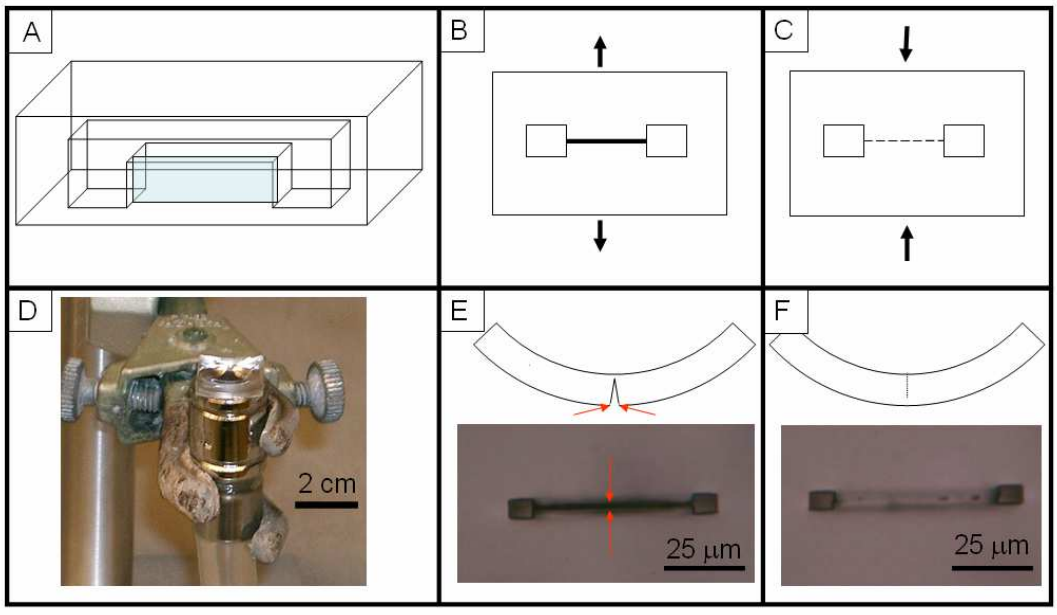

Figure 3.10 A) Schematic of a bridge structure showing the membrane area in light blue. B) and C) The surface of the mold flexing to open and close the membrane respectively. D) Photograph of equipment used to flex molds. The 1 cm × 1 cm × 2 mm mold rests on top of a section of metal tube connected to a vacuum line. E) and F) Diagram of how the membrane is flexed open/closed with optical micrographs of a mold after such a flex.

side it will be flexed ‘open’. Figure 3.10 shows this process schematically.

Membrane-assisted μTM can be used to replicate multiple structures over large length scales and with orthogonal membranes. Figure 3.11 shows three bridges spaced 100 μm apart, all of which have closed loops after replication. The orthogonal bridges are possible because the flexing mechanism shown in Figure 3.10D is isotropic and can close/open a membrane in any direction.

MA-μTM can also be used to ease the replication of structures without closed loops. For example, cantilever replication was demonstrated in Figure 3.6, but cantilevers molded in this manner will break if they extend much farther than 20 μm. MA-μTM can be used here to lengthen the cantilever indefinitely. By making a membrane under the cantilever, the mold can be released over the top of the cantilever, rather than having to slide the entire cantilever out of small hole in the mold. A master/replica of this structure is shown in Figure 3.11.

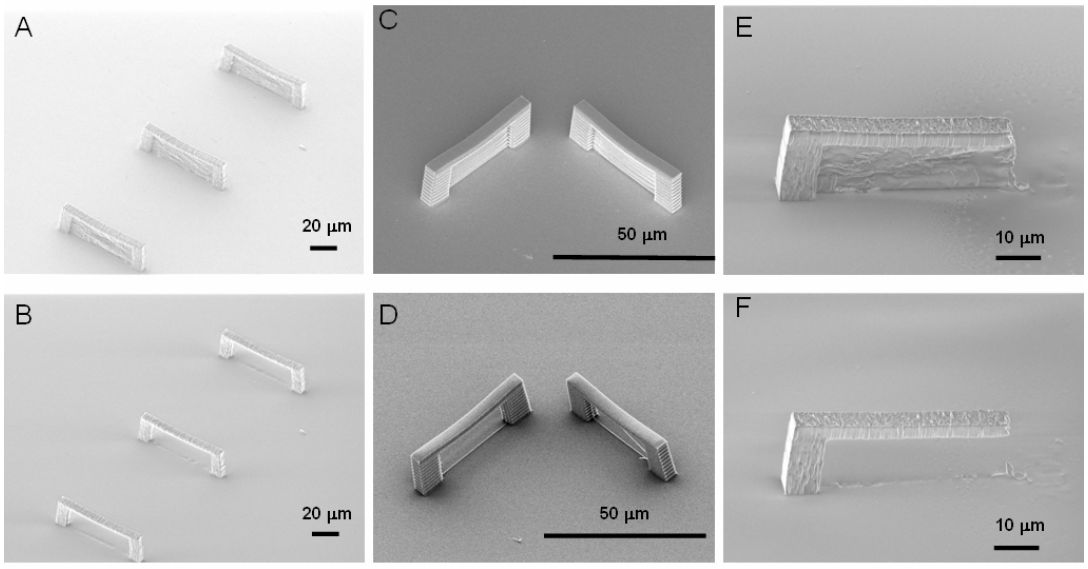

Figure 3.11 A,B) Master and replica of multiple bridges spaced 100 μm apart. C, D) Orthogonal bridges. E,F) Cantilever with membrane.

3.5.2 MA-μTM of more complex shapes

This technique of MA-μTM can be used to replicate an arch, but what other shapes are possible? Figure 3.12 shows three examples of more complex shapes. The first is a four-legged table made using a master having intersecting membranes under the table. The second structure also contains multiple membranes under the turns of a coil. Replication of this structure yields a 5 turn coil with 5 closed loops. Another application of membranes is to create free-moving parts. If a structure contained a part that was only connected to the substrate by a membrane, then if the membrane did not replicate that part would be free. A structure like this was made in the form of interlocked rings. In the master structure the rings are connected via membranes, but in the replica the top ring

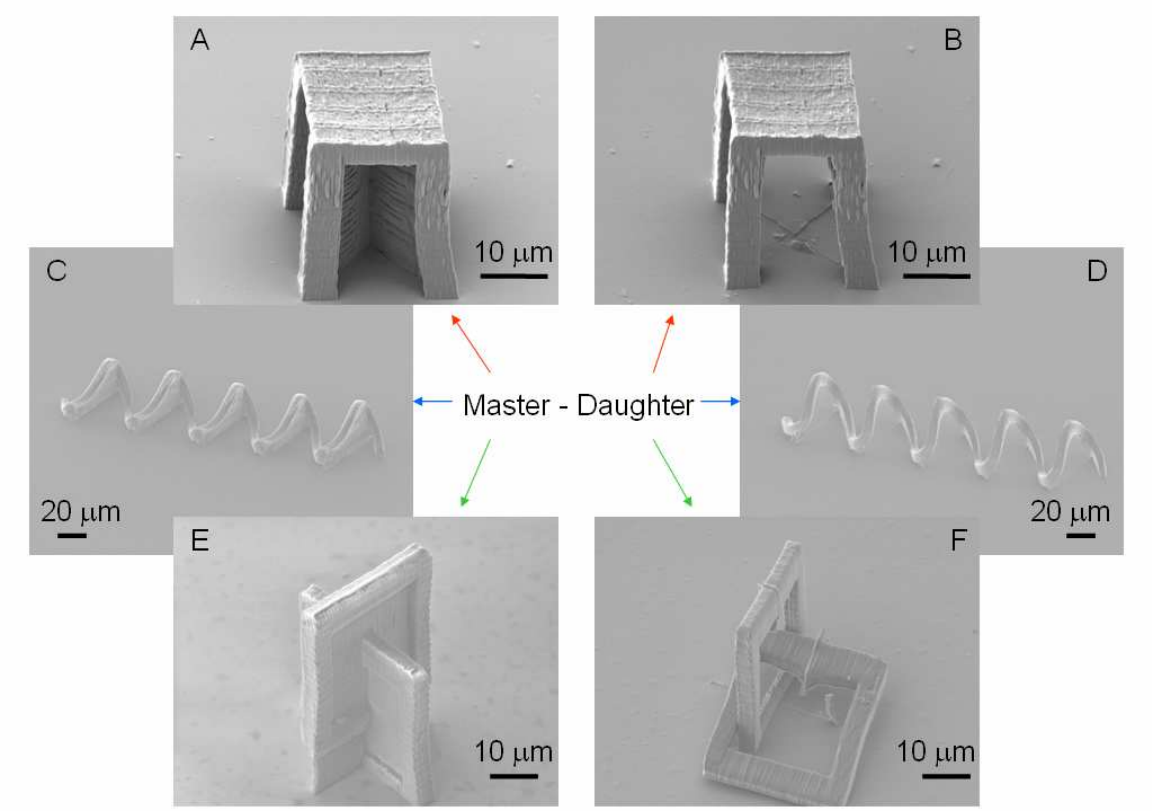

Figure 3.12 A, B) Four-legged table. C, D) 5-turn coil. E, F) Free-moving part.

is not connected to anything and comes out of the mold because it is interlocked with the bottom ring. This top ring could be moved around with an air gun and was completely free. Thus, by filling the mold with the membranes open and then applying pressure to close the membranes, free moving parts can be replicated.

3.5.3 Fundamental Limitations of MA-μTM

Membranes enable a much wider variety of structures to be made, but there are still topological limitations that prevent certain structures from being replicated. For example, while a close loop can be replicated, it is impossible to replicate a "hollow-sphere." If the goal were to replicate a lattice, like the diamond lattice shown in Figure 3.13A, then the central voids could not be hollow because the membranes in the master would prevent the PDMS from filling the inside (*A simple cubic lattice may be possible to replicate with MA-μTM, but this has not be demonstrated*). Lattice structures are of technological interest for applications in photonic crystals and tissue scaffolding.

Another fundamental issue with MA-μTM is the presence of seam lines at the edges of the membranes in the daughter structures. These seams are typically tiny in

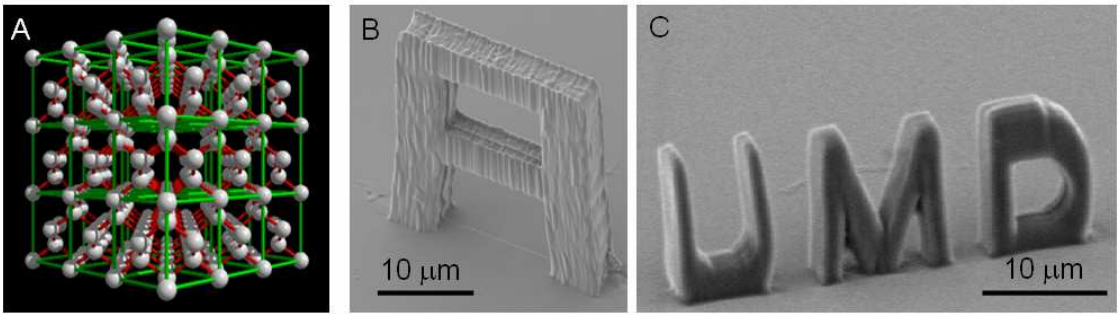

Figure 3.13 A) A diamond lattice is topologically impossible to replicate even with MA-μTM. B) Daughter structure showing seam lines around the area in which the membrane was. C) A daughter structure showing very small membranes under the 'M' where they are beginning to replicate unintentionally.

relation to the rest of the structure, but may cause a problem for some applications. If for example, a micro-optical component required optical smoothness, then a seam could affect its performance. As was the case with the shrinkage issue, there appears to be no easy solution to the seam problem. The mold is pressed to conform to a stressed state and cannot align perfectly, resulting in seams.

Another issue for MA-μTM is the ultimate size of a functioning membrane. As the cross-sectional area gets smaller, the force of adhesion will decrease, and there must be some limit in which the membrane will fail. While this phenomenon has not been explored systematically, some structures show evidence of breakdown when the area approaches just a few square micrometers, as in the 'M' in Figure 3.13C.

3.5.4 Practical Limitations of MA-μTM

Practical constraints also preclude the replication of some structures with MA-μTM. It may be possible topologically to remove PDMS from a given shape, but it may not be possible in reality. Two structures were made to demonstrate this point. One is a tunnel that has a membrane at the center running perpendicularly to the tunnel axis. The other is a pair of parallel bridges that are close to one another. In the tunnel experiment, the tunnel was made progressively longer, requiring longer and longer pieces of PDMS to slide out of it in opposite directions. For a long enough tunnel the PDMS under the tunnel will tear and the tunnel will not replicate. Likewise, in the parallel bridge experiment, the bridges were brought closer and closer together until the gap between them was comparable to the width of the PDMS underneath. A small gap will require a large portion of PDMS to squeeze through, and eventually the PDMS will tear rather than

squeeze through. Figure 3.14 shows these two examples near the limit of failure. The tunnel in Figure 3.14A is 30 μm wide, 15 μm tall, and 75 μm long. The optical micrographs show the mold after removing the master structure for a successful and a failed mold (left and right inset, respectively). The failure mechanism is that the PDMS partially tore inside the tunnel rather than sliding out. In Figure 3.14B the bridges are separated by 5 μm in the successful replica and 3 μm in the failed replica. The PDMS got locked within the 3 μm master, but what is remarkable is that in the 5-μm successful replica, the membranes are separated by 10 μm. Therefore, this 10-μm-wide section of PDMS is squeezed through a 5 μm gap between the bridges.

Another limitation of structures made with membranes is that the direction of the membrane is important. It has been demonstrated in Figures 3.11 and 3.12 that

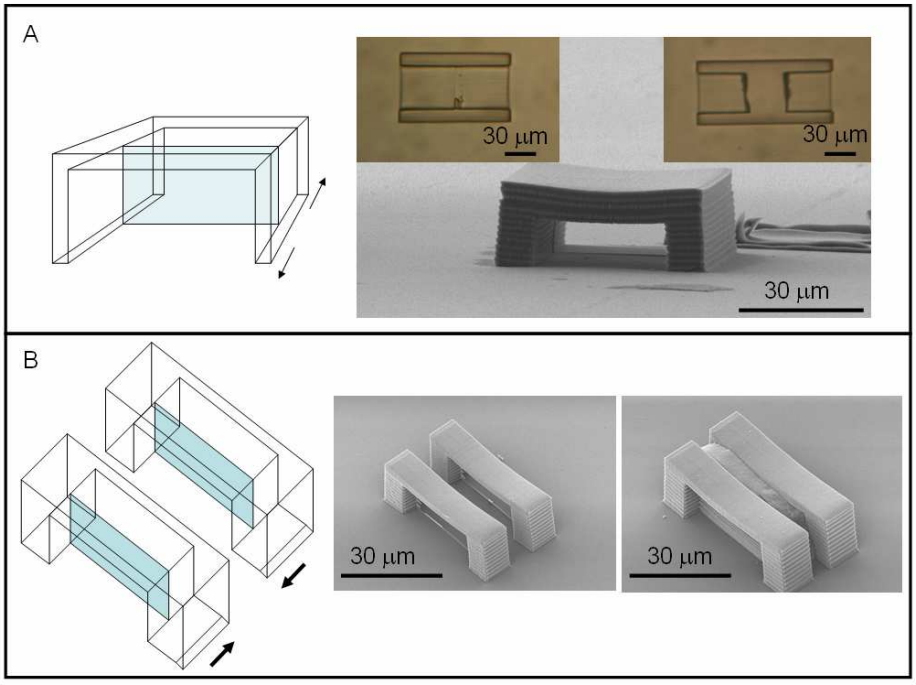

Figure 3.14 A) Lengthening tunnel experiment. An SEM micrograph shows a replica made using the successful mold shown in the left inset optical micrograph while the right inset shows a failed mold. B) A successful replica of bridges separated by 5 μm and a failed replica of bridges separated by 3 μm. The material in between the bridges is torn PDMS from the mold that was trapped there.

orthogonal membranes can be used successfully, but in these cases the direction in which the mold was peeled off (of either the master or replica), was of little consequence. In general, the direction of peeling does matter to some extent, whenever possible, peeling is performed parallel to the membrane. For structures with perpendicular membranes the peel direction bisected the angle made by the membranes. Thus, while perpendicular membranes have been demonstrated, there are practical limits outside of which they will fail. If, for example, the orthogonal bridges of Figure 3.11 B and C were widened into tunnel like the one in Figure 3.14A, it would be impossible to remove the mold successfully from both tunnels.

There is a final limitation of μTM that is indirectly related to membranes: the inadvertent creation of membranes during molding. It was found when the tunnel experiment from Figure 3.14A was being performed that several structures were failing to replicate correctly because they had a hole in the roof of the tunnel. The two slabs of PDMS that were inside the tunnel and pressed together to seal the membrane in the center also sealed to the bulk of the mold above the tunnel. This occurred because the slabs are only connected to the bulk by a small area and are quite flexible. To compound this problem, flexing the mold in the other direction by inverting it in order to open the membrane does not apply force in the right direction. Thus, an unintended skylight was created in the replica. The problem to be avoided, then, is large cross sectional areas separated by a small distance. The serendipitous discovery of this problem led to the conclusion that membranes need not be vertical with respect to the substrate. We originally assumed that because of the voxel size is significantly greater in the vertical direction, horizontal membranes would be too thick to be effective. However, it seems

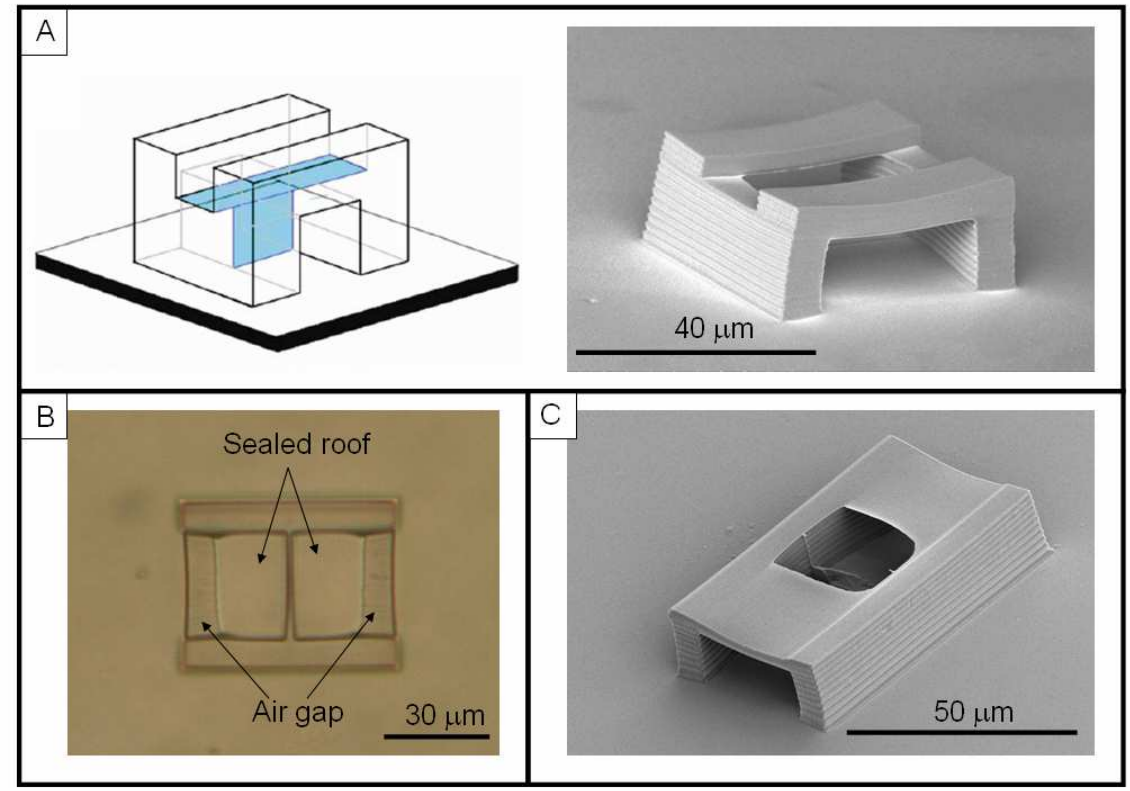

Figure 3.15 A) Intentional horizontal membrane, schematic and SEM. B) Optical micrograph of a mold of tunnel with unintentional roof collapse. C) SEM of a replica made from a mold similar to B.

that if the cross-section area is large enough, a thicker membrane can be tolerated. The Figure 3.15 below shows examples of such a 'thick' membranes, both intentional and unintentional.

3.6 Mold Longevity and Scale-up to mass production

The true power of μTM is in the ability to reuse the master and the molds to create numerous replicas from a single master structure. There are 3 routes by which to accomplish this: 1) making many molds from a master, 2) making replicas from a mold, and 3) using replicas to make new molds. If all of these are done together, millions of replicas could be made from a single master in tens of replication steps. In fact, since the

number of copies can double in each generation,[§] 10 generations will yield 1,024 (2^{10}) copies and 20 generations will yield over 1 million (2^{20}) copies, and 30 generations will yield over 1 billion (2^{30}) copies. Unfortunately, the propagation of defects is also exponential, so if a deformation occurs early on it could result in thousands of poor replicas. Defects can occur either by changes in the master after repeated molding or from changes in the mold after repeated use. These sources of defects have been studied and the results are presented below.

The first issue studied was how a mold deteriorates with continued use. Figure 3.16 below shows the 1st replica of a MAP microstructure, the 15th replica, and the 20th replica. Clearly, the latter replicas look withdrawn compared to the first replica. The exact reason for this degradation is not well understood. PDMS is known to swell,

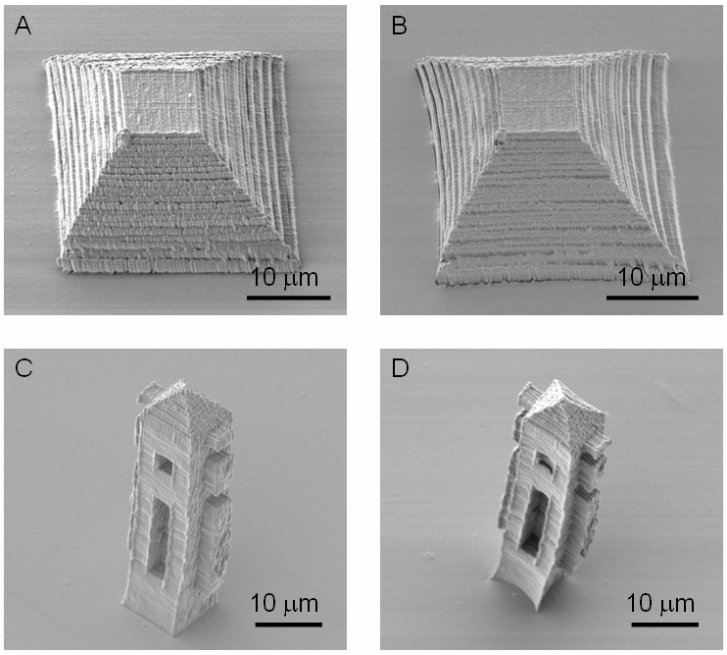

Figure 3.16 A) 1st replica from mold B) 20th replica from the same mold. C) Master structure and D) 18th replica from the same mold.

[§] The term generation refers to the cycle of using all existing molds to create replicas and using all existing replicas to create more molds.

sometime by more than 200% in organic solvents, and it is possible therefore that some components of the resin are dissolving in the mold and causing it to swell. The mold has not been cleaned between uses. It seems from this study that a mold can be used at least ten times without significant degradation.

At the point at which the mold begins to fail, a new mold can be made from of the original or from a replica to replace it. This raises the question of whether or not a master is altered by repeated moldings. Figure 3.17 below shows a master before and after twenty molds have been made from it; there does not seem to be a noticeable difference.

Molds can also be made from replicas; however, a surface treatment must be performed, as the PDMS does not cure well at the interface with the acrylic polymer. The surface treatment is done with 3-aminopropyl trimethoxysilane, and it is believed that the amine reacts via a Michael addition to unreacted acrylate groups. This reaction results in a surface of silanols, against which PDMS cures properly. This procedure has been demonstrated with the molding of the replica 5-turn coil shown in Figure 3.12. The

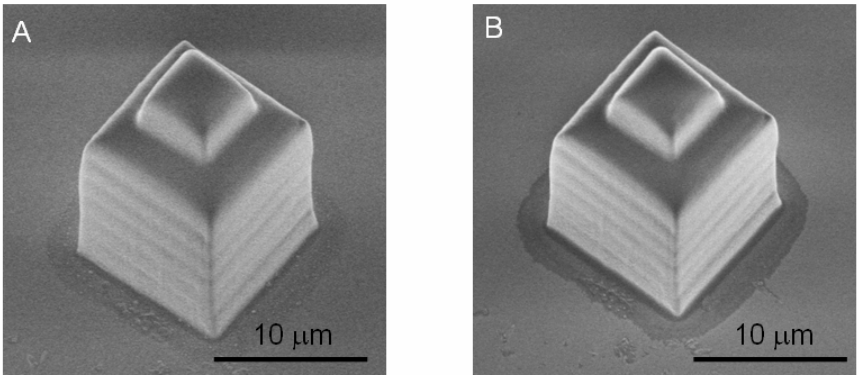

Figure 3.17 A) Master structure. B) Same master after having been use to create 20 molds.

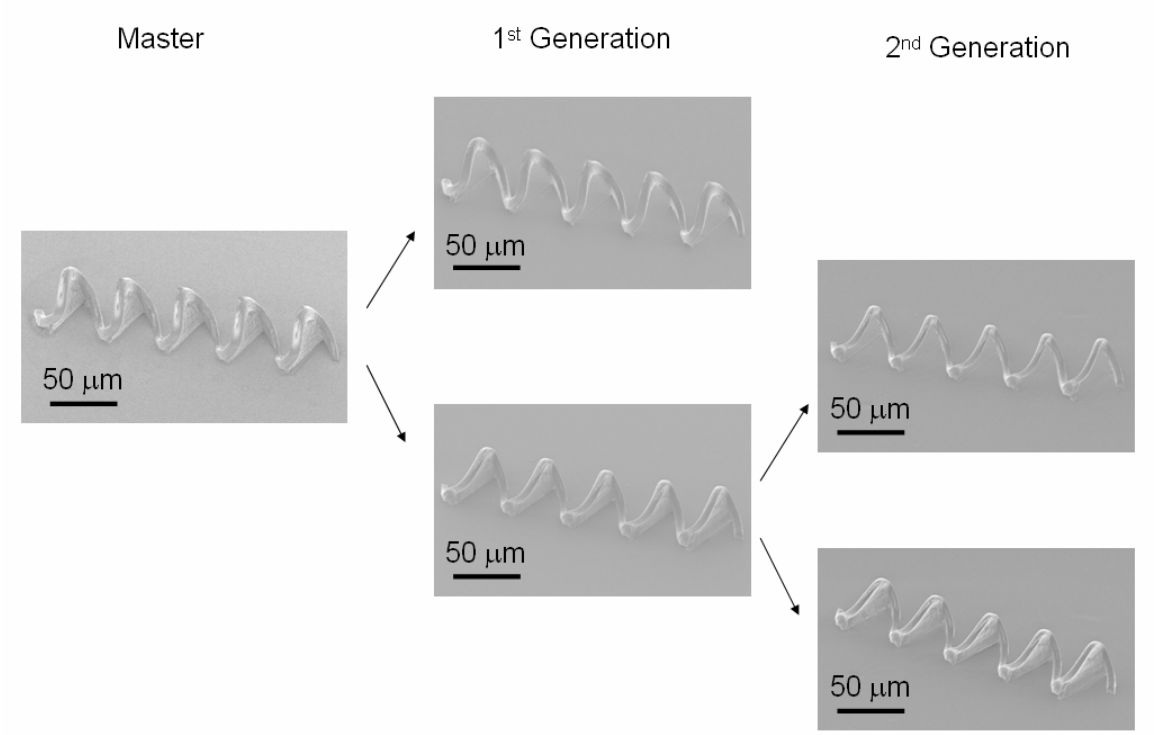

Figure 3.18. The master coil was molded and it was used to create the 1st generation of replicas with membranes (bottom) and without membranes (top). The replica with membranes was then molded to yield 2nd generation replicas.

replica used contained membranes, as in the original structure. Using this second-generation mold, replicas were produced with and without membranes. Figure 3.18 shows this sequence. Presumably a replica is as resilient to repeated moldings as is a master is made by MAP.

3.7 Conclusion

It has been shown that by applying μTM, the technique of MAP can be converted from a serial process to a parallel one. Due to the favorable physical properties of PDMS, particularly its low Young's modulus, a wide variety of geometries, including undercuts and high-aspect-ratio shapes can, be replicated. The low surface energy of

PDMS, which wets master structures well, enables replicas to be made quickly and easily with sub-100 nm resolution.

MA-μTM has been developed and used to form replicas that have closed loops, greatly expanding the possible topologies that can be replicated. Structures from simple arches to more complex coils and tables have been demonstrated. Membranes have been used to replicate free-moving parts, as well as to facilitate the release of fragile structures such as cantilevers. Despite some practical limitations, the flexibility of PDMS seems to enable some truly incredible shapes to be replicated, such as a 75 μm long tunnel. Horizontal membranes have also been shown in the replica of a tunnel with an intentional 'skylight'.

The proof-of-principle studies have been performed to use μTM for the mass production of MAP made microstructures. It has been shown that numerous molds can be made from a single master and that numerous replicas can be obtained from a single mold. Using these techniques in conjunction with MA-μTM will enable a host of microstructure of various geometries to be mass produced rapidly and cheaply.

Chapter 4: Polymeric Microstructure Metallization

4.1 Introduction

Previous chapters have shown that MAP is an effective way to create 3-D polymer microstructures; however, to be applicable in MEMS devices, additional functionality, such as electrical conductivity, must be incorporated. Electrical conductivity is fundamental for transferring information about a microsystem to the macroscopic world and for powering the microsystem. There are two strategies for patterning metal in three dimensions. The first is directly writing the pattern with a focused laser or stylus and the second is selectively coating an existing 3-D structure with metal. Both approaches have been demonstrated, and they will be the subject of this chapter.

4.2 Direct-Write Metal Patterning Techniques

Direct-write techniques for patterning metal in three dimensions include stylus-based methods such as localized electrochemical deposition (LECD) and laser-based methods such as laser chemical vapor deposition (LCVD) and multiphoton absorption metallization (MAM).

During LECD a finely-pointed metallic probe is placed in close proximity to a conductive substrate that is immersed in a metal-plating solution.[84] By applying a voltage between probe tip and substrate, metal can be reduced at the tip. Moving this probe tip in three dimensions allows arbitrary 3-D patterns to be created. LECD has been

used to create microcoils of nickel with a diameter of approximately 1 mm and line width of 100 μm.[88] Line widths depend on the size of the tip and can be made as small as 10 μm with speeds on the order of several μm/s. While LECD can fabricate metallic parts in three dimensions it has not been used for MEMS devices, probably because of the poor mechanical properties of the microstructures and the difficulties involved in the experimental setup.

LCVD uses localized heating at a laser focal point for the chemical transformation of a metal containing vapor into a solid metal and gaseous byproducts.[84] A generic chemical equation for this process is:

$$ML_{n(g)} \rightarrow M_{(s)} + nL_{(g)}.$$

The reaction takes place by focusing a high-powered laser into a closed chamber containing the reactive species.[89] Metals that have been used include nickel, tungsten, chromium, and iron. Resolution is limited to the focal spot size and can approach 1 μm. Multimaterial parts can be made easily by exchanging the metal vapor.

The method of metal patterning we chose to study was MAM, primarily because the equipment is the same as that needed for MAP. MAM is related to LCVD in that a laser focal point is used to spur a chemical reaction, except in MAM the starting materials are in the condensed phase. The sample may consist either of a metal precursor dissolved in a liquid[90,91] or suspended in a solid matrix, such as a polymer film.[92,93] Since multiphoton absorption is spatially localized, it can be used to pattern in three dimensions, as is done in MAP. However, fine metallic microstructures do not have the mechanical rigidity to support themselves, unlike the highly cross-linked polymeric microstructures created with MAP. There has been only one example in the literature of

a 3-D metallic microstructure created with MAM;[94] otherwise 2-D patterns have been generated. It is possible to fabricate 2-D patterns atop 3-D microstructures however, thereby patterning a conductor in three dimensions;[95] I will now describe this process in more detail.

4.3 Direct-Laser-Writing of a Conductor in Three Dimensions by MAM

4.3.1 Experimental Details of 2-D Silver Patterning

Our approach was inspired by previous work that used an argon-ion laser to deposit silver on a substrate from silver nitrate in liquid N-methyl pyrrolidone or in a film of polyamic acid.[96,97] Samples were prepared by dissolving 0.25 grams of polyvinylpyrrolidone (PVP, molecular weight 40,000 g/mol) in 10 mL of ethanol and adding to that a solution composed of 0.4 grams of silver nitrate in 2 mL of deionized water. This colorless solution was stirred for 25 minutes in the dark, during which time its color changed to dark yellow/orange. The surface of a one-inch-square piece of glass was modified with 3-acryloxypropyltrimethoxysilane. The glass was covered completely in the polymer solution and then a film was spin coated at 2000 rpm for 30 seconds. The film was baked at 110 °C for 10 minutes. The thickness of the film was approximately 1 μm, as measured by atomic force microscopy (AFM). Fabrication of silver structures took place on an upright multiphoton microscope with the same system used for MAP as described in Chapter 2. Once the laser had been focused at the surface of the glass slide, metal patterns were created by movement of the computer-controlled sample stage. Following silver deposition, the sample was washed in ethanol and then water. No

deposition of metal was observed at any intensity when the laser was not modelocked, which substantiates the multiphoton nature of the deposition process.

4.3.2 Silver Pattern Characterization

Figure 4.1 shows scanning electron microscope (SEM) images and transmitted light optical micrographs of the results of typical experiments. The patterns were created using a 20×, 0.5-NA objective to deliver 35 mW of power to the sample. The lines were created by translating the sample at a velocity of 80 μm/sec.

Although in reflected-light microscopy the metallic features appear quite shiny, the SEM images in Figure 4.1 show that the lines are composed of agglomerated silver

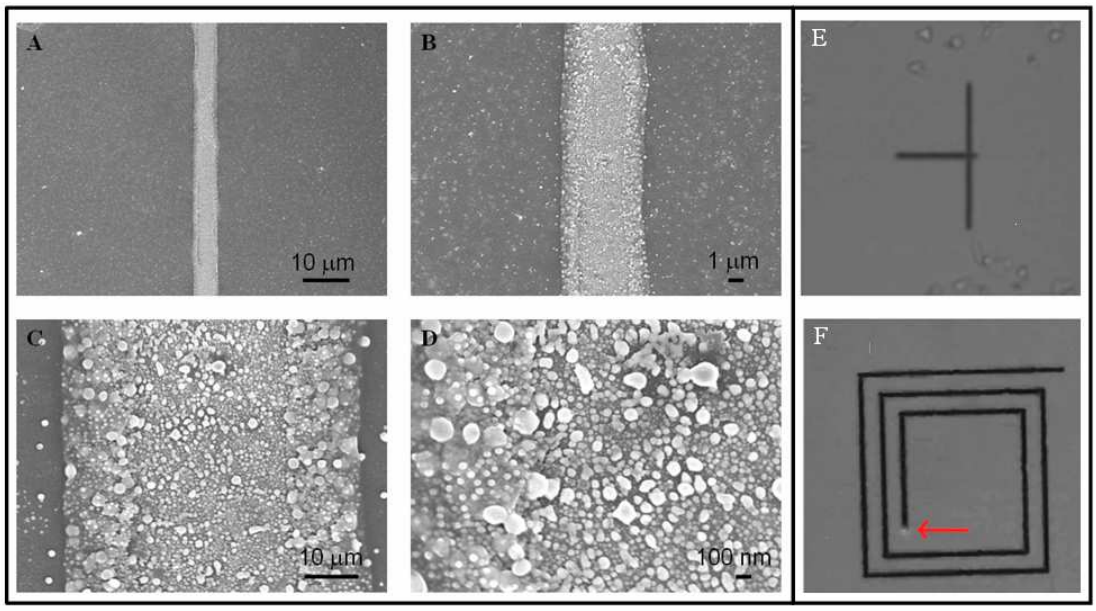

Figure 4.1 SEM images of representative photodeposited silver structures at different degrees of magnification. Panels (B)-(D) show close-ups of the line in panel (A). (E,F) Transmitted-light optical micrographs of deposited silver patterns. In (E) the 50-μm long vertical line was created first and the horizontal line was drawn from right to left starting at a position far from the vertical line. Deposition only commenced on the horizontal line when the laser focus reached the vertical line. The arrow in (F) indicates the position of the laser focus. Note that the silver luminesces as it is deposited. The spiral in this image is 100 μm across.

nanoparticles ranging in diameter from tens to hundreds of nanometers. The nanoparticles are interconnected, but because they do not form a continuous film they are not conductive. The lines are on the order of 5 μm across, and lines that are approximately 1 μm across can be fabricated using lower powers and faster scan speeds. These feature sizes are larger than might be expected from the diffraction limit, which suggests that local heating plays an important role in the deposition process. In support of this idea, as illustrated in Figure 4.1E it is more difficult to initiate deposition in a pristine portion of the sample than it is at the edge of a feature that has been deposited previously. Additionally, while metal is deposited across the diameter of each line, there are thicker ridges apparent at the edges of the lines.

To characterize the topology of the deposited lines an AFM study was performed. Representative results from this study are shown in Figure 4.2. Once again, the line can

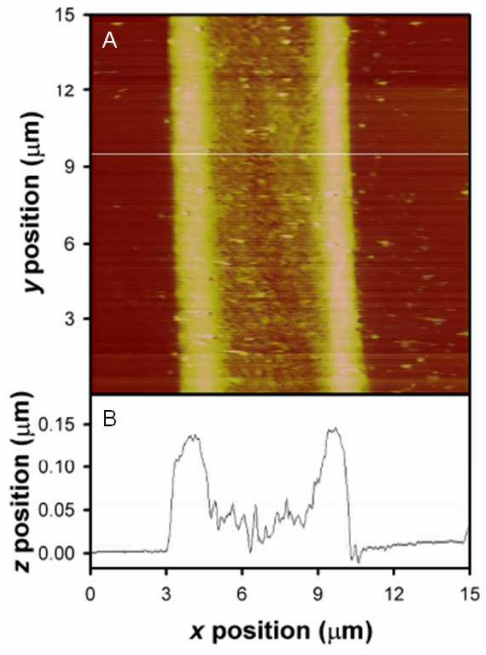

Fig. 4.2 Typical AFM image (A) and profile (B) of a photodeposited silver line. The horizontal line in (A) denotes the position of the profile in (B).

be seen to be comprised of individual nanoparticles with diameters up to hundreds of nanometers. Statistics obtained from several images indicate that the centers of the metallic lines are 21 ± 9 nm thick and the ridges at the edges of the lines are 126 ± 17 nm thick. Because the height of the centers of the lines is considerably less than the apparent diameter of many of the nanoparticles, we can conclude that the deposition process creates particles that are significantly oblate.

4.3.3 Silver Deposition Mechanism

We can use the two observations from Figure 4.1E and 4.1F along with SEM and AFM results to shed light into the metal deposition process. Stellacci et al. embedded silver nanoparticles into a polymeric matrix and were able to grow them via MPA;[98] we believe that a similar process is at work in our system. Figure 4.3 shows the transmission electron microscopy image that reveals the polydisperse silver nanoparticles in the PVP/silver nitrate solution that gives it its yellow-orange color.

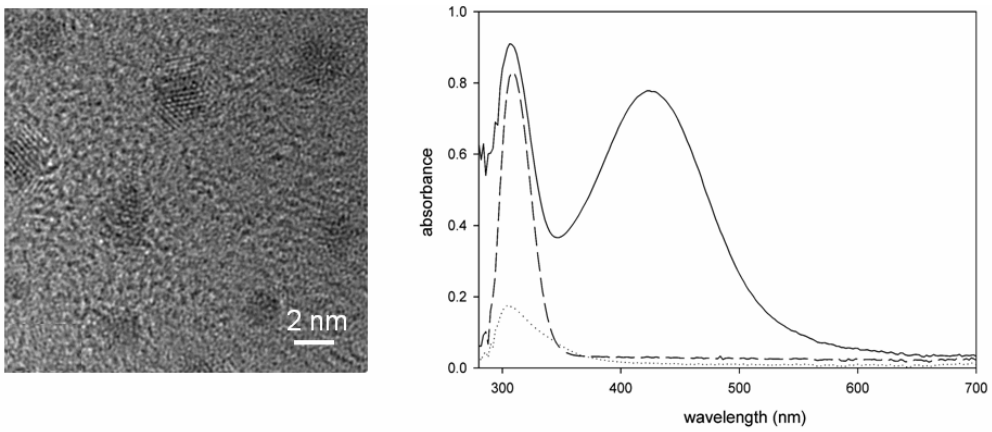

Figure 4.3 Left: TEM micrograph of silver nanoparticles obtained from the yellow-orange solution of $AgNO_3$ and PVP in ethanol. Right: UV-visible absorption spectra of the PVP in ethanol (dotted line), $AgNO_3$ in ethanol (dash line), and $AgNO_3$ and PVP in ethanol (solid line).

One possibility for the growth mechanism is that two-photon absorption into the plasmon band of these silver nanoparticles deposits heat that causes them to grow by electroless deposition. As shown in Fig. 4.1F, the silver features luminesce as they are deposited, which is consistent with strong luminescence from silver clusters from the literature.[99] If there is enough absorption by the clusters to generate luminescence, heating is expected to be present as well. This mechanism is consistent with the seeding of deposition by existing features, as in Figure 4.1E. In the areas in which silver clusters have not been deposited, the existing concentration of clusters may not be sufficient to deposit enough heat to promote deposition without increasing the laser intensity, whereas in the areas where silver has been deposited the concentration of absorbers is high enough to facilitate deposition at lower intensities. The ridges in the deposited lines may therefore result from deformation of the polymer film due to heating in the deposition process. However, the actual photodeposition mechanism is likely to be more complicated. Preliminary experiments on the wavelength dependence of the deposition process demonstrate that the efficiency of the process is linked more closely to the absorption spectrum of the polymer host than to that of the silver nanoparticles in the film, suggesting that it is photoreduction by PVP that is responsible for silver deposition. One possibility that is consistent with these observations is that existing silver features promote further silver deposition via local electric field enhancement by the silver particles that increase the effective two-photon absorption cross-section of the PVP. The microscopic details of the deposition process are a subject of continuing investigation.

4.3.4 Making the Silver Patterns Conductive by Copper Electroless Enhancement

The laser-deposited silver patterns are not conductive (resistance >20 MΩ) because of the granular nature of the silver. To make the silver patterns conductive they were enhanced electrolessly using a copper plating bath consisting of 3 g of $CuSO_4$, 4 g of NaOH, and 14 g of sodium potassium tartrate (Rochelle salt) in 100 mL of deionized water, which was combined in a 10:1 ratio with formaldehyde (37 wt %) before use.[100] Glass samples containing silver patterns were immersed in the solution for 7 min, after which they were immersed in deionized water, dried, and inspected using both transmission and reflection optical microscopes. Upon sufficient copper growth, the transmission image is opaque in the metallized regions and the reflection image shows shiny, copper colored lines. Samples that did not meet these criteria were placed back into the enhancement solution for an additional 3 min. All enhancement times were within the range of 7-13 min. Figure 4.4 shows the entire process to fabricate conducting patterns by MAM.

To characterize the conductivities of enhanced wires, 28 samples were prepared as described above. A gold wire with a diameter of 0.0005 in. (Sigmund Cohn) was glued to each lead in each four-point conductivity sample using Dupont 4929N silver paste. Conductivity measurements were made by using a programmable current source to apply a current ranging from -100 μA to +100 μA through the sample via two leads. A digital multimeter was used to measure the voltage across the sample via the other two leads, and the resistance of the sample was determined from the slope of the resultant current-voltage (*I-V*) curve. The lateral dimensions of the samples were measured using

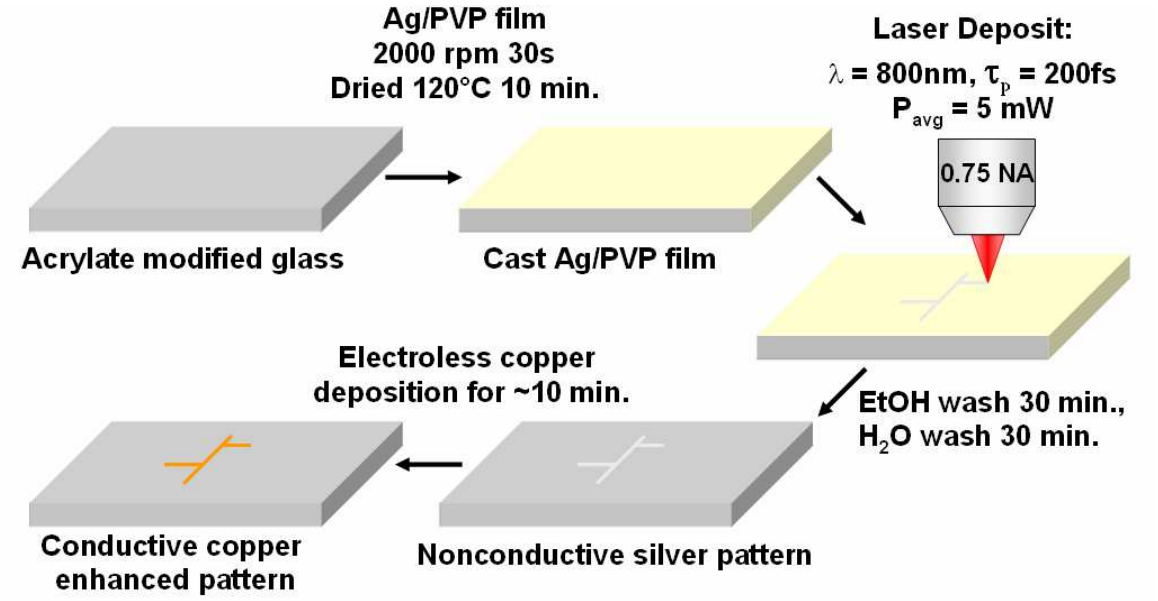

Figure 4.4 Schematic diagram for the direct laser writing of conductive wires onto glass substrates. A film of $AgNO_3$/PVP is cast onto an acrylate-modified glass substrate that is then exposed to focused, ultrafast, near-infrared radiation. The laser photoreduces Ag^+ onto existing Ag nanoparticles to form a nonconducting pattern of polydisperse Ag nanoparticles. This pattern is then electrolessly enhanced with copper to render it electrically conductive.

a scanning electron microscope (SEM). The thickness of the lines was measured using an AFM in tapping mode.

4.3.5 Conductivity Characterization

Shown in Figure 4.5A is a reflection optical micrograph of a typical four-point conductivity structure after copper enhancement and attachment of the gold leads. The deposited wires are shiny and metallic in appearance. Peel tests of the enhanced structures with Scotch tape[100] demonstrate complete adhesion. A representative *I-V* curve for the enhanced structures is shown in Figure 4.5 C. The plot is linear, and the slope yields a resistance of 2.35 Ω for the stretch of wire between the four leads. In total, 28

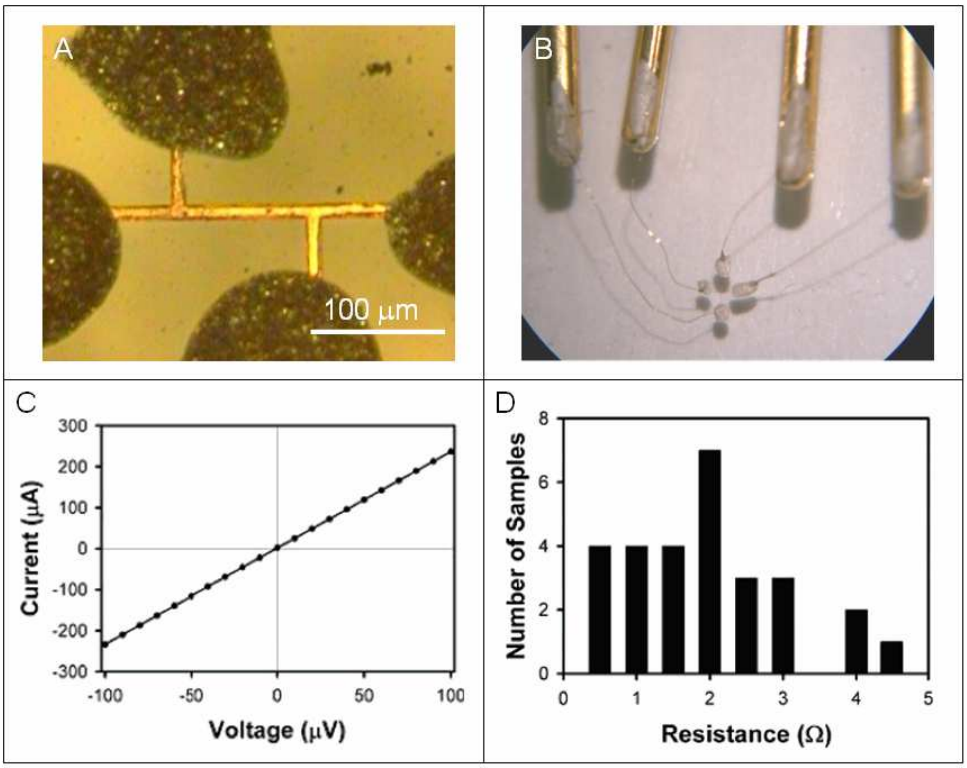

Figure 4.5 A) An optical micrograph of a copper-enhanced silver pattern that has been wired for a four-probe resistance measurement. B) Lower magnification micrograph of a wired sample such as the one shown in (A). C) Representative *I-V* curve data for a four-probe sample. The slope indicates a resistance of 2.35 Ω. D) Histogram for 28 identical samples with an average resistance of 2.4 ± 1.5 Ω.

silver four-point patterns were enhanced with copper, and the resistance data from these samples are summarized in the histogram in Figure 4.5 D.

On the basis of the data in the histogram, the average resistance of the common stretch of wire is 2.4 ± 1.5 Ω. To estimate the conductivity of the copper, it is necessary to determine the dimensions of the regions of the wires over which the resistance was measured. The lateral dimensions of the copper enhanced wires were measured via SEM. The average length was 90.6 ± 1.0 μm, and the average width was 9.5 ± 0.5 μm. Typical electron micrographs are shown in Figure 4.6 A and B. The cross-sectional area of the wires was measured using AFM. As shown in Figure 4.6 C and D, the wires are

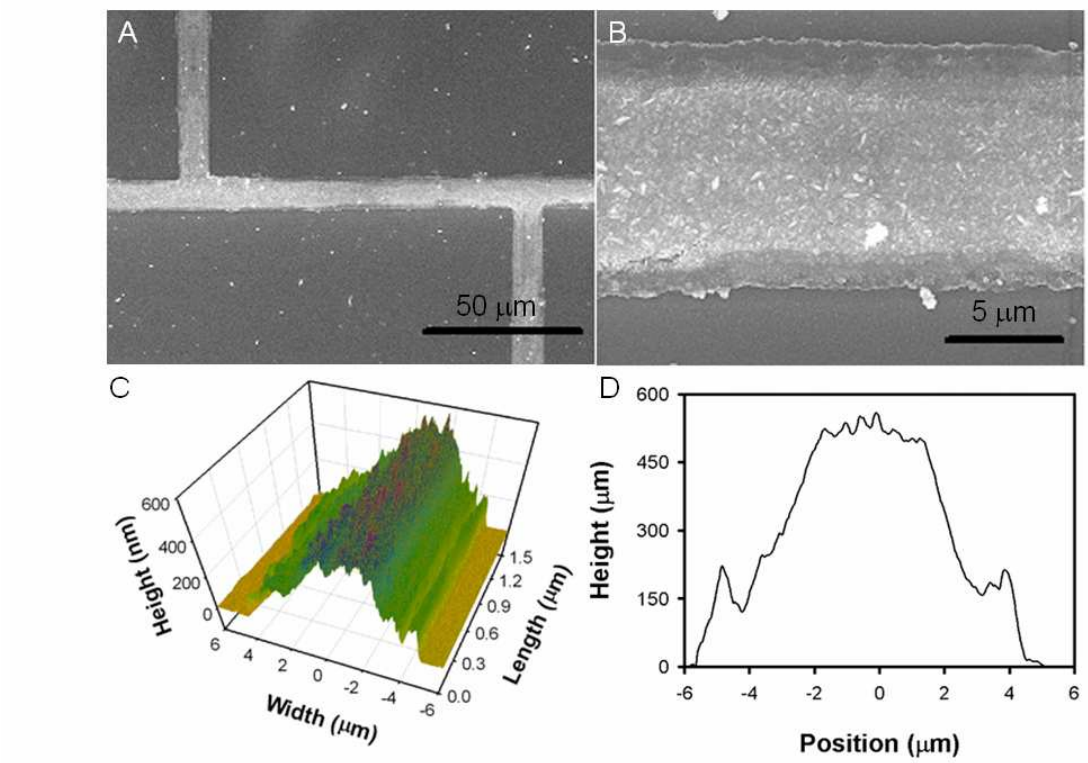

Figure 4.6 A, B) SEM micrographs of copper-enhanced four-probe sample for the measurement of length and width. C) Topological profile of wire obtained by AFM. D) Representative line scan from C.

approximately semicircular in cross section. This cross-section is in stark contrast to the one shown in Figure 4.2 before enhancement, where the silver structures are higher at the edges than in the middle. This phenomenon is believed to be related to deformation of the polymer film during silver deposition. There is still evidence of residual ridges at the edges of the enhanced lines, but the fact that the center of the lines enhances more efficiently than the edges suggests that there is less silver present in the ridges initially. The average thickness of the enhanced wires is 575 ± 150 nm, and the average cross-sectional area as determined from analysis of 4 μm lengths of wire from a dozen samples is 3.75 ± 1 μm^2. The conductivity, ρ, of a wire is given by the equation

$$\rho = \frac{L}{A \cdot R} \quad , \qquad \text{(eqn. 4.1)}$$

where *A* is the cross-sectional area, *L* is the length, and *R* is the resistance. On the basis of our data, the conductivity is found to be $1.0 \pm 0.7 \times 10^7\ \Omega^{-1}\ m^{-1}$. This value is within a factor of 6 of the $5.96 \times 10^7\ \Omega^{-1}\ m^{-1}$ conductivity of solid copper metal.[101] The lower conductivity of our wires is in line with previous measurements of electrolessly deposited copper[102] and is most likely due to the porosity of the copper layer. In addition, it is known that the underlying silver seed layer is not conductive, and the ridges are most likely not conductive either. As a result, the conductive cross-sectional area is likely to be roughly a third smaller than we have measured; this suggests that the conductivity of the electrolessly deposited copper is within approximately a factor of 4 of that of the bulk metal. The maximum current sustainable in these wires was approximately 100 mA. At high current, the wires exhibited localized melting at bottleneck points. Such bottlenecks arise from local inhomogeneities in the film that may be due to surface contaminants such as dust. Preparation and handling of samples under clean room conditions would presumably help to alleviate this problem. Conductive lines with widths as small as 1.5 μm have been fabricated with this technique. The resistance of these lines was on the order of 200 Ω, due to the considerably smaller cross-sectional area in comparison with the lines discussed above. It may be possible to improve the conductivity by performing additional electrodeposition of copper after electroless deposition has been used to make the wires conductive, as electrodeposited wires tend to be less porous.

4.3.6 Extension into Three Dimensions

The conductive patterns described thus far are 2-D but can be made 3-D if the $AgNO_3$/PVP film is cast onto a substrate having 3-D features. The experimental

procedure is shown in Figure 4.7. To prepare a sample like the one shown in Figure 4.7, a film of $AgNO_3$/PVP was spin coated over a substrate with a bridge made by MAP, and lead wires were patterned on the glass under the same conditions as before. A line was also made under the bridge; however, the film was too thin to allow deposition onto the bridge itself. After the lead wires and the wire under the bridge were made, a drop of the $AgNO_3$/PVP solution was added and allowed to dry in an oven at 110° C for 10 min. This drop-casting technique provides a thicker film than does spin-casting. A 40×, 0.75-NA objective was used to create a silver pattern on the bridge with a laser power of 3 mW at the sample. The silver was patterned on the bridge at a scan rate of about 1 μm/s. The scan speed was much slower on the bridge than on the substrate as a lower laser power was used to pattern silver on the bridge, both to prevent damage on the bridge and

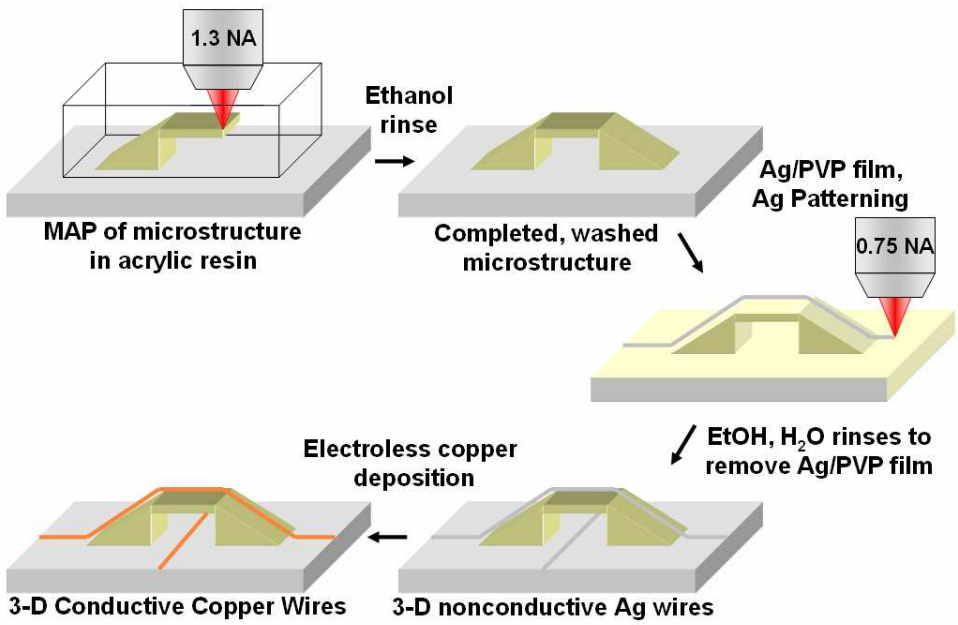

Figure 4.7 Five-step procedure for patterning 3-D wires. First, a microbridge is made by MAP. The completed bridge is washed and a Ag/PVP film is cast on top of the microstructure. Direct laser writing is used to create silver patterns in three dimensions. Following the rinsing of the film, the silver lines are made conductive by electroless copper enhancement.

because there was some uncertainty in determining the height of the surface of the bridge. The uncertainty arose because the line was made by hand with a joystick to control the stage position and not with a computer. A computer controlled stage is capable of scanning more accurately, but the system at the time could not smoothly coordinate motion in the x-z or y-z planes, only in the x-y plane (normal to the optical axis). After deposition of the silver, the sample was washed in ethanol and water. The sample was electrolessly enhanced in copper solution, and the resistances of the wires above and below the bridge were measured by the four-point method.

This hybrid polymer/metal structure is shown in Figure 4.8 and demonstrates the ability to pattern wires in three dimensions that can cross one another without shorting. As mentioned above, it is necessary to perform two separate silver deposition steps to create wires both on the substrate and across the bridge. If the $AgNO_3$/PVP solution is spin-cast onto a polymer microstructure, a circular region forms around the structure that

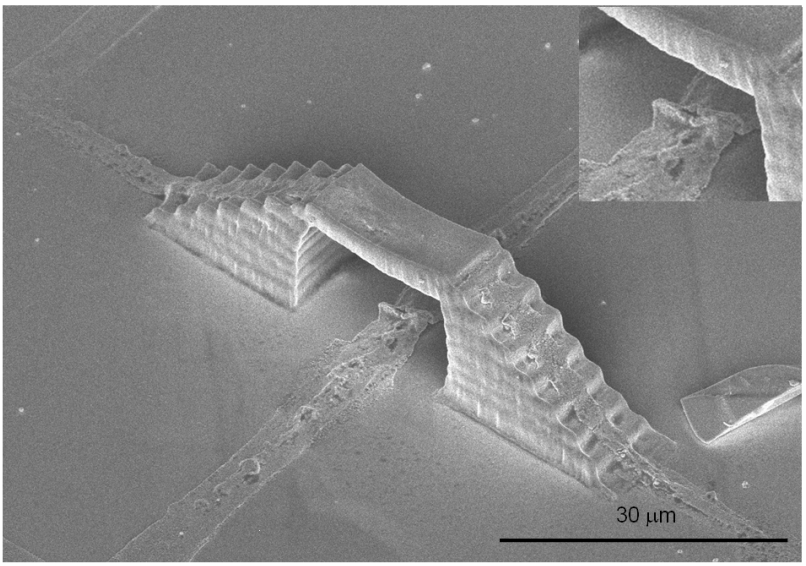

Figure 4.8 Field-emission SEM images of a polymeric bridge with conducting copper wires patterned across and below it. The inset shows the buckling of the wire under the bridge.

does not contain any film. This moat region, which extends for about 5 μm around the structure, makes formation of continuous silver lines emanating from the structure impossible. The reason for the formation of the moat is not entirely clear, but probably is related to the polymer solution wetting the acrylic microstructures poorly compared to the glass surface, which leaves the structure and the area immediately around it with little or no film. Thus, after initial patterning of silver wires on the substrate, a second film was made by drop-casting. This film made deposition of silver possible on and under the bridge, as well as in the moat region immediately adjacent to the structure. However, outside the moat region this film was too thick to allow the silver patterns to contact the substrate and was away when the film was rinsed off. While the second film does enable deposition in the moat region, the film atop the bridge is still quite thin. The SEM image in Figure 4.8 shows a polymer bridge with a copper coated silver wire running above and below it. Both wires are approximately 100 μm long and 5 μm wide. While the wire is continuous as it crosses the bridge, it is apparent that less metal has been deposited on the segment of the wire on top of the bridge. As a result, the wire that passes over the bridge has a resistance of 178 Ω, whereas the wire going under the bridge has a resistance of 29 Ω. There was no observable electrical cross talk between the two wires. For both wires, the conductivity is less than was observed for lines deposited on an open substrate. We did not attempt to measure the cross sections of these particular wires because they are not highly uniform, and because the area under the bridge is not accessible. In the case of the wire passing over the bridge, the decreased conductivity is almost certainly due to the thinness of the initial silver layer. For the wire passing under the bridge, the decreased conductivity probably arises from the buckle in the wire shown in the inset of Figure 4.8.

We have observed that thick films have a tendency to ablate if the focal point is positioned below the surface of the substrate. This effect likely stressed the silver pattern under the bridge, causing it to buckle. It seems, therefore, that film thickness critically affects ability to pattern the silver using MAM. Once again, it is likely that additional electrodeposition of copper could be used to improve the conductivity of the deposited wires.

In summary, the fabrication of conductive metal wires using MAM followed by electroless deposition of copper has been shown. This technique was combined with MAP to add conductive features to polymeric microstructures. These results demonstrate that 3-D metal/dielectric hybrid structures can be created using MPA-based techniques for all of the fabrication steps. This technique expands the capabilities of MPA-based fabrication by making it possible to add electrical functionality to 3-D polymeric microstructures.

4.4 Patterning 3-D Conductors by Coated Existing 3-D Structures

Laser direct writing can create 3-D metallic patterns, but it is laborious compared to an alternative technique that coats existing 3-D patterns with metal. The basic scheme to pattern metal in three dimensions by surface modification is shown in Figure 4.9.

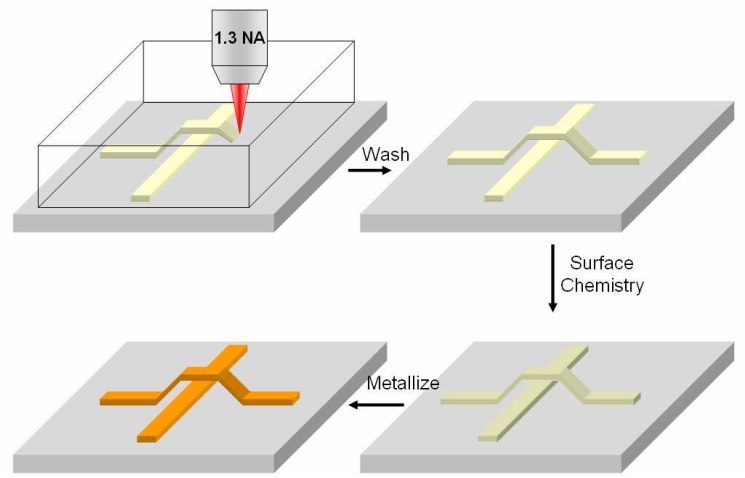

Figure 4.9 Four-step process to create 3-D conductors via surface coating. The first step is to fabricate a polymeric 3-D microstructure using MAP. After washing, the structures surface chemistry can be altered to make it reactive towards metallization. The final step is to coat the microstructure in metal, rendering it conductive.

A common way to coat polymers with metal is to use an adhesion promoting agent such as $SnCl_2$. Formanek *et al.* demonstrated that silver can be bound to a styrene-modified SCR500 resin that is treated with $SnCl_2$ after fabrication.[76,103] By making the substrate surface hydrophobic, silver can be reduced selectively onto polymeric microstructures from an aqueous solution. The conductivity of the coating is only about a factor of five lower than that of bulk silver.

We have developed a more general approach that enables selective surface modification by covalently bonding a new species to the polymer surface. The modified surfaces can be used to bind catalytic metals such as palladium, which can then be used to seed the electroless deposition of a number of metals or metal oxides.

4.4.1 Introduction to Polymer Surface Modification

The resins we most often use for MAP are acrylic-based, and are always multifunctional to ensure high cross-link density. This fact led us to believe there were unreacted acrylate moieties on the surface of microstructures made by MAP. We had found in the literature a precedent for the reaction of acrylate groups with nucleophiles, such as primary amines, via a Michael addition.[104,105] By reacting acrylic microstructures with diamines, such as ethylene diamine, we hypothesized that one amine group of the molecule should react with an acrylate group, thereby appending a primary amine to the polymer. This reaction is shown in Figure 4.10.

Although no direct detection of the amine presence has been performed, subsequent reactions on these modified surfaces strongly suggest that the amines are bound to the surface. This reaction, which is performed by immersing the sample in 20% (v/v) solution of ethylene diamine in ethanol for 20 minutes, has proved to be an effective method to add amine functionality to the polymer surface.

This reaction is also a useful way to modify the surface *selectively*, because

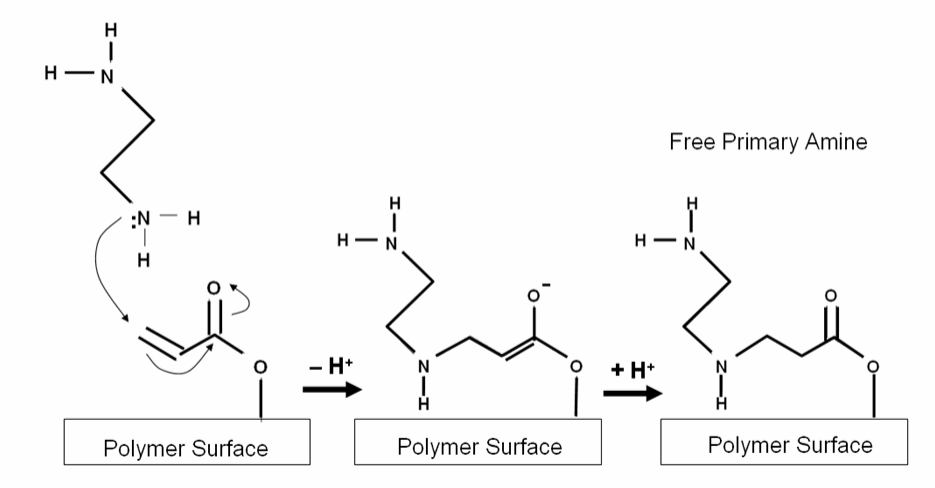

Figure 4.10 Michael addition of ethylene diamine onto an acrylate surface.

methacrylates undergo this reaction much more slowly than do acrylates. Indeed, compared to acrylates, methacrylates effectively do not react. Methacrylates and acrylates have similar chemistries in terms of polymerization. Methacrylates are slightly slower to polymerize and therefore require about twice the laser power for MAP, but structurally the monomers are available in the same vast range of compositions and their mechanical and optical properties are similar. Thus, hybrid structures can be made from methacrylate resin and then, in a second fabrication step, finished with an acrylate resin. The resulting structures can be reacted selectively with ethylene diamine, which can make possible a number of interesting reactions, such as metallization. Also, methacrylate groups can be used to modify the glass substrate surface for the adhesion of acrylate microstructures without fear of the substrate undergoing the same surface chemistry as the microstructure.

4.4.2 Selective Metallization

Reactive amine-coated surfaces can be useful for the seeding of a catalyst for metallization. Amine complexes of palladium form rapidly under mild reaction conditions. We have found that immersing diamine-modified acrylates in a solution of saturated palladium chloride in ethanol for 1 hr. is sufficient to coat the surface in a palladium complex. The palladium can then be used to catalyze electroless copper enhancement in a way similar to that used to create the silver pattern described in section 4.3.4. Using the same copper solution from section 4.3.4, polymeric microstructures can

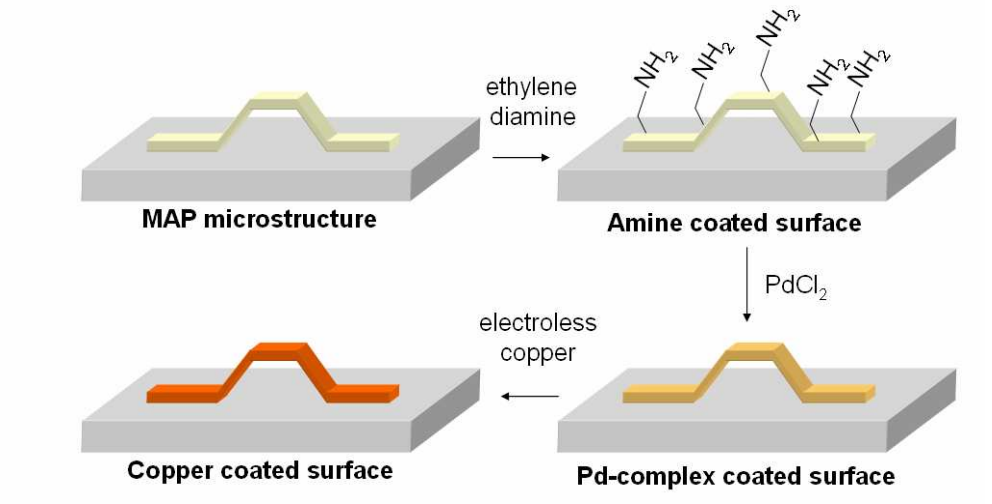

Figure 4.11 Metallization procedure for an acrylic MAP-made microstructure. The sample is treated in ethylene diamine to add amine functionality to the surface. The amines bind Pd^{+2}, which is reduced and used to catalyze the reduction of copper from an electroless plating bath.

be coated in copper metal in about 1 minute. This procedure is shown schematically in Figure 4.11.

This ability to metallize acrylic microstructures is very useful. Since methacrylates do not undergo the amine modification, this method can be used for the selective metallization of portions of a given structure. The two structures shown in Figure 4.12 are examples of hybrid methacrylate/acrylate microstructures in which part of the structure was made with methacrylate and then finished in acrylate resin.

The surface chemistry discussed thus far for copper-coating acrylate microstructures works with a success rate of about 50%. Over the past year and a half since its initial success, we have experienced periods of near 100% metallization and periods of near 0% metallization, with no apparent difference in reaction conditions. The cause for this fluctuation was difficult to pinpoint, but thanks to some previous work

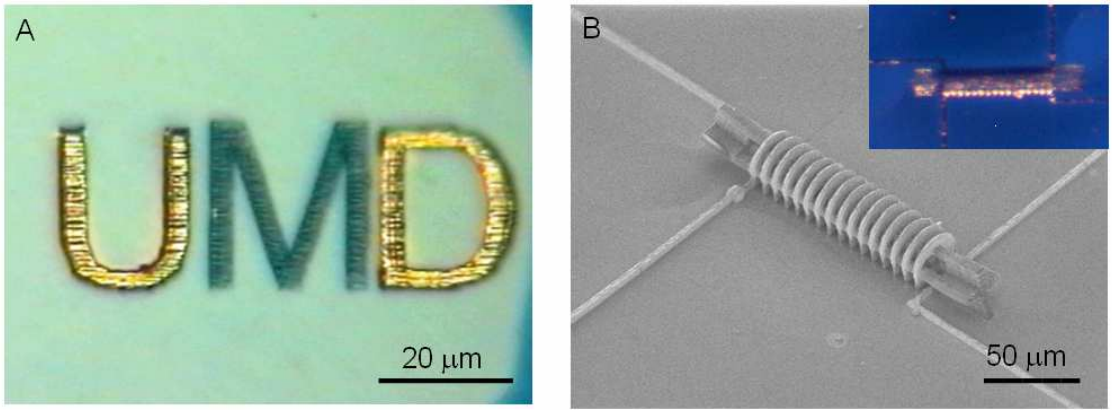

Figure 4.12 A) The letters 'U' and 'D' were made with acrylate resin and then the letter 'M' was made from methacrylate resin. The hybrid sample was then metallized following the procedure in Figure 4.11. This image was taken using a reflecting optical microscope and shows that no copper was deposited on the methacrylic 'M'. B) SEM micrograph of a 16-turn copper coated acrylate coil supported by a non-conducitve methacrylate core. The inset shows an optical micrograph of the same structure.

involving polymer surface modification, we believe we have narrowed down the problem to the oxidation state of the palladium.

4.4.3 Problems with Reproducibility of Metallization

Charbonnier and coworkers have reported on the surface treatment of polycarbonate films by first affixing nitrogen groups by NH_3 plasma treatment and then using these nitrogen groups to sequester Pd^{+2}.[106,107] They then proceeded to deposit nickel or copper electrolessly onto this palladium-seeded polymer. They found that nickel deposited very well but that copper did not. With the help of X-ray photoelectron spectroscopy (XPS) they concluded that the reducing agent in the nickel bath, hypophosphite, was first reducing the complexed Pd^{+2} to Pd^{0} which then catalyzed the reduction of Ni^{+2}. The copper solution, which has formaldehyde as a reducing agent, was not strong enough to reduce the Pd^{+2} and so failed to catalyze the reduction of Cu^{+2}. If

the Pd^{+2} surfaces were reduced first in a solution of hypophosphite then the copper electroless bath worked well to deposit the copper

.We performed a XPS analysis of our polymer samples and found similar results with regard to the oxidation state of the palladium. Four samples of polymer were prepared: 1) control sample, 2) a sample treated in ethylene diamine, 3) a sample treated with ethylene diamine then Pd^{+2}, and 4) a fourth sample treated with ethylene diamine, Pd^{+2}, and sodium hypophosphite. The XPS spectra for these four samples are shown in Figure 4.13.

After treatment in Pd^{+2}, XPS reveals that there is a mix of Pd^{+2} and Pd^{0} present on the surface, as is illustrated in the inset as a pair of shoulders at slightly higher binding

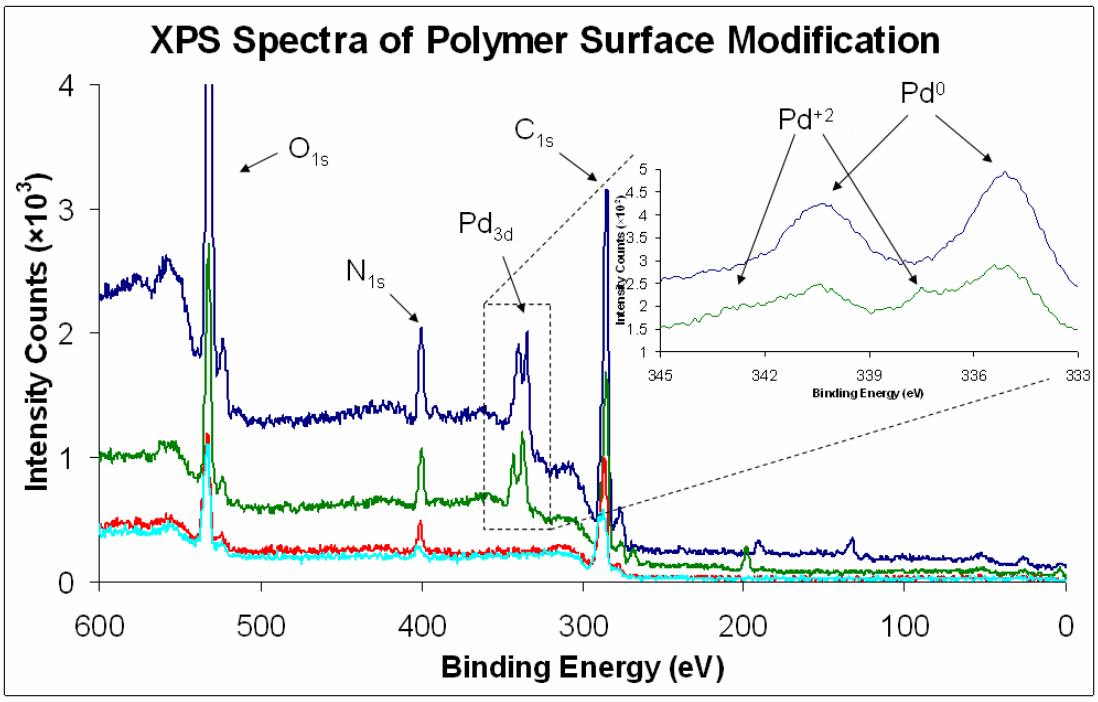

Figure 4.13 XPS spectra of four polymer samples at various stages of surface treatment. The control sample (light blue) shows the composition of the polymer which contains C, N, and O. The red spectrum shows the increase in surface N due after the binding of ethylene diamine. The green spectrum shows the presence of Pd^{+2} and Pd^{0} after treatment in Pd^{+2}, while the blue spectrum shows only Pd^{0} after reduction in hypophosphite.

energy than the Pd^0 peaks. The actual mechanism for the reduction of Pd^{+2} is not clear, and could possibly be caused by the polymer itself, but we believe this step is irreproducible. If the sample is reduced by hypophosphite, only Pd^0 is present in the XPS spectra. The end result is that after hypophosphite treatment, reproducible electroless copper growth is observed.

The experimental details for this modified procedure are as follows. Polymer samples made from a resin consisting of equal parts Sartomer SR-368 and Sartomer SR-399 with 3 wt. % Lucirin TPO-L (BASF) are fabricated on glass modified with 3-methacryloxypropyltrimethoxysilane. After fabrication, samples are washed in dimethylformamide and then ethanol. The sample is submerged in a 20% (by vol.) solution of ethylene diamine in ethanol for 20 min. Following this treatment, samples are washed three times, for about 1 min. each, in ethanol and then placed in an aqueous solution composed of 0.1 g/L $PdCl_2$ and 0.1 mL/L of concentrated HCl. After 15 min. in the Pd^{+2} solution the samples are dipped in ethanol for a minute before being placed in an 85° solution of 0.1 M NaH_2PO_2 for 10 min. Following that, the samples are dipped in water for 1 min. and then into the copper electroless solution for 5 minutes or more depending on the desired amount of copper. The copper solution consists of 0.6 M $NaKC_4H_4O_6 \cdot 4H_2O$ (Rochelle salt), 0.14 M NaOH, 0.28 M $CuSO_4 \cdot 5H_2O$, and 0.3 M EDTA.[107] The entire surface modification and metallization process can be completed in about 1 hour, and is highly selective towards acrylates and not methacrylates.

4.4.4 Electrical Characteristics of Copper Coated Polymer

The copper coating is electrically conductive, as in the case of the copper-coated silver lines. The conductivity has not been studied as systematically as it was in the case of the silver, but similar resistances for microstructures have been measured. For example, the structure shown in Figure 4.12B has a resistance of about 500 Ω and it is approximately 1,200 μm in total length and about 2 μm wide; the thickness was not measured but is approximately 100 nm. Given these dimensions, the conductivity of the coating is $1.2 \times 10^7\ \Omega^{-1}\ m^{-1}$, which is close to the value measured for copper-coated silver. Similar analysis on the sample shown in 4.14 also yields a conductivity of approximately $5 \times 10^6\ \Omega^{-1}\ m^{-1}$.

Although a detailed resolution study has yet to be performed, conducting patterns made with this method should have the resolution approaching that of MAP itself. A feature size as small as 200 nm should attainable, assuming a 100 nm polymer line width and a 50 nm metal coating.

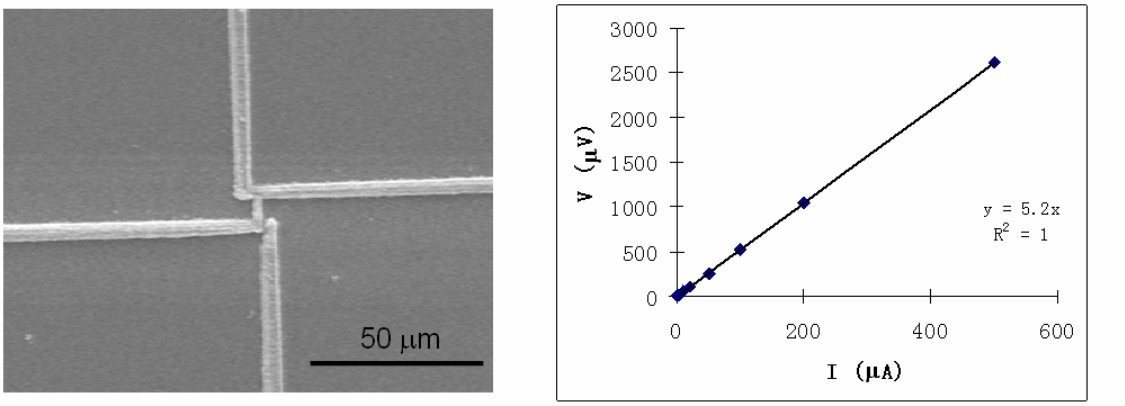

Figure 4.14 Left, an SEM micrograph of copper enhanced polymer sample wire that is approximately 2 μm wide by 5 μm long. Right, *I-V* curve for this sample showing a resistance of 5.21 Ω.

4.4.5 Metallization of Replicas

UV cured replica structures also can undergo the surface modification chemistry and subsequent metallization. Figure 4.15 shows a pair of pyramid replicas that have been copper enhanced.

One significant problem encountered when metallizing replicas is the leakage of resin beyond the form in the mold. The result is a thin film of polymer near the structure that is known as "flash." Figure 4.16 shows a copper enhanced pyramid surrounded by copper coated glass. This thin film could be eliminated by either reactive ion etching or by filling the mold via a capillary as is done in micromolding in capillaries (MIMIC).[2]

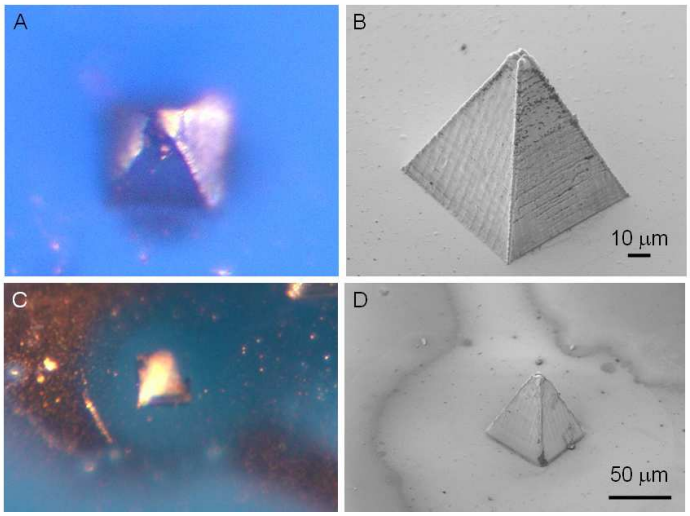

Figure 4.15 A) Optical image of a copper coated replicated pyramid. B) SEM micrograph of the sample from (A). C) Optical micrograph of unselective metallization due to a thin polymer film on the substrate. D) A scanning electron micrograph of the sample in (C).

4.5 Summary

Two methods to create conductive patterns in three dimensions have been demonstrated. The first method utilizes laser-direct-writing of silver by MAM and can be applied to 3-D substrates such as those created with MAP. Conductivity studies reveal that electrolessly grown copper, on top of these silver patterns, is somewhat less conductive than bulk copper. The second technique, which is experimentally more efficient and powerful, selectively metallizes polymeric microstructures made with MAP by controlling their surface chemistry. The Michael addition of a diamine onto an unpolymerized acrylate group is used to put amine functionality on the polymer surface. This is the gateway to a number of useful reactions, including metallization. Metal-coated polymer wires have been made with conductivities within a factor of 10 of bulk metal. The resolution of such structures should be only slightly less than that of MAP itself. In the next chapter, applications of this technique will be discussed.

Chapter 5: Applications of MAP

5.1 Introduction

A major goal of MAP technology is to create useful devices in conjunction with other microsystem techniques, such as photolithography and microfluidics, for use beyond the research laboratory. Such systems should ultimately be inexpensive, highly portable, and efficient for their particular application. No one yet knows exactly what the first killer application of such microsystems will be, but unquestionably its many advantages ensure that microsystem technology will be of great importance in the near future. At present, only simple devices made by MAP have been reported, and none have incorporated additional components to make more complex systems. However, this situation will soon change as much of the 'toolbox' for fabrication by MAP is complete.

The previous chapters have focused on solutions to issues with MAP, such as its limited throughput and lack of functionality, by using techniques such as micro-transfer molding (μTM) and surface modification chemistry. In this chapter functional devices will be described that take advantage of these solutions. The progress of a wide range of devices created in our laboratory will be described, in addition to selected applications from other groups. Applications are divided into four categories: electrical, optical, mechanical, and biological, although several devices span two or more categories. Current state-of-the-art devices in each category will be described, as well as some likely future applications. The chapter concludes with an outlook toward future improvements for MAP, such as the development of a technique to increase its resolution.

5.2 Electrical Applications

The ability to coat polymeric microstructures with metal enables the creation of true 3-D circuits or circuit elements. MAP could offer the promise of shrinking 3-D macroscopic electrical equipment, such as transformers or electric motors, down to the microscale in a way that is impossible using 2-D techniques such as photolithography. One such 3-D circuit element that we have created by MAP is a microinductor.

5.2.1 Microinductor

An inductor is a passive circuit element that resists changes in current by setting up a self-induced voltage. The induced voltage, or inductance, is caused by the change in the magnetic field that accompanies any current-carrying wire when the current in the wire changes. The ability of an inductor to resist changes in current is measured in henries (H). By definition, the inductance is 1 H when the current through a coil, changing at 1 A/s, induces 1 V across the coil.[108] For typical inductors the range of inductance is usually in the mH or μH range.

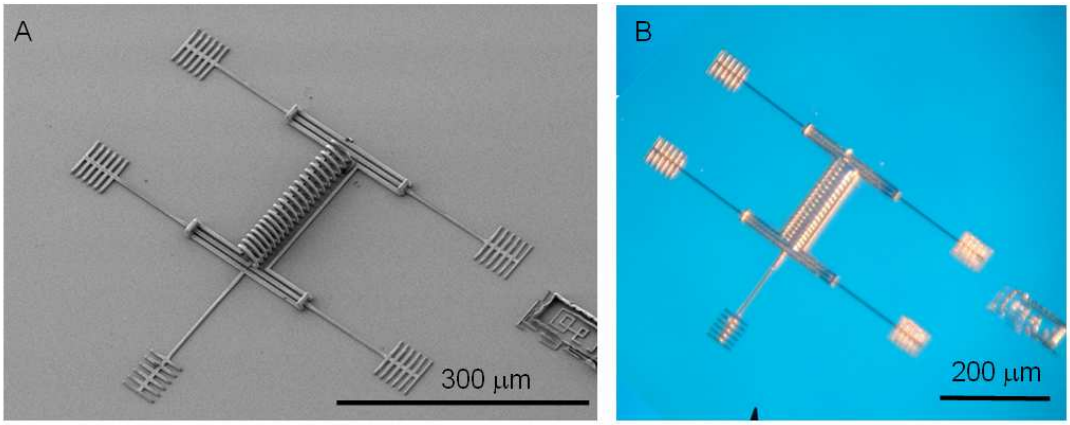

Figure 5.1 A) Electron micrograph of 20 turn inductor, length = 180 μm, diameter = 30 μm. B) Optical micrograph of the same structure showing the shiny copper coating.

Microinductors can be fabricated by MAP followed by surface modification and metallization (Figure 5.1). The coil portion of the circuit in Figure 5.1 was made in about 20 minutes. The four leads, terminated in contact pads, connect directly to the coil for 4-probe resistance and resonance measurements. The fifth contact pad is connected to ground and acts to ground the 'strip-line' wires that surround the coil and the leads close to it. The shielding wires 'bridge' the lead wires in four places to avoid shorting.

The inductance of a coil can be calculated from its dimensions and number of turns by the equation

$$L = \frac{N^2 \mu A}{l}, \qquad \text{(eqn 5.1)}$$

where L is the inductance (H), N is the number of turns, A is the area of a loop (m^2), l is the length (m), and μ is the permeability of the core material (H/m). Using this equation the theoretical inductance value for the coil shown in Figure 5.1 can be calculated:

$$L = \frac{20^2 (4\pi \times 10^7 H/m)(\pi (15 \times 10^{-6} m)^2)}{180 \times 10^{-6} m} = 2.0 \ nH$$

The inductance of this sample was measured by connecting the microinductor in series with a lock-in amplifier and measuring the voltage across the sample as a function of AC frequency with 100 μA of applied current. The inductor had a resistance of 220 Ω, and self-capacitance on the order of ~1pF.[109] This self-capacitance is an approximation, based on its dimensions, for the turn to turn capacitance. It should therefore act like an RLC circuit with resonance frequency, f_0 (Hz), at

$$f_0 = \frac{1}{2\pi\sqrt{LC}}, \qquad \text{(eqn 5.2)}$$

where *L* is the inductance (H) and C is the capacitance (F)[**]. The sample should have a resonance frequency of about 11.3 GHz. Strangely, a resonance was detected at 62 kHz, 6 orders of magnitude lower than expected. Initially, this resonance was thought to be caused by some sort of mechanical resonance of the spring-like structure. However, it was later determined to be an artifact of the Stanford Research 840 Lock-in Amplifier used for the measurement, as other lock-in amplifiers yielded no signal near this frequency. These data are shown in Figure 5.2.

The actual value of the inductance of these microcoils has not yet been well characterized. Despite shielding efforts to isolate stray inductance around the sample itself and the use of micro-coaxial lead-in wire, the inductance of the wires used to connect the sample is still similar to or higher in magnitude than that of the sample itself. The high resonance frequencies involved present additional complications in the measurements, such as the skin effect; therefore, these measurements are ongoing. Some changes we are considering to facilitate the measurements include making the coils

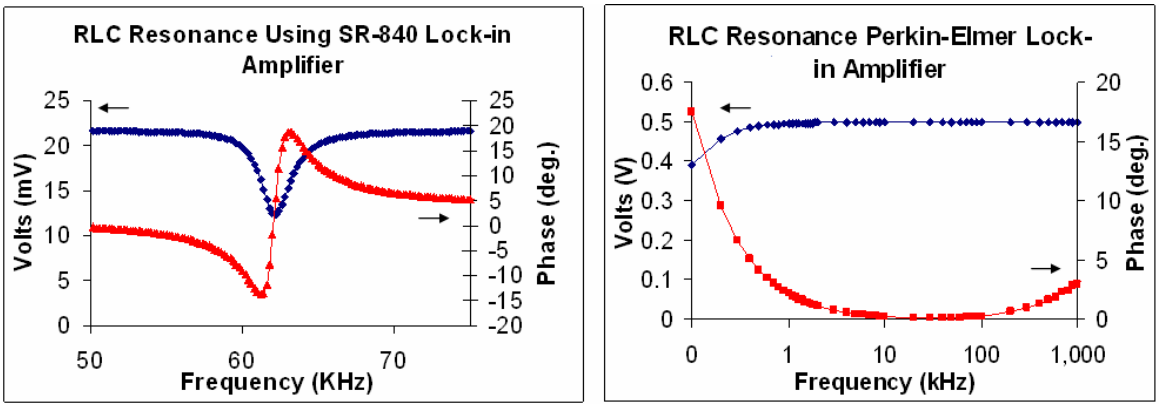

Figure 5.2 Left: The phantom resonance peak of a microinductor, which was an artifact of the SR-840 lock-in amplifier. Right: The same sample measured on a different lock-in amplifier showing no peak.

[**] The resistance does not affect the resonance frequency but it is inversely proportional to the Q-factor of the resonance.

slightly larger, using a ferrite core, and making these measurements at cryogenic temperatures at which the resistance would be greatly reduced. These changes would increase the inductance and the Q value of the coil, which should make measuring their inductance easier.

Inductors have numerous applications in electronic circuits such as filters, transformers, and oscillators. For microelectronics applications, real 3-D inductors are nearly impossible to make with conventional photolithography, and so they have been replaced by gyrator circuits. Gyrators are composed of transistors and capacitors in an arrangement that effectively simulates the response of an inductor. Thus, a circuit can be made to simulate a RLC filter without any inductor present at all. This method sidesteps the problem of not being able to fabricate a real inductor, but it fails to recreate all the features that inductors provide. For example, the simulated inductor cannot provide the expanding and contracting magnetic field that an inductor creates. This field is useful for magnetic resonance applications, magnetic actuation, transformers, and relay switches. The self-resonance frequencies of these microinductors should be in the GHz range, which is useful for communications devices, and can be lowered into the realm of MHz for applications in magnetic resonance. Microinductors with inductance values of just a few nanohenries have been used as rf coils in magnetic resonance force microscopy. [110]

5.2.2 Future Electrical Applications

Microscale NMR is an attractive application of small inductors because of the possibility of using a tiny volume of sample and the fact that the signal-to-noise ratio is inversely proportional to the diameter of the coil.[111] Tiny coils could also be fabricated

around microfluidic channels that are a part of a μTAS device. If these systems could be manufactured inexpensively it would be a vast improvement for μTAS.

5.3 Optical Applications

MAP, using optically transparent polymers, is well suited for the fabrication of micro-optical elements. The primary optical application for MAP by other groups has been the fabrication of photonic crystals.[48,112-117] Photonic crystals are structures having periodicity smaller than the wavelength of light, such that light propagation is prohibited because of diffraction. A band gap results, in which a range of colors cannot be transmitted through the material. An example of a 1-D photonic crystal is a Bragg reflector, which is commonly used in fiber optics. The reflector has a periodically varying index of refraction causing wavelengths that meet the diffraction criterion, to be reflected while others are transmitted. Scaling this concept to three dimensions requires the ability to pattern a periodic lattice of alternating refractive index. There are only a few ways to accomplish this other than MAP. One method is self-assembly, such as through the use of colloidal crystals or block copolymers. Photonic crystals can also be made by stacking 2-D patterns, but registration is difficult on the submicron scale. MAP is the only way to create 3-D patterns with complete freedom of geometry in a single fabrication step. While most photonic crystals will be highly periodic, one may engineer defects to have a desirable effect such as waveguiding or splitting a waveguide, as in a Y-junction. Photonic crystals made by MAP have been extensively reported in the literature with simple log-stack structures,[112] diamond unit cells,[114] spiral unit cells,[118] and with

engineered defects.[119] A functional distributed feedback micro-laser has also been made by MAP.[61]

While photonic crystals are of great interest, they suffer one severe problem: the need for high index contrast. To create a 'full stop' band gap an index contrast greater than 2 is necessary. Since polymers have an index close to 1.5, they cannot produce full stop gaps. However, recently progress has been made in patterning polymers by MAP and then replacing the polymer with a material having a higher index, such as silicon[120] or TiO_2.[70] These photonic crystals may be the first widespread successful application of MAP.

While our MAP setup allows for the fabrication of photonic crystals, we have not focused on this application. Instead, we have demonstrated a device that can electrically detect plasmon resonance in an individual gold nanowire and we have also fabricated micro-optical elements at the tip of fiber optics. These optical devices will be the subject of the next sections.

5.3.1 Electrical Detection of Au Plasmon Absorption

The plasmon absorption of noble metal nanoparticles has been known for over 150 years.[121,122] Plasmon surface waves are collective oscillations of free electrons at the surface of a metal in contact with a dielectric. A simple model can be envisioned when a metal nanoparticle experiences an alternating electric field (E-field), such as light. The free electrons of the metal are accelerated by the E-field and pushed to one side of the nanoparticle, leaving the other side positively charged. This electron cloud will be attracted back to the positive side of the nanoparticle by electrostatic attraction, and at

about the same time the E-field from the light will switch direction, pushing those electrons back. If the surface electrons oscillate at the same frequency as the incident light, the light is said to be resonant at the particle's plasmon frequency. Of course, what really happens is much more complex and depends on the type of metal, the refractive index of the surrounding medium, the size and shape of the particle, and the polarization of the incoming light. While it is not exact, this simple model can be used to visualize why particles of different sizes have different plasmon resonance frequencies. In general, the resonance frequency decreases (red shifts) with increasing particle size, and due to higher-order oscillation modes (quadrapole, etc.) the resonance peak also broadens.[123] Similarly, a nanowire will have two plasmon peaks, one for the short transverse axis and a red-shifted one for the longitudinal axis.

It is known that after excitation of a plasmon resonance the absorbed energy decays quickly into thermal energy.[124] This decay raises the temperature of the nanoparticle and can be used to localize heating, as in photodynamic therapy, or even to induce nanoparticle melting.[125] *In our experiments we detect this heating via a change in electrical resistance and then use it to infer information about the plasmon absorption.* This electronic plasmon detector therefore requires an electrically wired metal nanoparticle and an optically transparent substrate (to confine the photothermal absorption to the nanoparticle). Such a sample can be prepared by MAP followed by surface metallization according to the scheme in Figure 5.3.

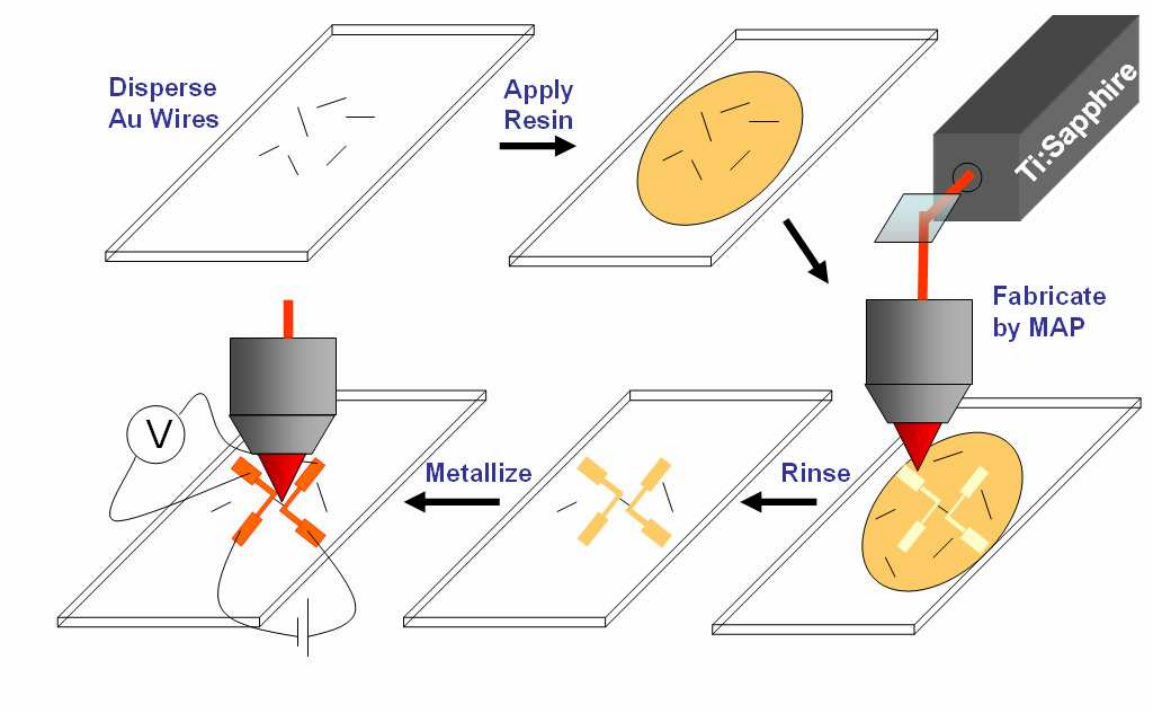

Figure 5.3 Preparation of the device to detect plasmon absorption electrically in nanoparticles. First, gold nanowires are dispersed on a methacrylate modified glass substrate. MAP is then employed to create polymer 'wires' connected to a particular nanowire. The polymer is coated with metal. Finally, a change in 4-probe resistance of the photoexcited nanowires is measured and compared to the resistance of non-excited wires.

In these experiments we have employed template-synthesized gold nanowires. Polycarbonate track-etched membranes with pore diameters of 10 nm have been used to create nanowires that are approximately 40 nm in diameter and 3-5 μm long. These nanowires show a plasmon absorption near 530 nm, corresponding to the transverse plasmon excitation. The longitudinal plasmon should be at a longer wavelength in the IR. Initially, these wires were created by electroless growth, but due to their non-uniformity an electrodeposition method is now used. Electrodeposition is performed by sputter coating one side of the polycarbonate template in silver and using the silver layer as the cathode in an electrochemical cell consisting of a DC current source, a platinum counter electrode, and an aqueous gold solution (Oromerse, Technic Inc.) (Figure 5.4).

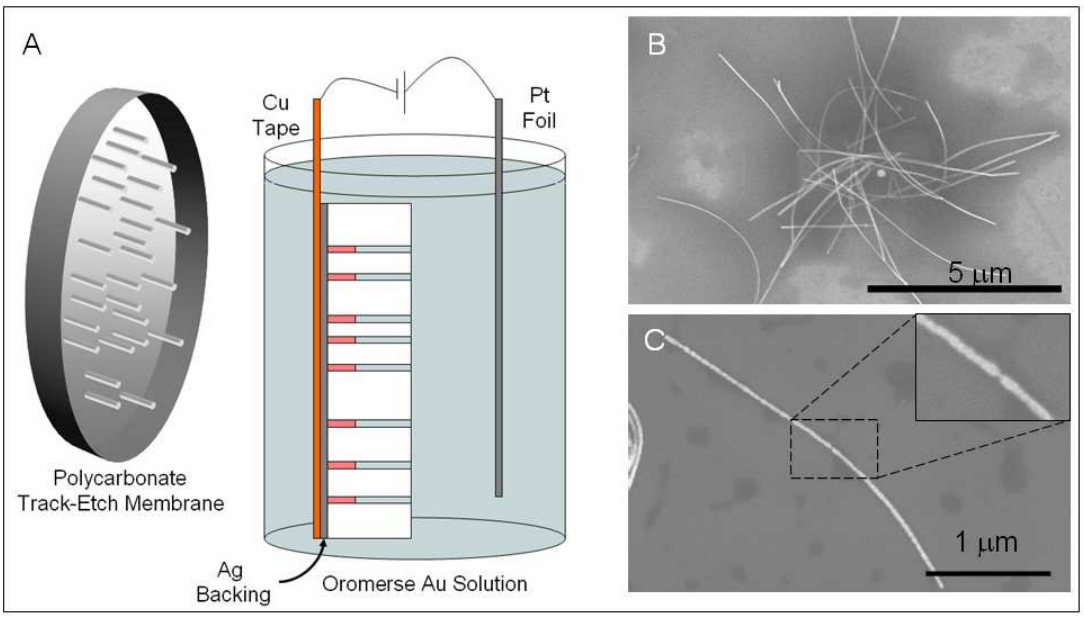

Figure 5.4 A) Electrodeposition setup for gold nanowire synthesis. B) SEM of typical electrodeposited gold nanowires. C) SEM of typical electrolessly-deposited gold nanowire. The inset shows non-uniformities in the wire.

Gold is deposited by applying pulses of DC current followed by periods of no current, which allows diffusion of depleted gold ions back into the pores.[126] Using this method, gold nanowires can be grown within the pores in several minutes. These wires can be released by dissolving the membrane in dichloromethane, which also solubilizes the nanowires.

After creating the Au nanowires they can be dispersed on a glass substrate and viewed on an optical microscope. Having the ability to see such nanostructures on an optical microscope means they can be incorporated into microstructures fabricated by MAP. Thus, surrounding the nanowires in a drop of prepolymer resin enables an individual Au nanowire to be 'tacked-down' and connected with polymer 'wires' (Figure 5.5).

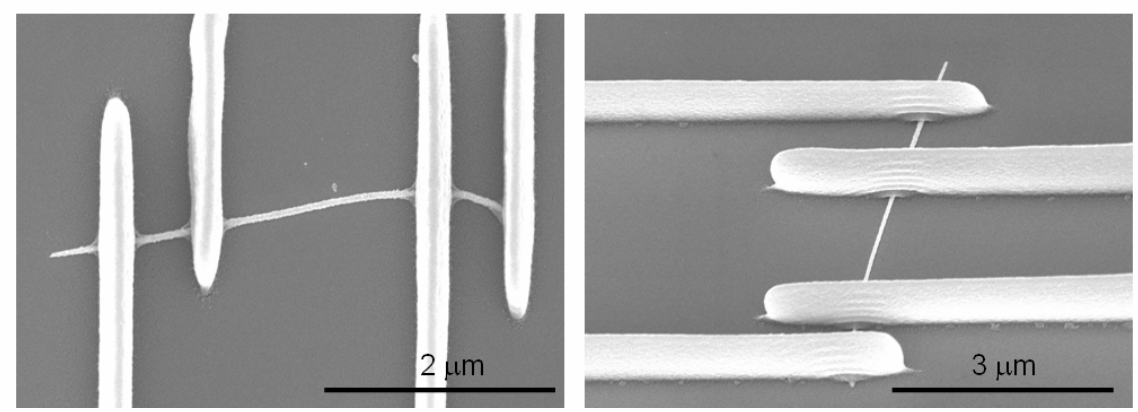

Figure 5.5 A 4-probe connection of polymer leads to an individual Au nanowire

The polymer leads can then be metallized using the scheme from Figure 4.12 to create an electrical connection through the nanostructure. The connection shown in Figure 5.6 can be used to measure the resistance of the nanowire. The resistance of nanowires is similar to the one shown in Figure 5.6, except made by electroless deposition instead of electrodeposition, was measured to be on the order of 100 Ω. This is close to the theoretical value of 56 Ω determined from the resistivity of gold, ρ_{Au} (2.44×10^{-8} W m), length, L (3×10^{-6} m), and cross-sectional area, A (1.3×10^{-15} m^2), of the gold nanowire using the equation

$$R = \frac{\rho_{Au} \cdot L}{A}. \qquad \text{(eqn. 5.3)}$$

Unfortunately, the electrolessly-deposited wires are extremely fragile and often break either during the electrical measurement or upon exposure to the laser. This breakage is likely due to the non-uniform cross-section, seen in Figure 5.4C.

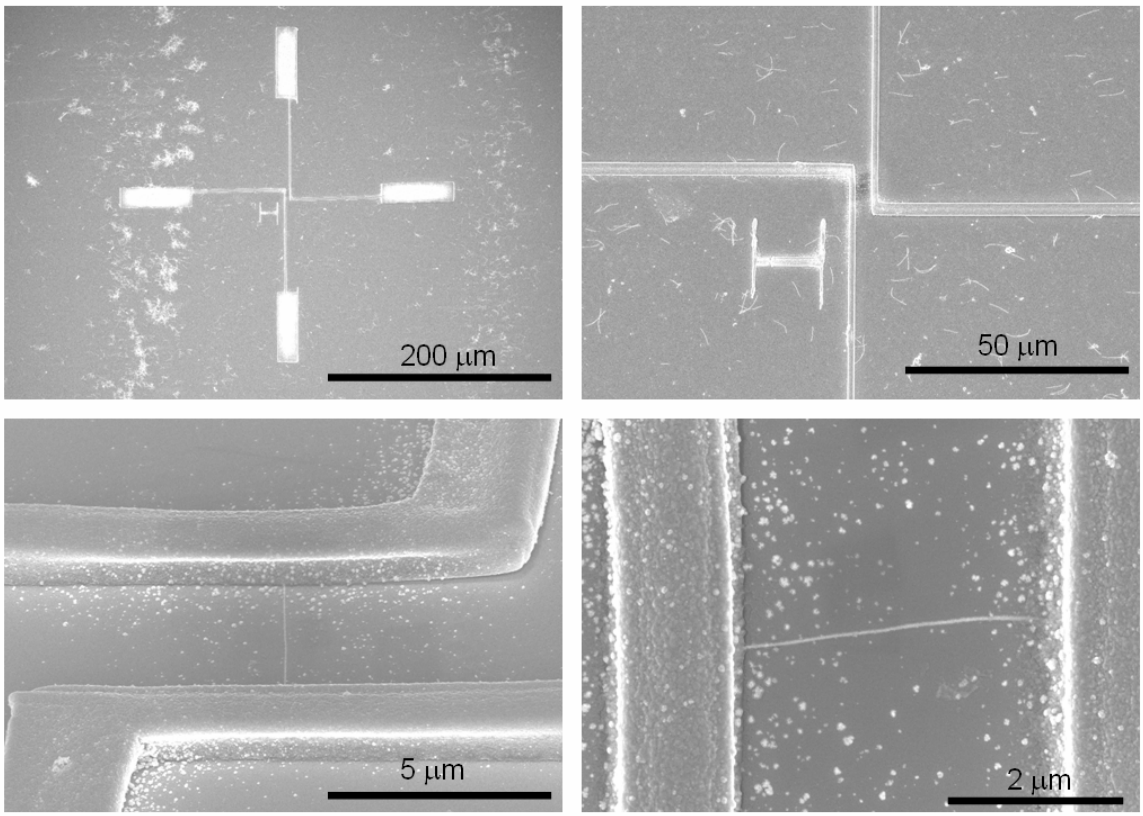

Figure 5.6 A connected Au nanowire with copper coated polymer leads. Note the texture of the copper coating on the polymer and the unselective copper deposits on the substrate.

Prior to synthesizing these 40-nm-diameter nanowires, nanowires of ~200 nm diameter were made to test the feasibility of electrically detecting plasmon absorption. These larger nanowires were more robust, despite having also been made electrolessly, and routinely survived the electrical measurement process and laser exposure. From these samples, preliminary results showing the effect of laser heating on the resistance of Au nanowires were obtained. An example of such data is shown in Figure 5.7.

Focused CW laser light with a wavelength of 800 nm and a power of a few milliwatts is enough to cause a transient increase of a few percent in the resistance of a Au nanowire. Assuming the nanowire acts like bulk metal, this change in resistance can

be converted to a change in temperature using the thermal coefficient of resistivity, α, which for gold is 3.4×10^{-3} K^{-1}.[127] The resistance is given by

$$\rho(T) = \rho_0(1 + \alpha(T - T_0)), \qquad \text{(eqn. 5.4)}$$

which can be rearranged to read,

$$\Delta T = \frac{\Delta R}{R_0} \cdot \frac{1}{\alpha}, \qquad \text{(eqn. 5.5)}$$

where $\rho(T)$ is the resistivity at temperature T and ρ_0 is the resistivity at T_0 (room temperature). Therefore, the change in resistance observed in Figure 5.7A, if caused exclusively by heating, would result in a change of temperature, averaged over the nanowire, of about 10 K. This temperature change may also cause the nanowire to expand and change dimensions, which could affect the resistance; however, this effect is considered negligible since the thermal coefficient of expansion for gold is 14.2×10^{6} K^{-1} and a change in 10 K would change the size by about 1 ppm. Figure 5.7B also shows an interesting polarization dependence that seems to support the hypothesis of plasmon

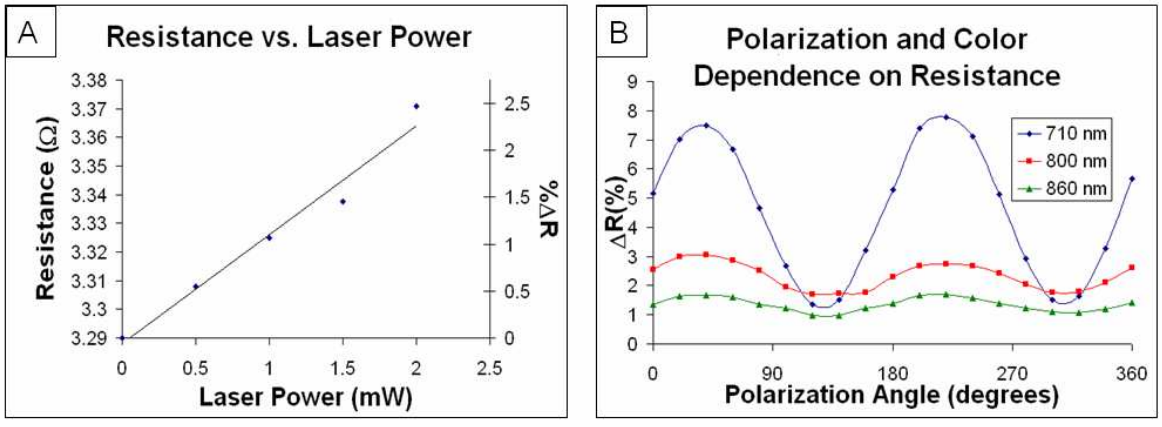

Figure 5.7 A) Laser-dependent change in resistance. B) Polarization-dependent resistance.

absorption, which should be highly polarization dependent. Strangely, though, the polarization dependence is reversed from what might be expected. It was expected that the peaks, the largest change in resistance due to heating, would occur when the polarization was parallel with the wire's short axis, because it has a plasmon band near 550 nm; however, this is not what was observed. Instead, the peaks occurred when the 800 nm laser light was polarized along the longitudinal axis, which is expected to have a plasmon peak somewhere in the IR. This phenomenon was somewhat puzzling, but a recent report in the literature suggests that it is likely due to multipole absorption along the longitudinal direction. A report by Schatz, Mirkin and coworkers showed that an 85-nm-diameter rod of length 1185 nm had several absorption peaks near 700 nm, 900 nm and 1400 nm when incident light was polarized along the longitudinal direction.[128] While multipole resonances do explain our observations, at the time of the experiment we were not aware of this effect. Thus, it was decided that nanowires with diameters closer to 40 nm with the well documented plasmon peak near 530 nm would be more suitable for this experiment. Unfortunately, these smaller nanowires, when made by electroless deposition, were more fragile and failed to produce data. After changing to electrodeposited nanowires, the polymer metallization stopped working reproducibly. For a time, samples either failed to metallize or metallized too rapidly and unselectively. Effort was then diverted to solve the metallization problem, which appears to be solved, via palladium reduction before copper enhancement. Additional devices have yet to be made incorporating the modified method of copper enhancement.

One problem that needs to be addressed is the catalysis of copper deposition by the gold wire. A copper-coated gold wire would not show characteristic gold plasmon

absorption. To circumvent this problem, an alkanethiol protection layer should be used to cover the gold wire by self-assembly. This problem was observed with our previous metallization procedure and attempts were made to protect the gold rod with an alkanethiol monolayer, however, the metallization failed either to deposit at all or to deposit selectively. We believe that the failure of alkanethiols to protect the nanorods may be related to non-uniform or rough surfaces of the electrolessly-deposited gold rods. The use of electrodeposited nanorods is expected to alleviate this problem.

While a functional sensor remains to be made, electrical plasmon detection will be an interesting application of MAP. If the plasmon absorption band could be sensitively detected electrically, one may envision simple sensor molecules attached to the gold wire that could bind analyte molecules to alter the plasmon absorption frequency of the gold wire. The shifted plasmon resonance could be detected by a brief light exposure that would cause a change in resistance. Thus, binding events could be detected electrically. This detection scheme lends itself to an array format where multiple analytes could be detector for in parallel. Since the gold substrate is about 10^8 times smaller than the substrate used for macroscopic plasmon detection, a complete monolayer of analyte is possible with only a fraction of the concentration that would be required in the macroscopic scheme.

The ability to fabricate such a device would have wider implications as well. For instance, materials besides gold nanowires could be electrically connected under an optical microscope. Currently, the predominant means to wire such tiny samples is through e-beam lithography. E-beam lithography is slow and typically requires 1-2 days to complete, compared to the technique described, which can be performed from start to

finish in about three hours and without any special clean-room precautions. The only requirements are that the samples be visible on the microscope and be chemically inert enough to withstand the polymer metallization procedure. Wiring of an assortment of interesting nanostructures could be envisioned, such as diode-structured nanowires[129] or tripod-shaped nanocrystals.

5.3.2 Fiber Optic Applications

Other groups have demonstrated the use of MAP fabricated fibers as light guides, and another application we thought would be interesting is fabrication at the end of silica waveguides. Micro-optical elements such as lenses, gratings, prisms, or spiral phase plates could be made directly on the cleaved surface of a fiber optic using MAP. Figure 5.8 shows an example of a micro-prism made on the core of a cleaved waveguide.

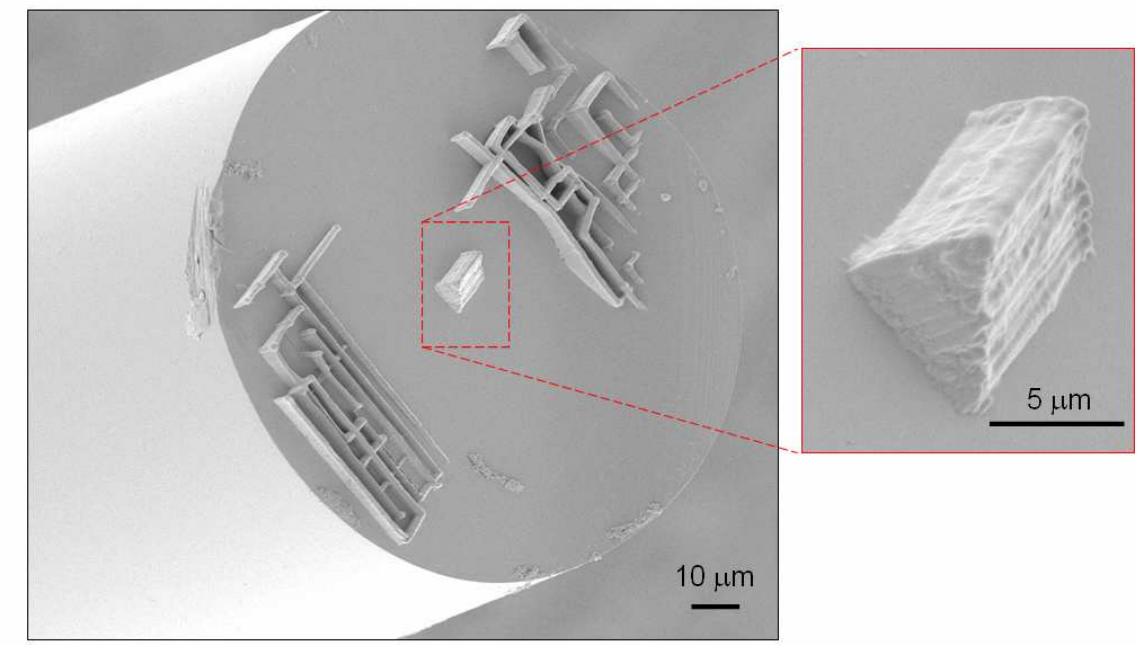

Figure 5.8 Microprism fabricated on the end of a fiber optic. The magnified image shows that the prism is not optically smooth.

The surface of the microstructure was not optically smooth. However, this sample was made using a mechanical stepper-motor stage, and structures made with the newer piezo-driven stage are significantly smoother (Figure 3.14) and, although never tested, are likely optical flat with roughness < 100 nm. It is thought, therefore, that elements that are optically smooth can be created and, using metallization chemistry, mirrored. This technique could be a useful way to couple light to micromechanical objects such as cantilevers. For instance, rather than aligning a focused beam to strike an independent cantilever, a cantilever could be made on the end of a fiber and would always remain aligned. Such a device may be useful for atomic force microscopy.

5.3.3 Future Optical Applications

Future optical applications will likely focus of the development of photonic crystals, as this application has been, in large part, responsible for progress in MAP by so many groups. MAP's ability to pattern in three dimensions makes it the best-suited technique for creating 3-D photonic crystals. Additional applications geared toward fiber optics will also likely emerge. For example, microring resonators are of increasing interest as a way to couple light evanescently from a fiber optic.[130] These devices are made by placing loop-shaped waveguides in close proximity (~100 nm) to an existing waveguide. At certain resonant wavelengths, which create standing waves within the loop, the light efficiently couples to the loop and is 'dropped' from its initial carrier waveguide. These devices could have applications ranging from sensing to eavesdropping. MAP offers a convenient way to fabricate such devices without the need for expensive photomasks or e-beam systems. Many micro-optic systems currently made

with conventional lithography or e-beam lithography could stand to benefit from MAP technology.

5.4 Mechanical Applications

Like so many other MEMS devices, our mechanical applications have centered around cantilevers. Cantilevers can couple microscopic motion to the macroscopic world via light. Used extensively in scanning-probe microscopy (SPM) and nanoindentation experiments, cantilevers can be used to apply picoNewton forces with nanometer accuracy.

Cantilevers for SPM are fabricated using conventional photolithography techniques, allowing for a range of dimensions and spring constants. Cantilevers are generally either rectangular prisms or V-shaped in geometry. They are typically composed of silicon or silicon nitride and can have additional functionality, such as magnetic or conductive tips, to image samples based on physical properties in addition to topology. Under normal imaging conditions the signal is obtained by monitoring laser light reflected from the back of the cantilever.

We foresaw several advantages in fabricating cantilevers by MAP. First, arbitrarily shaped cantilevers can be fabricated as easily as rectangular prisms. There have been reports that tapered cantilevers will have favorable thermal noise characteristics.[131] Also, polymeric cantilevers are optically transparent, enabling the sample under the cantilever to be visible during positioning. Finally, the mechanical and chemical properties of polymers are tunable by changing the material. For instance, a softer polymeric cantilever with suitable biochemical compatibility may be more

appropriate than a rigid silicon cantilever for some applications, such as scanning probe microscopy on biological species. One issue we encountered initially was the inability to reflect light off their surfaces due to the surface roughness. This issue will likely be solved by using the piezo-stage for fabrication rather than the stepper-motor stage as it capable of much smoother structures. Compare, for example, Figures 3.13 B and C which were made with piezo- and stepper-motor stages respectively.

5.4.1 Photochromic Cantilever

One goal we had was to make a polymeric cantilever that would have tunable mechanical properties. We sought to reach this goal using a photochromic monomer that reversibly isomerizes upon exposure to UV or white light. The structure of the photochromic diacrylate is shown in Figure 5.9.

Cantilevers were fabricated from this material, which was synthesized by the group of Prof. Neil Branda from the University of Alberta,[132] by adding 3 wt. % Lucirin TPO-L and fabricating in three stages with decreasing power. The resin absorbed the 800 nm laser light slightly. Thus, less power was required for fabrication at the top of the cantilever, where the laser penetrated less resin, than at the bottom. Cantilevers 250 μm long, 50 μm wide and 25 μm thick were fabricated. The photochromic nature of the monomer was retained after polymerization as can be seen by the color change upon exposure to UV and white light (Figure 5.9).

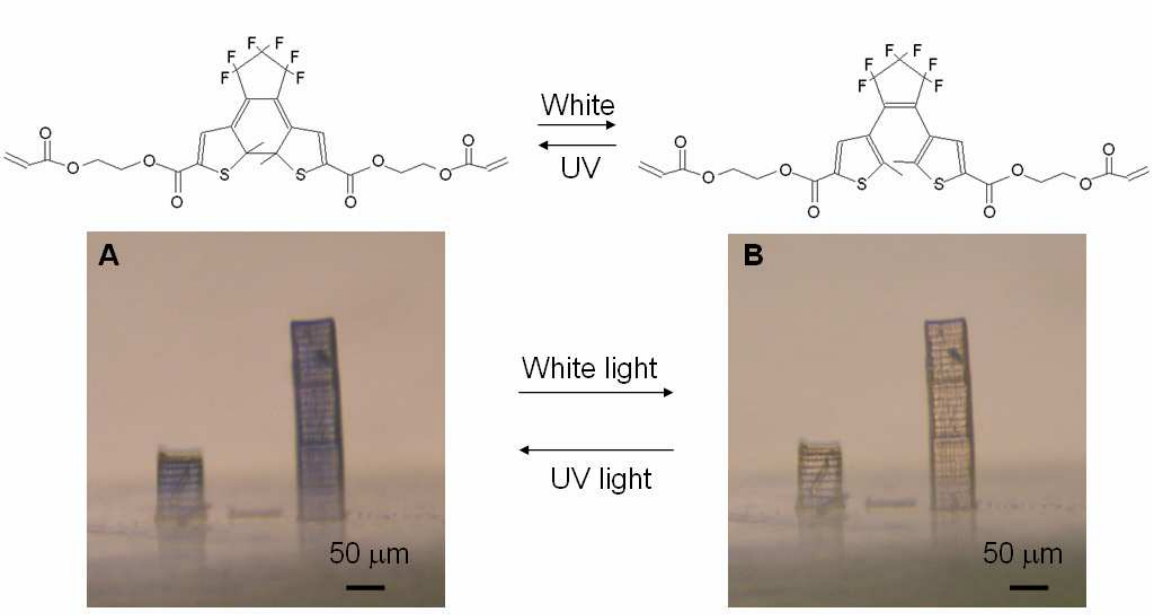

Figure 5.9 Top) Structure of photochromic diacrylate used to make cantilevers by MAP in both open and closed form. A) Photochromic cantilevers become blue after a brief exposure to UV light. B) The cantilevers return to their original orange color after being exposed to white light. Note that the larger cantilever is composed of three segments.

The change in mechanical strength was measured by observing the deflection of he polymer cantilever when pressed upon with a calibrated AFM cantilever.[††,86] If the unknown polymer cantilever has a spring constant comparable to that of the silicon AFM cantilever, the two cantilevers should deflect by approximately the same distance. By measuring the distances involved, the spring constant of the polymer cantilever can be calculated. The details of the theory are shown in Figure 5.10. After calibrating the known cantilever against a non-compliant surface, such as glass, displacement curves can be measured by pressing on the unknown cantilever and measuring the known cantilever's displacement compared to that of the AFM piezo. The slope of this curve, *m*, and the spring constant of the calibrated cantilever, k_{AFM}, can be used to calculate the

[††] The most accurate way to measure mechanical properties of cantilevers is to find the resonant frequency of the cantilever, however, this was not an option since the surface roughness did not permit the detection of reflected light.

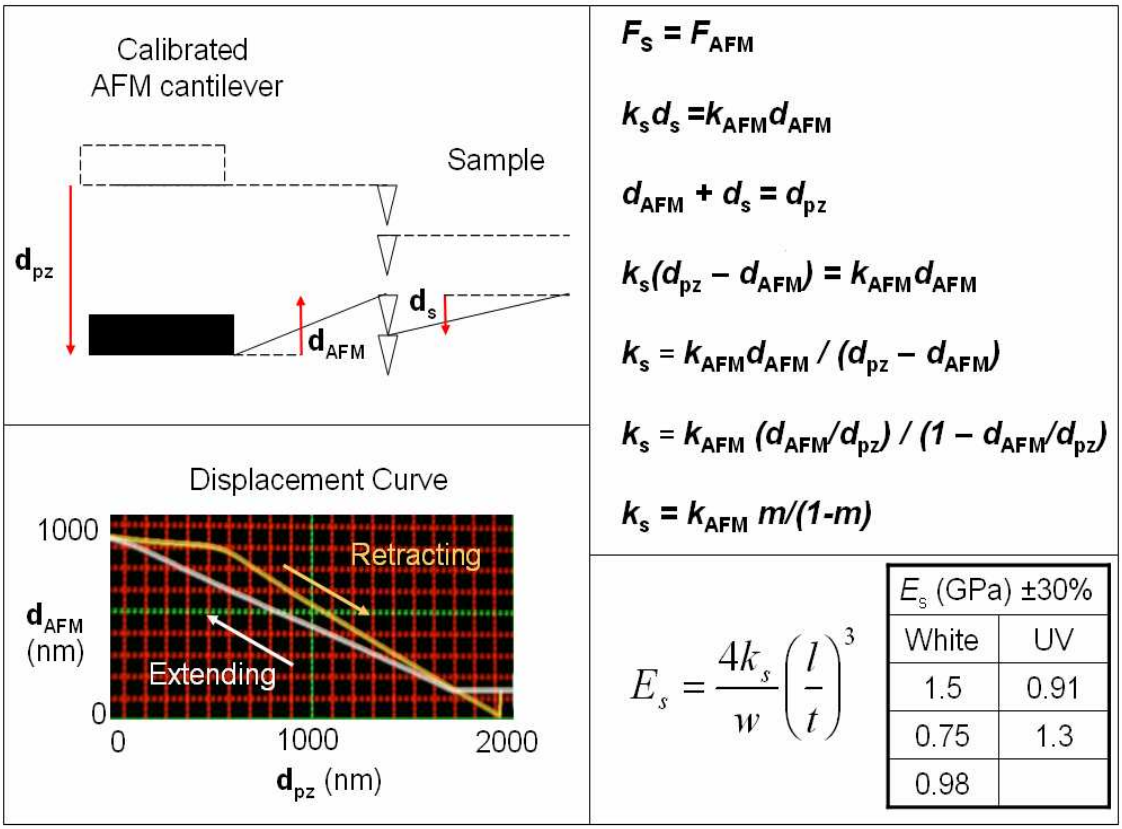

E_s (GPa) ±30%	
White	UV
1.5	0.91
0.75	1.3
0.98	

Figure 5.10 The top left panel shows a diagram of the experiment in which an AFM cantilever of known spring constant is used to deflect a sample cantilever. The top right panel gives the relevant equations, where *F* is force, *k* is spring constant, *d* is distance, and *m* is the slope of the displacement curve. The lower left panel shows a typical displacement curve with a slope near 0.5, indicating the two cantilevers have similar spring constants. The lower right panel shows the equation relating the Young's modulus, (*E*), to the spring constant, the length, (*l*), the width, (*w*), and the thickness, (*t*). Also shown are data obtained for the photochromic sample from Figure 5.9. Each value in the table is the average of 5 measurements taken over the course of two days.

unknown spring constant. Using the unknown cantilever's dimensions the Young's modulus of the material, *E*, can be found. Several measurements revealed that the average Young's modulus of the closed-form molecule and the open-form gave the same value, 1.1 ± .3 GPa. From this observation it can be concluded that the change in mechanical properties between the isomers is small and that this method is not accurate

enough to detect the difference. Unfortunately, this photochromic material does not seem offer the tunable mechanical properties that we had hoped.

5.4.2 Magnetic Cantilever

Another device that uses a cantilever can be made using a ferromagnetic material, such as magnetite (Fe_3O_4), for magnetic actuation. After using the method described in section 4.4 to seed palladium on the polymer, magnetite can be deposited by dipping the sample in a solution of 2.5 mM $Fe(NO_3)_3$ and 0.03 M dimethylamine-borane at 80° C for 30 minutes.[133] The deposited film appears black and is grown selectively where palladium is present. A cantilever was made first out of methacrylate, and then in a second fabrication step was fitted with acrylic 'wires' that were later coated in copper. Finally, in a third fabrication step, an acrylic tip was put on the end of the cantilever. This tip was coated in magnetite to demonstrate both that microstructures with multiple coatings could be made and that magnetic actuation could be incorporated. This structure is shown in Figure 5.11A.

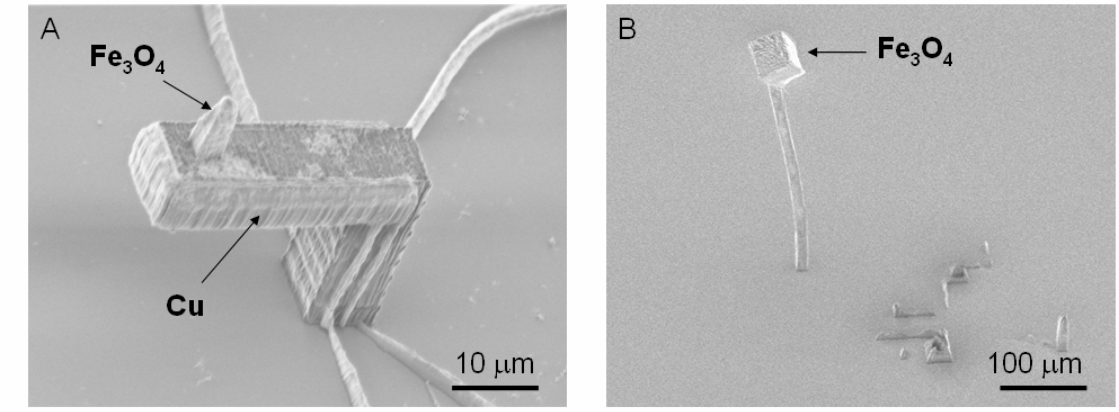

Figure 5.11 A) 4-probe wire cantilever, similar to that in Figure 5.11, except for the addition of a magnetite-coated acrylic tip. B) Methacrylate tower, ~1 mm tall, with a magnetite-coated acrylic tip. This tower was exposed to a strong magnetic field, but it did not bend in response.

Given the dimensions of the cantilever in Figure 5.11A, it was not expected to deflect significantly in a magnetic field. Another structure was fabricated to exhibit greater deflection in a magnetic field. This structure is shown in Figure 5.11B; it is a methacrylic tower with an acrylic cube affixed to its top. The cube was coated in magnetite and the structure was placed in close proximity (i.e. in contact) to a samarium-cobalt magnet. No attraction was observed, presumably due to the small quantity of Fe_3O_4 on the structure. Unlike copper, which is deposited auto-catalytically, Fe_3O_4 does not continue growing after the palladium catalyst is covered. The resulting thin film is made of randomly oriented crystallites approximately 20 nm in diameter, whose magnetic character, is similar to that of bulk magnetite.[134] This small quantity of magnetic material is insufficient for magnetic actuation.

The following calculation approximates the amount of magnetite that would be necessary to observe motion in the cantilever. The relevant equations are,

$$F_{cant} = kd$$
$$F_{mag} = MV\frac{dB}{dz} \qquad \text{(Eqn. 5.6)}$$

where, F_{cant} is the force on the cantilever, k is the cantilever spring constant (~0.02 N/m), d is the displacement, and F_{mag} is the magnetic force on a volume, V, of ferromagnetic material in a magnetic field with gradient dB/dz. M is the magnetization constant of a material, which for magnetite is 4.8×10^5 A/m.[135] Setting the forces equal to one another and solving for V yields,

$$V = \frac{kd}{M}\frac{dB}{dz}. \qquad \text{(Eqn 5.7)}$$

For a permanent magnet, such as SmCo, the magnetic field gradient can be ~100 T/m at close range, and if the displacement is to be observable under a microscope is should be

on the order of 10 μm, which would require a volume of magnetite of approximately 4×10^{-15} m^3 or 4000 μm^3. The cubic structure atop the tower in Figure 5.11B is 50 μm on an edge. Given its surface area of 15,000 μm^2, it would require a film of magnetite to be at least 0.25 μm thick to be noticeably deflected by a permanent magnetic when viewed under a microscope. This thickness of 250 nm is a factor of ten thicker than the film is believed to be.

Attaching iron atop a long tower, similar to the one in Figure 5.11B, can result in the ability to actuate a microstructure magnetically. The images in Figure 5.12 are screenshots from a movie that shows the tower, topped with micron-sized iron filings, repeatedly springing back and forth at it is attracted to the magnet shown on the right of the images. The iron filings were placed there by first wetting the tower tip with liquid resin and then touch iron powder to the liquid. The liquid resin was then photocured to fix the iron atop the tower.

Two striking aspects of the movie are the flexibility of the polymeric microstructure and its strong adhesion to the substrate. Clearly, given enough iron, the cantilever can be actuated. A possibility for future experiments is to deposit Fe_3O_4

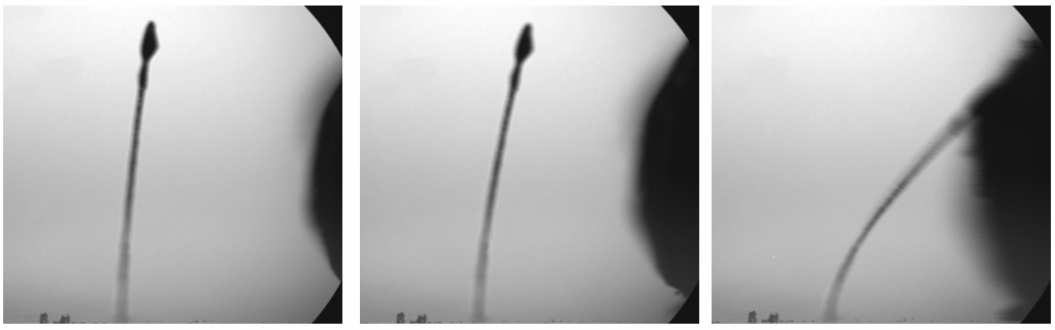

Figure 5.12 Three micrographs showing an acrylic tower, (20 μm × 20 μm × 1000 μm) with iron filings glued to the tip, being flexed by a magnet. The magnet is approaching from the right.

electrolessly on a high-surface-area structure, such as a scaffold, to incorporate as large a quantity of Fe_3O_4 as possible.

5.4.3 Future Mechanical Applications

Further development of mechanical applications of MAP will likely continue to involve cantilevers as they are the very simple mechanical devices with predictable behavior. Other devices may include valves or switches for systems such as microfluidic channels.

Two issues with mechanical devices in this size regime are actuation and control. For example, gears and axles can be made easily by MAP, but without a good way to rotate them they are useless. One way to apply force with microscopic control is with optical tweezers. This technique has been shown by other groups to be an effective means of manipulating objects made by MAP. For example, a polymeric nanoneedle with two-degrees of motion has been used to lance a living cell by optical manipulation.[136] This kind of micromanipulation tool will likely grow to be a useful application of structures fabricated by MAP.

Given the ability to pattern conductors and magnetic materials, electromagnetic actuation should also be possible. Though there was no success demonstration presented here, the first steps have been taken.

5.5 Biological Applications

We have not focused our attention on biological application of MAP, but there are several reports in the literature that suggest that such applications will soon be a major avenue for MAP. The reported work shows the ability to crosslink biological molecules such as bovine serum albumin, fibrinogen, alkaline phosphatase, and cytochrome c by multiphoton absorption[137,138]. Enzymes patterned by MAP have been shown to retain their activity, and the degree of cross-linking can tailored by the polymerization conditions. In addition, such polymerization has been performed *in vivo* in cells, and has also been used to create corral-type structures that can alter neuron growth.[139,140]

5.5.1 Future Biological Applications

The ability to create 3-D patterns *in vivo* is remarkable, and could result in a better understanding of the inner workings of cellular components. Another application that is emerging is the use of MAP fabricated scaffolds for tissue engineering.[141] Creating 3-D scaffolds that are biologically compatible has been a goal for biomedical engineers for a number of years. There are a number of possible approaches to this problem, ranging from rapid prototyping techniques to soft lithography to micropart microassembly.[142] MAP offers the unique ability to pattern in three dimensions with sub-micron resolution using biocompatible materials. Shear and coworkers used a compact, inexpensive, turnkey, Nd:YAG laser system to create 3-D biomolecular structures; this technique will facilitate the spread of multiphoton technology in biological applications.[62]

Another application is the use of 3-D structures to develop a better understanding of cell mobility and interaction with their surroundings. Structures such as 3-D micro-

mazes could easily be made by MAP, and the courses that cells take through such mazes may prove informative about their response to stimuli such as nutrients or toxins. The mechanical properties of the surroundings have also been shown to influence cell mobility in two dimensions.[143] Similar studies would certainly be of interest in three dimensions and could be performed easily with MAP-made structures.

5.6 Future Technical Challenges

5.6.1 Resolution Improvements

The ability of MAP to create 100-nm features using 800-nm light is impressive. However, the ability to create even smaller features may be crucial to many applications. For instance, the 'wiring' of nanostructures, as described in section 5.3.1, currently requires the nanostructure to have one dimension larger then 1 μm, in so that multiple polymer wires can be patterned without shorting one another. If the voxel resolution could be improved by a factor of 2 or 3, nanoparticles that are submicron in all dimensions could be wired and measured. In addition to reducing the voxel size, it would be desirable to be able to create spherical voxels rather than prolate spheroids.

Part of the solution to the resolution problem may be chemical. For instance, it has been reported that the addition of radical inhibitors to a resin appears to decrease the voxel size.[144] Careful control of the polymerization chemistry may yield further improvements in voxel size, although probably only in the range of ten or twenty percent. It is unclear whether chemistry can be used to improve the voxel shape as well.

Optical techniques probably offer the greatest hope for significant reductions in voxel volumes and significant improvements in voxel shapes. One promising technique, which has been developed in the context of fluorescence microscopy, is called stimulated emission depletion (STED).[145] STED employs two laser beams, one to excite the molecules and one, which is tuned to the red of the absorption spectrum, to stimulate emission back down to the ground state. The depletion beam passes through a phase mask that causes it to be dark in the center of the focal region, so that no emission is stimulated there. As a result, it has proven possible to attain resolution of tens of nanometers in fluorescence microscopy using visible light.[145] STED also assists in creating a considerably more spherical point-spread-function than does standard focused laser excitation.

STED should be directly applicable to MAP. Using a setup like the cross-correlation scheme shown in Figure 2.3, two lasers of with different colors can be overlapped in space with a fixed time delay between them. The first beam can excite the photoinitiator by two-photon absorption and the second beam, which is at the fundamental wavelength for depletion, can be used for STED. Typical radical photoinitiators become singlet diradicals upon excitation, and it is only after intersystem crossing that homolysis occurs and polymerization can be initiated.[146] The intersystem crossing time is in the range of 100 ps, so there is ample opportunity to stimulate emission before polymerization is initiated. In fluorescence microscopy, ideally more than 95% of molecules should be deexcited to improve resolution. In MAP it is only necessary to deexcite enough molecules to fall below the polymerization threshold; thus, stimulating emission from even 10% of the molecules may be sufficient to reduce voxel

size significantly. STED may ultimately enable the creation of 20-nm voxels using 800-nm light.

5.6.2 System Improvements

It is desirable to be able to make MAP fabrication systems more compact and less expensive. Both of these goals rely to some extent on improving photoinitiator efficiency. Beyond that, the desirable improvements in fabrication systems depend on the fabrication goals.

In a laboratory setting, it would be desirable to have a single-point fabrication system consisting of nothing more than a microscope, a laptop computer, and an inexpensive, compact, turnkey laser system. Such a fabrication system could easily fit on top of a desk or a lab bench. As described above, the use of inexpensive microlasers in place of ultrafast Ti:sapphire systems for MAP-based fabrication has already been demonstrated. Compact ultrafast laser systems with tens of milliwatts of power at 800 nm are also available, albeit at a somewhat greater cost. The commercial availability of highly efficient photoinitiators makes either of these laser options quite attractive.

In an industrial setting, it would be desirable to have high-throughput, multi-point fabrication capability. With efficient enough photoinitiators, such a system should be possible with a Ti:sapphire oscillator rather than an amplified laser system. Development of a multipoint fabrication system based on a micro-lens array, to create several hundred individual beams, and a spatial light modulator, to control the intensity of each beam, should enable independent fabrication at hundreds of points simultaneously. These

points could be used to create hundreds of copies of a given structure or they could act in unison to fabricate large structures rapidly.

Chapter 6: Conclusion

This thesis has discussed the technique of multiphoton absorption polymerization, a unique method for fabrication on the submicron scale with arbitrary 3-D complexity. The mechanism and chemistry of MAP was described in the first chapter, along with the motivation for creating microsystems. Several issues were also raised in the introduction, such as the novelty of designing a MAP fabrication system, MAP's slow serial nature, and the lack of additional functionality, such as conductivity.

In chapter 2 the five necessary components of a MAP system were identified: a laser, a microscope, a sample, a device to move the beam with respect to the sample, and software to control the motion. The working details of each subsystem were explained and the setup we currently use was described. Fabrication techniques, such as 3-D pattern design and sample washing methods, were also explained. One of the central tenets of the chapter was that while the complexity of a MAP setup can vary from simple to complex, a basic working system requires little expertise to assemble and should be within reach of a wide range of scientists, including those inexperienced in ultrafast optics.

The next chapter dealt with the serial nature of MAP by using μTM to replicate complex, MAP-made structures on a fast time scale. The elastomeric nature of the molding material, PDMS, was shown to be useful in the replication of structures with high aspect ratios and severe undercuts. A method was also developed to extend μTM to replicate structures with closed loops, such as arches. MA-μTM was demonstrated to

replicate daughter structures such as bridges, cantilevers, tables, and coils from master structures that contained thin wall-like membranes under closed-loop portions of the structure. This technique can also control the presence or absence of a membrane in daughter structures, which gives us the ability to use daughter structures to create new molds. These molding techniques demonstrate that the serial process of MAP can be converted to a parallel process, in analogy with the serial process of mask writing and its parallel use in photolithography.

The issue of surface chemistry was discussed in chapter 4, in which two techniques were described to add conductive functionality to 3-D microstructures. The first technique involved creating a 3-D pattern such as a bridge and using multiphoton absorption metallization (MAM) to deposit silver above and below the bridge. This silver, which is granular, was rendered conductive by electroless copper enhancement. The second method is more general and efficient than the first, and involves adding amine functionality to the acrylic surface. This amine functionality can be used for applications requiring biocompatibility or as a complexing agent to bind palladium. Reduction of bound palladium results in a highly catalytic surface for a number of reactions, including the electroless deposition of copper and magnetite. It was also shown that the amine functionalization is selective to acrylate surfaces versus methacrylate surfaces, enabling portions of composite acrylate-methacrylate microstructures to be functionalized while leaving other portions unaffected.

Several applications of these techniques were described in chapter 5, including the wiring of nanostructures by MAP for the electrical detection of surface plasmon resonance and the fabrication of a working microinductor. Other potential devices, for

applications ranging from optical to mechanical were described, including work done by other groups practicing MAP. The future seems bright for MAP, with a number of applications close on the horizon, such as tissue scaffolding and ‘full-stop’ band gap photonic crystals. The solutions to the issues described above (the assembly of a MAP system, the use μTM to speed device creation, and the use of selective surface chemistry to add functionality) will be helpful to future applications of MAP.

REFERENCES

(1) Wang, Y.; Miyamatsu, T.; Furukawa, T.; Yamada, K.; Tominaga, T.; Makita, Y.; Nakagawa, H.; Nakamura, A.; Shima, M.; Kusumoto, S.; Shimokawa, T.; Hieda, K. *Proceedings of SPIE-The International Society for Optical Engineering* **2006**, *6153*, 61530A/1.

(2) Xia, Y.; Whitesides, G. M. *Angewandte Chemie, International Edition* **1998**, *37*, 550.

(3) Spadaccini, C. M.; Zhang, X.; Cadou, C. P.; Miki, N.; Waitz, I. A. *Sensors and Actuators, A: Physical* **2003**, *A103*, 219.

(4) Lu, C.-J.; Steinecker, W. H.; Tian, W.-C.; Oborny, M. C.; Nichols, J. M.; Agah, M.; Potkay, J. A.; Chan, H. K. L.; Driscoll, J.; Sacks, R. D.; Wise, K. D.; Pang, S. W.; Zellers, E. T. *Lab on a Chip* **2005**, *5*, 1123.

(5) Hruby, J. *MRS Bulletin* **2001**, *26*, 337.

(6) Odom, T. W.; Love, J. C.; Wolfe, D. B.; Paul, K. E.; Whitesides, G. M. *Langmuir* **2002**, *18*, 5314.

(7) Campbell, C. J.; Baker, E.; Fialkowski, M.; Bitner, A.; Smoukov, S. K.; Grzybowski, B. A. *Journal of Applied Physics* **2005**, *97*, 126102/1.

(8) Grzybowski, B. A.; Radkowski, M.; Campbell, C. J.; Lee, J. N.; Whitesides, G. M. *Applied Physics Letters* **2004**, *84*, 1798.

(9) Grzybowski, B. A.; Winkleman, A.; Wiles, J. A.; Brumer, Y.; Whitesides, G. M. *Nature Materials* **2003**, *2*, 241.

(10) Kalsin, A. M.; Fialkowski, M.; Paszewski, M.; Smoukov, S. K.; Bishop, K. J. M.; Grzybowski, B. A. *Science (Washington, DC, United States)* **2006**, *312*, 420.

(11) Xia, Y.; Gates, B.; Yin, Y.; Lu, Y. *Advanced Materials (Weinheim, Germany)* **2000**, *12*, 693.

(12) Yoon, J.; Lee, W.; Thomas, E. L. *MRS Bulletin* **2005**, *30*, 721.

(13) Fleming, J. G.; Lin, S. Y.; El-Kady, I.; Biswas, R.; Ho, K. M. *Nature (London, United Kingdom)* **2002**, *417*, 52.

(14) Campbell, M.; Sharp, D. N.; Harrison, M. T.; Denning, R. G.; Turberfield, A. J. *Nature (London)* **2000**, *404*, 53.

(15) Lewis, J. A.; Gratson, G. M. *Materials Today (Oxford, United Kingdom)* **2004**, *7*, 32.

(16) Gratson, G. M.; Garcia-Santamaria, F.; Lousse, V.; Xu, M.; Fan, S.; Lewis, J. A.; Braun, P. V. *Advanced Materials (Weinheim, Germany)* **2006**, *18*, 461.

(17) Gratson, G. M.; Xu, M.; Lewis, J. A. *Nature* **2004**, *428*, 386.

(18) Smay, J. E.; Cesarano, J., III; Lewis, J. A. *Langmuir* **2002**, *18*, 5429.

(19) Therriault, D.; Shepherd, R. F.; White, S. R.; Lewis, J. A. *Advanced Materials (Weinheim, Germany)* **2005**, *17*, 395.

(20) Bertsch, A.; Jiguet, S.; Bernhard, P.; Renaud, P. *Materials Research Society Symposium Proceedings* **2003**, *758*, 3.

(21) Maruo, S.; Ikuta, K. *Sensors and Actuators, A: Physical* **2002**, *A100*, 70.
(22) Cumpston, B. H.; Ananthavel, S. P.; Barlow, S.; Dyer, D. L.; Ehrlich, J. E.; Erskine, L. L.; Heikal, A. A.; Kuebler, S. M.; Lee, I. Y. S.; McCord-Maughon, D.; Qin, J.; Rockel, H.; Rumi, M.; Wu, X.-L.; Marder, S. R.; Perry, J. W. *Nature (London)* **1999**, *398*, 51.
(23) Kawata, S.; Sun, H.-B.; Tianaka, T.; Takada, K. *Nature (London, United Kingdom)* **2001**, *412*, 697.
(24) Goppert-Mayer, M. *Annalen der Physik (Berlin, Germany)* **1931**, *9*, 273.
(25) Kaiser, W.; Garrett, C. G. B. *Physical Review Letters* **1961**, *7*, 229.
(26) Nakamura, O. *Microscopy Research and Technique* **1999**, *47*, 165.
(27) So, P. T. C.; Dong, C. Y.; Masters, B. R.; Berland, K. M. *Annual Review of Biomedical Engineering* **2000**, *2*, 399.
(28) Denk, W.; Strickler, J. H.; Webb, W. W. *Science (Washington, DC, United States)* **1990**, *248*, 73.
(29) Soeller, C.; Cannell, M. B. *Microscopy Research and Technique* **1999**, *47*, 182.
(30) Odian, G. *Principles of Polymerization. 2nd Ed*, 1981.
(31) Sun, H.-B.; Kawata, S. *Journal of Lightwave Technology* **2003**, *21*, 624.
(32) Baldacchini, T.; Chen, H.; Farrer, R. A.; Previte, M. J. R.; Moser, J.; Naughton, M. J.; Fourkas, J. T. *Proceedings of SPIE-The International Society for Optical Engineering* **2002**, *4633*, 136.
(33) Baldacchini, T.; Farrer, R. A.; Moser, J.; Fourkas, J. T.; Naughton, M. J. *Synthetic Metals* **2003**, *135-136*, 11.
(34) Baldacchini, T.; Fourkas, J. T. *Three-Dimensional Nanofabrication Using Multiphoton Absorption*; Marcel Dekker: New York, 2004.
(35) Baldacchini, T.; LaFratta, C. N.; Farrer, R. A.; Teich, M. C.; Saleh, B. E. A.; Naughton, M. J.; Fourkas, J. T. *Journal of Applied Physics* **2004**, *95*, 6072.
(36) Belfield, K. D.; Schafer, K. J.; Liu, Y.; Liu, J.; Ren, X.; Van Stryland, E. W. *Journal of Physical Organic Chemistry* **2000**, *13*, 837.
(37) Albota, M.; Beljonne, D.; Bredas, J.-L.; Ehrlich, J. E.; Fu, J.-Y.; Heikal, A. A.; Hess, S. E.; Kogej, T.; Levin, M. D.; Marder, S. R.; McCord-Maughon, D.; Perry, J. W.; Rockel, H.; Rumi, M.; Subramaniam, G.; Webb, W. W.; Wu, X.-L.; Xu, C. *Science (Washington, D. C.)* **1998**, *281*, 1653.
(38) Rumi, M.; Ehrlich, J. E.; Heikal, A. A.; Perry, J. W.; Barlow, S.; Hu, Z.; McCord-Maughon, D.; Parker, T. C.; Roeckel, H.; Thayumanavan, S.; Marder, S. R.; Beljonne, D.; Bredas, J.-L. *Journal of the American Chemical Society* **2000**, *122*, 9500.
(39) Reinhardt, B. A.; Brott, L. L.; Clarson, S. J.; Dillard, A. G.; Bhatt, J. C.; Kannan, R.; Yuan, L.; He, G. S.; Prasad, P. N. *Chemistry of Materials* **1998**, *10*, 1863.
(40) Wang, I.; Bouriau, M.; Baldeck, P. L.; Martineau, C.; Andraud, C. *Optics Letters* **2002**, *27*, 1348.

(41) Lemercier, G.; Mulatier, J.-C.; Martineau, C.; Anemian, R.; Andraud, C.; Wang, I.; Stephan, O.; Amari, N.; Baldeck, P. *Comptes Rendus Chimie* **2005**, *8*, 1308.
(42) Martineau, C.; Anemian, R.; Andraud, C.; Wang, I.; Bouriau, M.; Baldeck, P. L. *Chemical Physics Letters* **2002**, *362*, 291.
(43) Campagnola, P. J.; Delguidice, D. M.; Epling, G. A.; Hoffacker, K. D.; Howell, A. R.; Pitts, J. D.; Goodman, S. L. *Macromolecules* **2000**, *33*, 1511.
(44) Li, C.; Luo, L.; Wang, S.; Huang, W.; Gong, Q.; Yang, Y.; Feng, S. *Chemical Physics Letters* **2001**, *340*, 444.
(45) Teh, W. H.; Durig, U.; Salis, G.; Harbers, R.; Drechsler, U.; Mahrt, R. F.; Smith, C. G.; Guntherodt, H. J. *Applied Physics Letters* **2004**, *84*, 4095.
(46) Teh, W. H.; Duerig, U.; Drechsler, U.; Smith, C. G.; Guentherodt, H. J. *Journal of Applied Physics* **2005**, *97*, 054907/1.
(47) Yin, X.; Fang, N.; Zhang, X.; Martini, I. B.; Schwartz, B. J. *Applied Physics Letters* **2002**, *81*, 3663.
(48) Deubel, M.; von Freymann, G.; Wegener, M.; Pereira, S.; Busch, K.; Soukoulis, C. M. *Nature Materials* **2004**, *3*, 444.
(49) Guerin, L. J.; Bossel, M.; Demierre, M.; Calmes, S.; Renaud, P. *Transducers 97, International Conference on Solid-State Sensors and Actuators, Chicago, June 16-19, 1997* **1997**, *2*, 1419.
(50) Kuebler, S. M.; Braun, K. L.; Zhou, W.; Cammack, J. K.; Yu, T.; Ober, C. K.; Marder, S. R.; Perry, J. W. *Journal of Photochemistry and Photobiology, A: Chemistry* **2003**, *158*, 163.
(51) Yu, T.; Ober, C. K.; Kuebler, S. M.; Zhou, W.; Marder, S. R.; Perry, J. W. *Advanced Materials (Weinheim, Germany)* **2003**, *15*, 517.
(52) Zhou, W.; Kuebler Stephen, M.; Braun Kevin, L.; Yu, T.; Cammack, J. K.; Ober Christopher, K.; Perry Joseph, W.; Marder Seth, R. *Science* **2002**, *296*, 1106.
(53) Takada, K.; Sun, H.-B.; Kawata, S. *Applied Physics Letters* **2005**, *86*, 071122/1.
(54) Juodkazis, S.; Mizeikis, V.; Seet, K. K.; Miwa, M.; Misawa, H. *Nanotechnology* **2005**, *16*, 846.
(55) Sun, H.-B.; Tanaka, T.; Kawata, S. *Applied Physics Letters* **2002**, *80*, 3673.
(56) Tanaka, T.; Sun, H.-B.; Kawata, S. *Applied Physics Letters* **2002**, *80*, 312.
(57) Wu, E. S.; Strickler, J. H.; Harrell, W. R.; Webb, W. W. *Proceedings of SPIE-The International Society for Optical Engineering* **1992**, *1674*, 776.
(58) Sridhar, M.; Basu, S.; Scranton, V. L.; Campagnola, P. J. *Review of Scientific Instruments* **2003**, *74*, 3474.
(59) Maruo, S.; Nakamura, O.; Kawata, S. *Optics Letters* **1997**, *22*, 132.
(60) Fuji, T.; Unterhuber, A.; Yakovlev, V. S.; Tempea, G.; Stingl, A.; Krausz, F.; Drexler, W. *Applied Physics B: Lasers and Optics* **2003**, *77*, 125.
(61) Yokoyama, S.; Nakahama, T.; Miki, H.; Mashiko, S. *Thin Solid Films* **2003**, *438-439*, 452.

(62) Kaehr, B.; Ertas, N.; Nielson, R.; Allen, R.; Hill, R. T.; Plenert, M.; Shear, J. B. *Analytical Chemistry* **2006**, *78*, 3198.
(63) Reid, D. T.; Sibbett, W.; Dudley, J. M.; Barry, L. P.; Thomsen, B.; Harvey, J. D. *Applied Optics* **1998**, *37*, 8142.
(64) Santran, S.; Martinez-Rosas, M. E.; Canioni, L.; Sarger, L. *IEEE Journal of Quantum Electronics* **2004**, *40*, 1687.
(65) Millard, A. C.; Fittinghoff, D. N.; Squier, J. A.; Muller, M.; Gaeta, A. L. *Journal of Microscopy* **1999**, *193*, 179.
(66) Ranka, J. K.; Gaeta, A. L.; Baltuska, A.; Pshenichnikov, M. S.; Wiersma, D. A. *Optics Letters* **1997**, *22*, 1344.
(67) Coenjarts, C. A.; Ober, C. K. *Chemistry of Materials* **2004**, *16*, 5556.
(68) Watanabe, T.; Akiyama, M.; Totani, K.; Kuebler, S. M.; Stellacci, F.; Wenseleers, W.; Braun, K.; Marder, S. R.; Perry, J. W. *Advanced Functional Materials* **2002**, *12*, 611.
(69) Wong, S.; Deubel, M.; Perez-Willard, F.; John, S.; Ozin, G. A.; Wegener, M.; von Freymann, G. *Advanced Materials (Weinheim, Germany)* **2006**, *18*, 265.
(70) Serbin, J.; Egbert, A.; Ostendorf, A.; Chichkov, B. N.; Houbertz, R.; Domann, G.; Schulz, J.; Cronauer, C.; Frohlich, L.; Popall, M. *Optics letters* **2003**, *28*, 301.
(71) Lu, Y.; Hasegawa, F.; Goto, T.; Ohkuma, S.; Fukuhara, S.; Kawazu, Y.; Totani, K.; Yamashita, T.; Watanabe, T. *Journal of Materials Chemistry* **2004**, *14*, 75.
(72) Klein, S.; Barsella, A.; Leblond, H.; Bulou, H.; Fort, A.; Andraud, C.; Lemercier, G.; Mulatier, J. C.; Dorkenoo, K. *Applied Physics Letters* **2005**, *86*, 211118/1.
(73) Kuebler, S. M.; Rumi, M.; Watanabe, T.; Braun, K.; Cumpston, B. H.; Heikal, A. A.; Erskine, L. L.; Thayumanavan, S.; Barlow, S.; Marder, S. R.; Perry, J. W. *Journal of Photopolymer Science and Technology* **2001**, *14*, 657.
(74) Qi, F.; Li, Y.; Guo, H.; Yang, H.; Gong, Q. *Optics Express* **2004**, *12*, 4725.
(75) Kato, J.-i.; Takeyasu, N.; Adachi, Y.; Sun, H.-B.; Kawata, S. *Applied Physics Letters* **2005**, *86*, 044102/1.
(76) Formanek, F.; Takeyasu, N.; Tanaka, T.; Chiyoda, K.; Ishikawa, A.; Kawata, S. *Optics Express* **2006**, *14*, 800.
(77) Choi, K. M.; Rogers, J., A. *Journal of the American Chemical Society* **2003**, *125*, 4060.
(78) Hui, C. Y.; Jagota, A.; Lin, Y. Y. *Langmuir* **2002**, *18*, 1394.
(79) Schmid, H.; Michel, B. *Macromolecules* **2000**, *33*, 3042.
(80) Xia, Y.; McClelland, J. J.; Gupta, R.; Qin, D.; Zho, X.-M.; Sohn, L. L.; Celotta, R. J.; Whitesides, G. M. *Advanced Materials* **1997**, *9*, 147.
(81) Corning, D. Product Information about Dow Corning brand Silicone Encapsulants.
(82) Gates, B.; Whitesides, G. M. *Journal of the American Chemical Society* **2003**, *125*, 14986.

(83) Rogers, J., A. “Techniques and Applications for Non-Planar Lithography”; Materials Research Society, 2003, Boston.
(84) Kadekar, V.; Fang, W.; Liou, F. *Journal of Manufacturing Science and Engineering* **2004**, *126*, 9.
(85) LaFratta, C. N.; Baldacchini, T.; Farrer, R. A.; Fourkas, J. T.; Teich, M. C.; Saleh, B. E. A.; Naughton, M. J. *Journal of Physical Chemistry B* **2004**, *108*, 11256.
(86) Bayindir, Z.; Sun, Y.; Naughton, M. J.; LaFratta, C. N.; Baldacchini, T.; Fourkas, J. T.; Stewart, J.; Saleh, B. E. A.; Teich, M. C. *Applied Physics Letters* **2005**, *86*, 064105/1.
(87) LaFratta, C. N.; Li, L.; Fourkas, J. T. *PNAS* **2006**, *103*, 8589.
(88) Madden, J. D.; Hunter, I. W. *Journal of Microelectromechanical Systems* **1996**, *5*, 24.
(89) Conde, O.; Kar, A.; Mazumder, J. *Journal of Applied Physics* **1992**, *72*, 754.
(90) Xu, X.; Steinfeld, J. I. *Applied Surface Science* **1990**, *45*, 281.
(91) Wexler, D.; Zink, J. I.; Tutt, L. W.; Lunt, S. R. *Journal of Physical Chemistry* **1993**, *97*, 13563.
(92) Baldacchini, T.; Pons, A.-C.; Pons, J.; LaFratta, C. N.; Fourkas, J. T.; Sun, Y.; Naughton, M. J. *Optics Express* **2005**, *13*, 1275.
(93) Kaneko, K.; Sun, H.-B.; Duan, X.-M.; Kawata, S. *Applied Physics Letters* **2003**, *83*, 1426.
(94) Tanaka, T.; Ishikawa, A.; Kawata, S. *Applied Physics Letters* **2006**, *88*, 081107/1.
(95) LaFratta, C. N.; Lim, D.; O'Malley, K.; Baldacchini, T.; Fourkas, J. T. *Chemistry of Materials* **2006**, *18*, 2038.
(96) Auerbach, A. *Journal of the Electrochemical Society* **1985**, *132*, 130.
(97) Auerbach, A. *Journal of the Electrochemical Society* **1985**, *132*, 1437.
(98) Stellacci, F.; Bauer, C. A.; Meyer-Friedrichsen, T.; Wenseleers, W.; Alain, V.; Kuebler, S. M.; Pond, S. J. K.; Zhang, Y.; Marder, S. R.; Perry, J. W. *Advanced Materials (Weinheim, Germany)* **2002**, *14*, 194.
(99) Peyser, L. A.; Vinson, A. E.; Bartko, A. P.; Dickson, R. M. *Science (Washington, D. C.)* **2001**, *291*, 103.
(100) Hidber, P. C.; Helbig, W.; Kim, E.; Whitesides, G. M. *Langmuir* **1996**, *12*, 1375.
(101) *CRC Handbook of Chemistry and Physics, 66th ed.*; Weast, R. C., Ed.; CRC Press: Boca Raton, 1985; Vol. 66.
(102) Radoeva, M.; Radoev, B.; Stoeckelhuber, K. W. *Journal of Materials Science* **2003**, *38*, 2703.
(103) Formanek, F.; Takeyasu, N.; Tanaka, T.; Chiyoda, K.; Ishikawa, A.; Kawata, S. *Applied Physics Letters* **2006**, *88*, 083110/1.
(104) Ekkehard Müh, H. W. J. E. K. H. F. R. M. Acrylate-Terminated Macromonomers by Michael Addition, 2001; Vol. 202; pp 3484.
(105) Mueh, E.; Marquardt, J.; Klee, J. E.; Frey, H.; Muelhaupt, R. *Macromolecules* **2001**, *34*, 5778.

(106) Charbonnier, M.; Alami, M.; Romand, M. *Journal of Applied Electrochemistry* **1998**, *28*, 449.
(107) Charbonnier, M.; Romand, M.; Harry, E.; Alami, M. *Journal of Applied Electrochemistry* **2001**, *31*, 57.
(108) Floyd, T. L. *Electronics fundamentals: circuits, devices, and applications*; Prentise-Hall, Inc.: Upper Saddle River, NJ, 2001.
(109) Medhurst, R. G. *Wireless Engineering* **1947**, *24*, 35.
(110) Ruskell, T. G.; Lohndorf, M.; Moreland, J. *Journal of Applied Physics* **1999**, *86*.
(111) Trumbull, J. D.; Glasgow, I. K.; Beebe, D. J.; Magin, R. L. *IEEE transactions on bio-medical engineering* **2000**, *47*, 3.
(112) Sun, H.-B.; Matsuo, S.; Misawa, H. *Applied Physics Letters* **1999**, *74*, 786.
(113) Borisov, R. A.; Dorojkina, G. N.; Koroteev, N. I.; Kozenkov, V. M.; Magnitskii, S. A.; Malakhov, D. V.; Tarasishin, A. V.; Zheltikov, A. M. *Applied Physics B: Lasers and Optics* **1998**, *67*, 765.
(114) Kaneko, K.; Sun, H.-B.; Duan, X.-M.; Kawata, S. *Applied Physics Letters* **2003**, *83*, 2091.
(115) Korte, F.; Serbin, J.; Koch, J.; Egbert, A.; Fallnich, C.; Ostendorf, A.; Chichkov, B. N. *Applied Physics A: Materials Science & Processing* **2003**, *77*, 229.
(116) Guo, R.; Li, Z.; Jiang, Z.; Yuan, D.; Huang, W.; Xia, A. *Journal of Optics A: Pure and Applied Optics* **2005**, *7*, 396.
(117) Straub, M.; Nguyen, L. H.; Fazlic, A.; Gu, M. *Optical Materials (Amsterdam, Netherlands)* **2005**, *27*, 359.
(118) Seet, K. K.; Mizeikis, V.; Matsuo, S.; Juodkazis, S.; Misawa, H. *Advanced Materials (Weinheim, Germany)* **2005**, *17*, 541.
(119) Sun, H.-B.; Mizeikis, V.; Xu, Y.; Juodkazis, S.; Ye, J.-Y.; Matsuo, S.; Misawa, H. *Applied Physics Letters* **2001**, *79*, 1.
(120) Tetreault, N.; von Freymann, G.; Deubel, M.; Hermatschweiler, M.; Perez-Willard, F.; John, S.; Wegener, M.; Ozin, G. A. *Advanced Materials (Weinheim, Germany)* **2006**, *18*, 457.
(121) Faraday, M. *Philosophical Transactions of the Royal Society* **1857**, *147*.
(122) Mie, G. *Ann. Phys.* **1908**, *25*.
(123) Link, S.; El-Sayed, M. A. *International Reviews in Physical Chemistry* **2000**, *19*, 409.
(124) Chou, C.-H.; Chen, C.-D.; Wang, C. R. C. *Journal of Physical Chemistry B* **2005**, *109*, 11135.
(125) Link, S.; Wang, Z. L.; El-Sayed, M. A. *Journal of Physical Chemistry B* **2000**, *104*, 7867.
(126) Nielsch, K.; Muller, F.; Li, A.-P.; Gosele, U. *Advanced Materials (Weinheim, Germany)* **2000**, *12*, 582.
(127) *CRC Handbook of Chemistry and Physics*; 66th ed.; Weast, R. C., Ed.; CRC Press: Boca Raton, 1985.
(128) Payne, E. K.; Shuford, K. L.; Park, S.; Schatz, G. C.; Mirkin, C. A. *Journal of Physical Chemistry B* **2006**, *110*, 2150.

(129) Park, S.; Chung, S.-W.; Mirkin, C. A. *Journal of the American Chemical Society* **2004**, *126*, 11772.
(130) Ibrahim, T. A.; Cao, W.; Kim, Y.; Li, J.; Goldhar, J.; Ho, P. T.; Lee, C. H. *Journal of Lightwave Technology* **2003**, *21*, 2997.
(131) Mamin, H. J.; Budakian, R.; Chui, B. W.; Rugar, D. *Physical Review Letters* **2003**, *91*, 207604/1.
(132) Myles, A. J.; Zhang, Z.; Liu, G.; Branda, N. R. *Organic Letters* **2000**, *2*, 2749.
(133) Nakanishi, T.; Masuda, Y.; Koumoto, K. *Chemistry of Materials* **2004**, *16*, 3484.
(134) Nakanishi, T.; Masuda, Y.; Koumoto, K. *Journal of Crystal Growth* **2005**, *284*, 176.
(135) Butler, R. F. *Paleomagnetism: Magnetic Domains to Geologic Terranes*; Blackwell Science
1992.
(136) Maruo, S.; Ikuta, K.; Korogi, H. *Applied Physics Letters* **2003**, *82*, 133.
(137) Pitts, J. D.; Campagnola, P. J.; Epling, G. A.; Goodman, S. L. *Macromolecules* **2000**, *33*, 1514.
(138) Allen, R.; Nielson, R.; Wise Dana, D.; Shear Jason, B. *Analytical chemistry* **2005**, *77*, 5089.
(139) Kaehr, B.; Allen, R.; Javier, D. J.; Currie, J.; Shear, J. B. *Proceedings of the National Academy of Sciences of the United States of America* **2004**, *101*, 16104.
(140) Basu, S.; Rodionov, V.; Terasaki, M.; Campagnola Paul, J. *Optics letters* **2005**, *30*, 159.
(141) Pitts, J. D.; Howell, A. R.; Taboada, R.; Banerjee, I.; Wang, J.; Goodman, S. L.; Campagnola, P. J. *Photochemistry and Photobiology* **2002**, *76*, 135.
(142) Zhang, H.; Hutmacher, D. W.; Chollet, F.; Poo, A. N.; Burdet, E. *Macromolecular Bioscience* **2005**, *5*, 477.
(143) Zaari, N.; Rajagopalan, P.; Kim, S. K.; Engler, A. J.; Wong, J. Y. *Advanced Materials (Weinheim, Germany)* **2004**, *16*, 2133.
(144) Leatherdale, C. A.; DeVoe, R. J. *Proceedings of SPIE-The International Society for Optical Engineering* **2003**, *5211*, 112.
(145) Klar, T. A.; Jakobs, S.; Dyba, M.; Egner, A.; Hell, S. W. *Proceedings of the National Academy of Sciences of the United States of America* **2000**, *97*, 8206.
(146) Colley, C. S.; Grills, D. C.; Besley, N. A.; Jockusch, S.; Matousek, P.; Parker, A. W.; Towrie, M.; Turro, N. J.; Gill, P. M. W.; George, M. W. *Journal of the American Chemical Society* **2002**, *124*, 14952.